

CRYSTALLOGRAPHIC STUDY OF CALCIUM METASILICATES

by

Felix John Trojer

Dr.phil., University of Graz

(1964)

M.S., Massachusetts Institute of

Technology (1966)

SUBMITTED IN PARTIAL FULFILLMENT

OF THE REQUIREMENTS FOR THE

DEGREE OF DOCTOR OF PHILOSOPHY

at the

MASSACHUSETTS INSTITUTE OF TECHNOLOGY

February, 1969

Signature of Author

Department of Geology, February 18, 1969  
and Geophysics i.e. Dept. of Earth  
and Planetary Sciences

Certified by

Thesis Supervisor

Accepted by

Chairman, Departmental Committee  
on Graduate Students

Archives



TABLE OF CONTENTS

	Page
Abstract.....	1
List of figures.....	4
List of tables.....	8
General background.....	10
Scope of the thesis.....	12
Chapter I, parawollastonite	
Introduction.....	17
Material and experimental data.....	19
Refinement.....	22
Discussion of the structure.....	27
Pseudosymmetry and substructure.....	35
Disorder in parawollastonite.....	39
Chapter II, high-pressure phase of CaSiO <sub>3</sub>	
Introduction.....	50
Material.....	53
X-ray diffraction experiment.....	57
Structure determination and refinement.....	60
Discussion of the structure.....	67
Chapter III, structural types of calcium metasilicate	
Introduction.....	92
Structural relation between wollastonite and parawollastonite.....	94
Common structural features in walstromite, high- pressure CaSiO <sub>3</sub> , and pseudowollastonite.....	99
Comparison of wollastonite and parawollastonite with high-pressure CaSiO <sub>3</sub> .....	109

	Page
Classification of the calcium metasilicates.....	118
The $p$ - $T$ stability field of the calcium metasilicates in relation to their structures.....	123
Acknowledgement.....	126
References.....	127
Biography.....	132
Publications by the author.....	133

## Crystallographic Study of Calcium Metasilicates

by

Felix J. Trojer

Submitted to the Department of Geology and Geophysics on  
February 18, 1969, in partial fulfillment of the requirements  
for the degree of Doctor of Philosophy.

### ABSTRACT

Two crystal structure investigations form the initial part of this research on calcium metasilicate. The structure of parawollastonite was analyzed and the results essentially confirm a proposal suggested by Mamedov and Belov (1956). In continuing the work a high-pressure phase of  $\text{CaSiO}_3$  was studied and a detailed structure determination is presented in this thesis.

Parawollastonite crystallizes in space group  $P2_1/a$  and has following cell dimensions:  $a=15.426 \text{ \AA}$ ,  $b=7.310 \text{ \AA}$ ,  $c=7.066 \text{ \AA}$ , and  $\beta=95^\circ 24'$ . Twelve formula units of  $\text{CaSiO}_3$  are found within the cell. Several previous investigators have reported unusual non-space group extinctions in addition to the absences caused by the respective symmetry elements. However, with modern counter methods applied in the present diffraction experiment these strange extinctions proved to be very weak reflections which eluded earlier diffraction records made on film. These weak reflections were found to be the consequence of a distinct substructure. With the aid of the least-squares method it was possible to reduce the discrepancy between the observed and calculated structure factors

to 6.6%. The principal structural features of parawollastonite can be described as follows: The silicon-oxygen tetrahedra form infinite chains with a repeat unit of three tetrahedra. These chains are sandwiched by slabs of calcium-oxygen octahedra. Within such a slab the octahedra share edges and form a layer-like arrangement as has been observed in brucite.

The second compound, a high-pressure phase of  $\text{CaSiO}_3$ , was crystallized at 65 kilobars and about  $1300^\circ \text{C}$ . The space group and cell dimensions are:  $\overline{P}1$ ,  $a=6.695 \text{ \AA}$ ,  $b=9.257 \text{ \AA}$ ,  $c=6.666 \text{ \AA}$ ,  $\alpha=86^\circ 38'$ ,  $\beta=76^\circ 08'$ , and  $\gamma=70^\circ 23'$ . The cell contains six formula units of  $\text{CaSiO}_3$ . The structure was solved by interpretation of a three-dimensional Patterson map and also with the aid of statistical methods. The model of the structure was then refined by the least-squares method so that the error in the agreement between the observed and computed structure factors was lowered to 6.5%. The structure of high-pressure  $\text{CaSiO}_3$  has following important characteristics: The silicons are tetrahedrally coordinated by oxygens. The tetrahedra form three-member rings and are located between irregular layers composed by calcium-oxygen polyhedra. The three crystallographically different Ca atoms within the cell appear in two distinct coordinations, two Ca atoms are surrounded by six oxygens and one Ca atom is surrounded by eight oxygens.

A comparison of the structures of wollastonite and parawollastonite with the structure of high-pressure  $\text{CaSiO}_3$  reveals several interesting similarities. In lieu of parallel Ca-O slabs found in the two wollastonites, the high-pressure phase of  $\text{CaSiO}_3$  has layers based on an irregular, hexagonal network of Ca atoms. The  $\text{Si}_3 \text{O}_9$  rings are arranged in bands which correspond to the location of the chains in the wollastonites. As a result of the close relation of the chain

structure of the wollastonites with the ring structure of the high-pressure phase, a transformation mechanism between these two structural types is proposed. In addition it is assumed that this transformation is reversible like the one found between wollastonite and pseudowollastonite. The structure of high-pressure  $\text{CaSiO}_3$  is furthermore related to walstromite,  $\text{Ca}_2\text{BaSi}_3\text{O}_9$ , and pseudowollastonite, the latter being assumed analogous with  $\text{SrGeO}_3$ . All three compounds have more or less hexagonal Ca layers in common. The individual structures can be distinguished by the number of layers in each structure and by the stacking sequence of the layers and their adjacent rings. Based on the examination of the structural characteristics of the calcium metasilicates it can be stated that the four known phases appear in two distinct structural types. The low-temperature modifications wollastonite and parawollastonite have pyroxenoid structures, while the high-temperature and high-pressure modifications such as pseudowollastonite and the phase analyzed in this investigation belong to the cyclosilicates with three-member rings.

Thesis Supervisor: Martin J. Buerger

Title: Professor of Mineralogy and  
Crystallography.

LIST OF FIGURES		Page
Fig. 1.	Projection of the structure of parawollastonite along $\underline{c}$ .....	32
Fig. 2.	Symmetry in parawollastonite.	
(a)	Pseudomonoclinic unit.	
(b)	Symmetry in the pseudomonoclinic unit.	
(c)	True and pseudosymmetry in parawollastonite.	
(d)	Symmetry of the subcell as illustrated by the atoms of the substructure.....	36
Fig. 3.	Projection along $\underline{c}$ of the idealized parawollastonite structure.	
(a)	Substructure based on Ca and Si atoms.	
(b) and (c)	Two substructures based on oxygen atoms.....	37
Fig. 4.	Precession photograph showing $(\underline{hk}0)$ of a disordered parawollastonite from Žulova, Moravia in ČSR.....	40
Fig. 5.	Schematic picture of diffraction patterns representing various stages of disorder in parawollastonite.	
(a)	$\alpha=0$ , no disorder.	
(b)	$\alpha=0.5$ .	
(c)	Schematic diffraction pattern of disordered parawollastonite from Žulova showing diffuse reflections and continuous radiation streaks.	
(d)	$\alpha= 0.8$ .....	41

Fig. 6.	Two interpretations of disorder in parawollastonite.	
(a)	Cells of parawollastonite are displaced in respect to each other by the amount $b/2$ .	
(b)	Intergrowth of parawollastonite with wollastonite giving rise to an almost identical type of disorder as given in the figure above.....	43
Fig. 7.	Guinier powder photograph using $\text{CuK}\alpha$ radiation.	
(a)	High-pressure $\text{CaSiO}_3$ .	
(b)	Pseudowollastonite.....	54
Fig. 8.	Powder photograph with $\text{CuK}\alpha$ radiation.	
(a)	High-pressure $\text{CaSiO}_3$ .	
(b)	Ringwood and Major's high-pressure phase of $\text{CaSiO}_3$ ...	55
Fig. 9.	Schematic presentation of the substructure of high-pressure $\text{CaSiO}_3$ .	
(a)	Idealized substructure Patterson projected along $\underline{a}$ , showing only the high peaks.	
(b)	Idealized substructure as a model derived from the Patterson map shown in Fig. 9a.....	61
Fig. 10.	Comparison of the atomic positions suggested by the substructure with the actual locations of the Ca and Si atoms in high-pressure $\text{CaSiO}_3$ .....	62
Fig. 11.	Projection along $\underline{a}$ of the structure of high-pressure $\text{CaSiO}_3$ .....	68
Fig. 12.	The Ca-O layer in high-pressure $\text{CaSiO}_3$ .....	71
Fig. 13.	Graphic presentation of the Ca(2) octahedra connecting two parts of neighboring layers in high-pressure $\text{CaSiO}_3$ .....	72



Fig. 14.	Schematic projection of the structure of high-pressure $\text{CaSiO}_3$ parallel (101).....	73
Fig. 15.	A silicon-oxygen ring in high-pressure $\text{CaSiO}_3$ .....	
(a)	Projected in direction normal to the Ca planes.	
(b)	Viewed parallel to the Ca planes.....	74
Fig. 16.	The orientation of the Ca planes in the reduced cell of high-pressure $\text{CaSiO}_3$ .....	75
Fig. 17.	Precession photographs of the reciprocal plane ( $hk0$ ) using $\text{MoK}\alpha$ radiation.	
(a)	Parawollastonite.	
(b)	Wollastonite.....	95
Fig. 18.	Structural relation between wollastonite and parawollastonite.	
(a)	Selection of the pseudomonoclinic unit.	
(b)	Stacking scheme of the pseudomonoclinic units in parawollastonite.....	96
Fig. 19.	The orientation of the Ca planes in the reduced cell of walstromite.....	101
Fig. 20.	Walstromite: Selection of a cell whose basal plane is a Ca-O layer.....	103
Fig. 21.	High-pressure $\text{CaSiO}_3$ : Selection of a cell whose basal plane is a Ca-O layer.....	104
Fig. 22.	Stacking sequence of the $\text{Si}_3\text{O}_9$ rings in walstromite, high-pressure $\text{CaSiO}_3$ , pseudowollastonite, and wadeite.	
(a)	Walstromite.	

- (b) High-pressure  $\text{CaSiO}_3$  .
- (c) Pseudowollastonite assumed analogous  
with  $\text{SrGeO}_3$  .
- (d) Wadeite..... 107
- Fig. 23. A schematic picture of the structure of wollastonite  
as well as parawollastonite, viewed along the  
direction of the chains..... 110
- Fig. 24. A schematic picture of the structure of high-  
pressure  $\text{CaSiO}_3$  viewed along a direction  
parallel to the Ca layers..... 111
- Fig. 25. Two pseudomonoclinic units of wollastonite  
displaced in respect to each other by the amount  
 $b/2$  parallel the plane (001)..... 112
- Fig. 26. A possible mechanism for constructing  
 $\text{Si}_3\text{O}_9$  rings out of  $\text{Si}_3\text{O}_9$  chains.
- (a)  $\text{Si}_3\text{O}_9$  chain in wollastonite and parawollastonite.
- (b)  $\text{Si}_3\text{O}_9$  ring in high-pressure  $\text{CaSiO}_3$  ..... 114
- Fig. 27. An idealized structure of wollastonite  
projected perpendicular to the Ca network.
- (a) The  $\text{SiO}_4$  tetrahedra form chains
- (b) The  $\text{SiO}_4$  tetrahedra are rearranged into rings..... 115

LIST OF TABLES		Page
Table 1.	Cell dimension of parawollastonite.....	20
Table 2.	Mamedov and Belov's coordinates for wollastonite based upon a monoclinic cell.....	23
Table 3.	Some observed structure factors with the corresponding $F$ 's based on Mamedov and Belov's coordinates and the final refined $F_{cal}$ 's for parawollastonite.....	24
Table 4.	Positional coordinates for parawollastonite.....	28
Table 5.	Interatomic distances in parawollastonite.....	29
Table 6.	Bond Angles between atoms in parawollastonite.....	30
Table 7.	Anisotropic temperature coefficients for parawollastonite.....	33
Table 8.	Thermal parameters for parawollastonite.....	34
Table 9.	Observed and computed structure factors of parawollastonite.....	46
Table 10.	Theoretical and observed statistical averages of normalized structure factors for high- pressure $CaSiO_3$ .....	58
Table 11.	Symmetry and cell data for the high-pressure polymorph of $CaSiO_3$ .....	59
Table 12 .	Summary of the sixteen models obtained by application of R.E. Long's sign determination program for high-pressure $CaSiO_3$ .....	64
Table 13 .	Atomic coordinates for the high-pressure polymorph of $CaSiO_3$ .....	69

Table 14.	Interatomic distances for high-pressure $\text{CaSiO}_3$ .....	76
Table 15.	Bond angles for high-pressure $\text{CaSiO}_3$ .....	78
Table 16.	Anisotropic temperature coefficients for high-pressure $\text{CaSiO}_3$ .....	81
Table 17.	Thermal parameters for high-pressure $\text{CaSiO}_3$ .....	82
Table 18.	Observed and calculated structure factors of high-pressure $\text{CaSiO}_3$ .....	83
Table 19.	Comparison of the $y$ coordinate of atoms in parawollastonite with the position $(2n+1)/8$ .....	97
Table 20.	Cell constants of walstromite and high- pressure $\text{CaSiO}_3$ .....	100

## GENERAL BACKGROUND

The silicates form the most abundant mineral group in nature, about ninety per cent of the earth's mantle is composed of silicates. In addition, the silicates play an ever increasing role in industrial products such as glass, cement, porcelain, bricks and other innumerable synthetic products. Naturally many attempts were made to establish a systematic of this important group of minerals. The first classification was based on chemical considerations, and the silicates were interpreted as salts of the various silicic acids. This preliminary classification was abandoned when the first structural knowledge was obtained by x-ray diffraction and replaced by a systematic based upon the arrangement of the  $\text{SiO}_4$  tetrahedra. In this respect pioneering work was performed by Machatschki (1928) and especially by Bragg (1930) whose systematic of silicates remained virtually unchallenged until today. Bragg divided the silicates into five classes:

- I Separate  $\text{SiO}_4$  tetrahedra.
- II Separate silicon-oxygen complexes.
- III Silicon-oxygen chains.
- IV Silicon-oxygen sheets.
- V Framework silicates.

Another classification frequently used is the one established by Strunz; for example published in Strunz (1966):

- I Nesosilicates (separate  $\text{SiO}_4$  tetrahedra)
- II Sorosilicates (double tetrahedra).
- III Cyclosilicates (ring-silicates).
- IV Ionosilicates (chain-silicates).

V Phyllosilicates (sheet-silicates).

VI Tectosilicates (framework silicates).

The present investigation represents a study of the various phases of calcium metasilicate,  $\text{CaSiO}_3$ . As the chemical formula indicates by its silicon-oxygen ratio, the calcium metasilicates belong either to the ring-silicates or to the chain-silicates or include both structural types. These two structural types are the only ones where the silicon-oxygen ratio is 1:3 or multiples of it. A detailed systematic of silicates by Liebau (1962) was found very useful to define a rough outline of the problems to be considered in this investigation. Liebau gives an excellent survey about the hitherto known crystals chemistry of chain-silicates and ring-silicates. Hence a thorough study of the calcium metasilicates ought to encompass following criteria:

I Examination of the nature of the  $\text{SiO}_4$  assemblage.

a Silicon-oxygen chains. Determination of the chain type.

As of now chains with a repeating unit of 2, 3, 4, 5, 7, and 9 tetrahedra are known, other repeating units are predicted but have not yet been found in silicates.

b Silicon-oxygen rings. Determination of the ring type.

Rings composed of 3, 4, and 6 tetrahedra are known to exist.

II Examination of the arrangement of the calcium-oxygen polyhedra.

Recent studies of silicates have shown that the size of the large cations as well as the way they are coordinated and linked together by oxygens have a strong influence upon the arrangement of the  $\text{SiO}_4$  tetrahedra.

## SCOPE OF THE THESIS

The mineral wollastonite, the most prominent member of the calcium metasilicates, was discovered 150 years ago. It is a well known constituent in metamorphosed limestone and is also found in contact altered calcareous sediments. Based on morphological studies, wollastonite was originally classified as a pyroxene. With the introduction of x-ray diffraction technique as a powerful tool to identify crystals, many pyroxenes were investigated and their structures worked out. The main characteristic was found to be the arrangement of the  $\text{SiO}_4$  tetrahedra in the form of infinite chains with a repeating unit of two tetrahedra. When wollastonite was investigated with x-rays by Warren (1931), it became evident that this mineral probably had a structure different from the one found in pyroxenes such as diopside. Wollastonite and all the other modifications of calcium metasilicate were therefore classed as pyroxene-like minerals and were assigned to a related structural group, namely the pyroxenoids. Many years later Mamedov and Belov (1956) determined the crystal structure of wollastonite and found silicon-oxygen chains to be present which have a repeating unit of three tetrahedra. The different length of the chain repeat is henceforth considered to be the most important criterion to differentiate pyroxenes, which have a repeat of two tetrahedra, from pyroxenoids, which have a repeat of three or more tetrahedra.

The occurrence of several modifications of calcium metasilicate was already known at the end of the last century. However, only one phase, namely wollastonite was given a careful x-ray investigation. Mamedov and

Belov determined the crystal structure of triclinic wollastonite and suggested a proposal for the monoclinic variety, called parawollastonite. Another modification was discovered by Bourgeois (1882). The symmetry of this compound was determined by Dölter (1886) by optical means, and he reported it to be either hexagonal or orthorhombic. Later this phase was named pseudowollastonite by Allen, White, and Wright (1906), and several attempts were made to solve its structure. Jeffrey and Heller (1953) made a preliminary x-ray investigation but could not proceed with a structure determination because of bad crystalline material. Hilmer (1963) circumvented this difficulty by solving the structure of strontium germanate, which is considered to be analogous with pseudowollastonite.

This brief outline shows that the knowledge of calcium metasilicates is a rather limited one. Of the three minerals only triclinic wollastonite has been studied in detail. Since this phase has been classed as a mineral belonging to the pyroxenoid group, it is natural to ask whether the other modifications of calcium metasilicate such as parawollastonite, pseudowollastonite, and perhaps other high-temperature, high-pressure phases of  $\text{CaSiO}_3$  adhere to the same chain structure type. As a consequence the investigation of structural features in common with the various phases of  $\text{CaSiO}_3$  as well as those which are different in each structure will be of great interest. This in turn lays the ground for a study of possible transformation mechanisms between these structures.

In view of these questions it was considered desirable to determine and refine the crystal structures of parawollastonite and a high-pressure phase of  $\text{CaSiO}_3$ . The latter compound was chosen because single crystals



of pseudowollastonite suitable for crystal structure analysis were not available until now. Moreover the powder pattern of this compound shows a remarkable resemblance with the one obtained from pseudowollastonite, thus promising to reveal some structural relation with pseudowollastonite. The crystallographic examination was undertaken according to the following plan.

The first chapter deals with parawollastonite. A careful structure analysis essentially confirms the proposal by Mamedov and Belov. The dispute over the correct space group,  $P2_1/a$  or  $P2_1$ , for parawollastonite is solved by comparing the agreement of the computed structure factors with the observed ones for both space groups. The considerably better agreement obtained for  $P2_1/a$  warrants the assumption that the centrosymmetric space group is the correct one for parawollastonite. Previous investigators reported so called non-space group extinctions. This problem is studied and explained in terms of a distinct substructure. This substructure also gives the answer to the presence of pseudosymmetry elements in parawollastonite. The last section in this chapter is concerned with the disorder frequently observed in wollastonite, as well as in parawollastonite. An attempt is made to explain this disorder in terms of stacking faults between neighboring cells and intergrowth of wollastonite and parawollastonite.

The second chapter presents the structure determination and refinement of a high-pressure, high-temperature phase of calcium metasilicate. It was the deliberate aim not to use a substitute analogous compound in order to establish the actual structure of such a phase in the  $CaSiO_3$  system. The most surprising result of this structure determination was the discovery of

the silicon-oxygen tetrahedra forming three-member rings. The calcium-oxygen polyhedra form imperfect layers. In the discussion of this structure it is shown that it is possible to conceive of an idealized structure of high-pressure  $\text{CaSiO}_3$ , with hexagonal, octahedral layers. The idealized structure can be used to describe the relation to the proposed structure of pseudowollastonite.

The third and last chapter is dedicated to comparative studies. The first section in this chapter relates the structures of wollastonite and parawollastonite. It confirms Ito's (1950) proposal that the different arrangement of pseudomonoclinic units determines either structure. Of great interest, however, is a comparison of the chain structures of the two modifications of wollastonite with the ring structure of this high-pressure phase of  $\text{CaSiO}_3$ . Although, at the first glance, one is inclined not to find any similarities, a number of surprising, common structural features are found in both structures. Hence it seems quite possible that wollastonite transforms into this new phase of  $\text{CaSiO}_3$  under the proper environmental conditions. A possible transformation mechanism is proposed in this chapter. The changes required by this **transition** are such that they are probably reversible, since they do not alter the basic layer-like arrangement of the calcium-oxygen polyhedra. There is some credibility to this assumption since a similar inversion, namely of wollastonite to pseudowollastonite, is known to be fairly easily reversible. In addition, a comparison of high-pressure  $\text{CaSiO}_3$ , pseudowollastonite and walstromite with each other reveals that these three compounds can be considered as members of the same polymorphic set. The third chapter concludes with a structural classification. The various modifications of

calcium metasilicate are examined in light of several criteria suggested by Prewitt and Peacor (1964) for the pyroxenes and pyroxenoids as well as those proposed by Dornberger-Schiff (1962) for pseudowollastonite.

CHAPTER I  
PARAWOLLASTONITE

Introduction

In the year 1818 the mineral wollastonite was first identified by Monticelli (1825) in volcanic bombs from Mt. Somma, Italy. Early morphological studies suggested that wollastonite has monoclinic symmetry and belongs to the pyroxene group. Eakle (1917), however, observed triclinic symmetry on some wollastonite crystals. This in turn raised the question whether wollastonite is monoclinic or triclinic. This ambiguity was solved by Warren (1931) who clearly found triclinic symmetry for wollastonite in an x-ray investigation using oscillation and rotation photographs. In addition, Warren observed that even layer lines show monoclinic symmetry. This made him conclude that a monoclinic variety could be obtained where successive cells are shifted by the amount  $\pm b/2$ . Using these results Peacock (1935) established the existence of two phases of low temperature calcium meta-silicate: triclinic wollastonite and monoclinic parawollastonite.

In an attempt to solve the structure of the monoclinic variety, Barnik (1936) proposed  $\text{Si}_3\text{O}_9$  rings as the main structural feature for parawollastonite. He also reported the systematic absence of  $hkl$  reflections of the type  $2h + k = 4n + 2$ , which is not required by space group  $P2_1/a$ . His proposal was strongly criticized, mainly because the ring structure could not explain the fibrous character of the crystals.

The similarity of x-ray diffraction patterns from wollastonite with those of the Madrell salt  $(\text{NaPO}_3)_x$  sodium polyarsenate  $(\text{NaAsO}_3)_x$ , and xonotlite  $\text{Ca}_6\text{Si}_6\text{O}_{17}(\text{OH})_2$  led to a series of structure investigations. Based on

chemical considerations, Thilo and Plaetschke (1949) assumed a chain structure for sodium polyarsenate and the Madrell salt. Dornberger-Schiff, Liebau, and Thilo (1955) were able to determine the structure of sodium polyarsenate. These authors confirmed the chain character and hence ruled out the ring arrangement for similar compounds such as wollastonite. Further evidence for a chain structure in wollastonite was presented by the structure determination of xonotlite by Mamedov and Belov (1955) and of pectolite by Buerger (1956).

With the aid of direct methods Mamedov and Belov (1956) were able to determine the structure of wollastonite in which  $\text{Si}_3\text{O}_9$  chains parallel to the  $b$  axis were found to be a basic structural feature. They used two-dimensional film data and indexed only the strong reflections of layers with  $k$  even. Their indexing was based on both a triclinic cell,  $\bar{P}1$ , and on a double monoclinic cell  $P2_1/a$ . The 204 strong reflections satisfied the condition  $2h + k = 4n$ ; this characterization bears a kind of complementary relation to Barnik's systematic absence  $2h + k = 4n + 2$ , but is not equivalent to it. The Russian authors reported an  $R$  value of 24% for the strong  $h0l$  reflections.

Tolliday (1958) proposed a structure for monoclinic parawollastonite. She started the refinement using the centric space group  $P2_1/a$ . This attempt was not satisfactory, so  $P2_1/a$  was replaced by the noncentric space group  $P2_1$ . After making this change, Tolliday reported that the refinement was progressing well. Unfortunately no coordinates, structure factors, or  $R$  values were published so that the validity of her findings can be appraised. In the view of this unsatisfactory state of affairs, a reinvestigation of the structure of parawollastonite appeared desirable.

### Material and Experimental Data

A specimen of parawollastonite crystals from Crestmore, California, was kindly provided by Dr. Charles T. Prewitt. The crystal used in the present investigation was carefully examined, and the quality of the diffraction pattern was sufficient to proceed with the intensity determination.

The space group  $P2_1/a$  was determined from precession photographs, which is consistent with Barnik's (1936) result. In addition to the extinctions caused by the two fold screw axis and the glide plane, the reflections  $hkl$  of the type  $2h + k = 4n + 2$ , were considered to be absent until now, due to some specialised locations of the atoms in the structure. This unusual phenomenon seemed to be worth checking. Although the results of film data were inconclusive on this matter a very weak diffracted x-ray beam, especially in upper levels of the index  $k$ , could be detected with a single-crystal diffractometer using advanced counter methods. Therefore these reflections were classified as present, but very weak, and hence were included in the intensity measurements.

Precise lattice constants were obtained by evaluating data from back-reflection Weissenberg films. These data were refined by least-squares methods. The dimensions for the cell of parawollastonite are given in Table 1, which shows that the new values are in good agreement with results published by Barnik (1936), and by Tolliday (1958).

Table 1. Cell Dimensions of Parawollastonite.

Parameter	Barnik (1936)	Tolliday (1958)	Present Work
$a$	15.33 Å	$15.417 \pm 0.004$ Å	$15.426 \pm 0.004$ Å
$b$	7.28	$7.321 \pm 0.002$	$7.320 \pm 0.003$
$c$	7.07	$7.066 \pm 0.002$	$7.066 \pm 0.003$
$\beta$	95° 24' 30"	95° 24' + 3'	95° 24' 15" $\pm$ 50"

Nickel-filtered  $\text{CuK}\alpha$  radiation was used to record 1290 reflections with an equi-inclination single-crystal diffractometer. In order to obtain accurate experimental data, a proportional counter was employed in connection with pulse-height discrimination. Weissenberg photographs using the same geometry as the diffractometer showed that white radiation streaks of strong reflections extend to the next lattice point on the same lattice line. For this reason, the recorded intensity of a reflection with a strong, neighboring reflection of lower  $\sin^2\theta$  on the same lattice line, was usually recorded too high. Hence the integrated intensities had to be corrected for this residual white radiation which could not be eliminated by pulse-height discrimination and the Ni filter. The method applied is similar to the procedure outlined by Larson (1965), a detailed description of it is given by Trojer (1966). The improved data were corrected for Lorentz and polarization factors as well as for absorption. The observed structure factors are listed in Table 9.



## Refinement

The coordinates published by Mamedov and Belov (1956) for wollastonite, as referred to a double monoclinic cell, were tested with the present data and a preliminary set of structure factors calculated. With the proper scale factor and an overall isotropic temperature factor of  $B = 0.6 \text{ \AA}^2$ , the discrepancy between the computed and observed structure factors, also called  $R$ , had the rather large value of 52%. Mamedov and Belov's atomic parameters are presented in Table 2. With the exception of their Si I, Si I', O IV, and IV', all positions listed in this table have  $y$  coordinates of  $(2n + 1)/8$ ; these coordinates require absences of  $hkl$  reflections with  $2h + k = 4n + 2$ . Tolliday (1958) reported having observed this extinction rule. Table 3 gives a representative sample of observed and computed structure factors for those reflections. This table shows that the non-space group extinctions are almost obeyed by Mamedov and Belov's model for wollastonite. Actually, as observed in the present investigation, the structure amplitudes of the reflections corresponding to this extinction rule, although small, are not zero.

Tolliday's view that parawollastonite should be refined in the noncentric space group  $P2_1$  was tried without success. The refinement came to a halt at an  $R$  value of 16% and gave no indication of further improvement. Accordingly space group  $P2_1/a$  was retained and several cycles of least-squares refinement were carried out with the SFLSQ 3 program written by C.T. Prewitt and recorded by Onken (1964). The scattering curves used in the refinement program were adjusted for anomalous dispersion. For  $\text{CuK}\alpha$  radiation the following correction terms were used for the metal atoms: Ca:  $\Delta f' = 0.3$ ,  $\Delta f'' = 1.4$ , and Si:  $\Delta f' = 0.2$ ,

Table 2. Mamedov and Belov's Coordinates for Wollastonite  
Based upon a Monoclinic Cell.

Atom	$\underline{x}$	$\underline{y}$	$\underline{z}$
Ca I	0.250	0.375	0.000
Ca II	0.602	0.375	0.263
Ca II'	0.602	0.875	0.263
Si I	0.406	0.080	0.232
Si I'	0.406	0.670	0.232
Si II	0.300	0.375	0.443
O I	0.297	0.375	0.667
O I'	0.297	0.875	0.667
O II	0.345	0.125	0.047
O II'	0.345	0.625	0.047
O III	0.507	0.125	0.229
O III'	0.507	0.625	0.229
O IV	0.362	0.198	0.406
O IV'	0.362	0.552	0.406
O V	0.406	0.875	0.232

Table 3. Some Observed Structure Factors with the Corresponding  $F$ 's based on Mamedov and Belov's Coordinates and the Final Refined  $F_{\text{cal}}$ 's for Parawollastonite. Indices with an Asterisk refer to "absences" in  $hkl$  with  $2h + k = 4n + 2$ . All Structure Factors are in Electron Units.

$h$	$k$	$l$	$F_{\text{obs}}$ , parawollastonite	$F_{\text{cal}}$ , M. and B.	$F_{\text{cal}}$ , parawollastonite
2	4	0	31.48	57.00	28.17
*3	4	0	2.00	0.00	-3.80
4	4	0	38.48	38.24	35.15
*5	4	0	0.00	0.00	-0.26
6	4	0	97.96	32.42	97.84
*7	4	0	1.48	0.00	1.39
8	4	0	55.76	-92.45	-52.66
*9	4	0	4.02	0.00	1.24
10	4	0	109.23	-64.59	-114.13
*11	4	0	1.94	0.00	-2.60
12	4	0	60.41	13.82	-59.62
*13	4	0	4.11	0.00	-1.98
*2	6	0	1.40	0.00	-2.99
*4	6	0	0.71	0.00	-2.55
5	6	0	37.82	-83.52	-34.56
*6	6	0	0.00	0.00	0.86
7	6	0	46.97	-24.68	-45.30
*8	6	0	0.00	0.00	-5.65
9	6	0	52.89	-33.86	-52.43
*10	6	0	3.11	0.00	-7.54

Table 3. Continued.

<u>h</u>	<u>k</u>	<u>l</u>	$\bar{F}_{\text{obs}}$ , parawollastonite	$\bar{F}_{\text{cal}}$ , M. and B.	$\bar{F}_{\text{cal}}$ , parawollastonite
0	4	-1	43.59	-41.01	-36.55
0	4	1	43.24	41.01	-36.55
*1	4	-1	2.02	0.18	0.81
*1	4	1	1.67	0.02	3.11
2	4	-1	24.20	-44.97	-23.13
2	4	1	60.81	76.14	60.93
*3	4	-1	0.60	0.08	-5.47
*3	4	1	3.02	-0.18	5.84
4	4	-1	25.60	12.49	-25.65
4	4	1	7.03	-32.25	-7.94
*5	4	-1	1.40	0.14	2.13
*5	4	1	1.25	0.04	5.38
6	4	-1	31.19	74.60	31.80
6	4	1	25.85	-20.39	21.41
*7	4	-1	2.21	-0.10	-3.70
*7	4	1	0.00	0.11	2.10
8	4	-1	42.36	-81.02	-39.91
8	4	1	98.31	-57.32	-99.14
*9	4	-1	4.82	-0.08	2.37
*9	4	1	3.27	-0.06	3.48

$\Delta f'' = 0.4$ . Employing an equal weighting scheme and allowing all parameters to vary, the best  $\underline{R}$  value with individual, isotropic temperature factors for each atom was 8.4%.

At this stage of the investigation it became evident that the shifts performed by the least-squares refinement showed no tendency to locate atoms on positions responsible for the non-space group extinctions. In order to obtain an excellent agreement between observed and computed data with a least-squares refinement a proper weighting scheme is necessary, thus a weighting factor  $\underline{w} = |\underline{F}_{\text{obs}}|$  was attributed to each reflection. This weighting procedure is described in detail by de Vries (1965). With introduction of anisotropic thermal parameters the final  $\underline{R}$  values were obtained:  $\underline{R}$  (unweighted) = 6.6%,  $\underline{R}$  (weighted) = 4.9%. In contrast to Mamedov and Belov's proposal this refined model of the structure of parawollastonite does not demand absences of hkl reflections with  $2\underline{h} + \underline{k} = 4\underline{n} + 2$ . A comparison of these observed structure factors with the corresponding final ones in Table 3 shows a fairly good agreement considering the fact that the counting statistics are very poor for such weak intensities.

### Discussion of the Structure

The low residual value of 6.6%, compared with the  $R = 16\%$  for the noncentric space group  $P2_1$ , confirms the centric space group  $P2_1/a$  as the correct one for parawollastonite. All the atoms in this structure occupy the general position  $4e$ . The final coordinates are listed in Table 4. Table 5 gives the interatomic distances and Table 6 the bond angles between atoms. A projection of the structure of parawollastonite along  $c$  is illustrated in Fig. 1.

The Ca atoms are surrounded by distorted oxygen octahedra which form three slabs within the cell parallel  $b$ . A slab consists of three rows of Ca octahedra sharing edges with each other. The center row built up by Ca(1) and its surrounding oxygens has an average Ca(1)-O distance of 2.368 Å. The two rows, one composed by Ca(2), the other by Ca(3), on either side of the center row have octahedra with a slightly larger, average Ca-O distance of 2.402 Å. This average distance is the same for Ca(2) and Ca(3). Ca(1) is linked to an additional seventh oxygen, O(9), at a rather large distance of 2.895 Å. Similar Ca-O distances are reported by Peacor and Buerger (1962) for bustamite, such as  $Ca_1-O_9 = 2.899$  Å and  $Ca_2-O_9 = 2.891$  Å.

The Si atoms are tetrahedrally coordinated. The deviations from the ideal tetrahedral angle =  $109^{\circ}28'$  are considerable, the values varying between  $96^{\circ}10'$  and  $129^{\circ}30'$ . Prewitt and Buerger (1963) reported three nonequivalent Si-O-Si angles in wollastonite as well as in bustamite. The corresponding angles for parawollastonite lie between those for wollastonite and bustamite:

bustamite	$161^{\circ}$ , $135^{\circ}$ , $137^{\circ}$
parawollastonite	$152^{\circ}$ , $135^{\circ}$ , $137^{\circ}$
wollastonite	$149^{\circ}$ , $139^{\circ}$ , $137^{\circ}$

Table 4. Positional Coordinate for Parawollastonite

Atom	$\underline{x}$	$\sigma(\underline{x})$	$\underline{y}$	$\sigma(\underline{y})$	$\underline{z}$	$\sigma(\underline{z})$
Ca(1)	0.2482	0.0001	0.3758	0.0004	0.9712	0.0002
Ca(2)	0.4011	0.0001	0.6265	0.0006	0.7397	0.0002
Ca(3)	0.3987	0.0001	0.1209	0.0006	0.7364	0.0002
Si(1)	0.4076	0.0001	0.0907	0.0003	0.2313	0.0003
Si(2)	0.4075	0.0001	0.6598	0.0003	0.2313	0.0003
Si(3)	0.3016	0.0001	0.3761	0.0004	0.4432	0.0002
O(1)	0.3000	0.0003	0.3747	0.0013	0.6685	0.0006
O(2)	0.2156	0.0003	0.3759	0.0013	0.3031	0.0007
O(3)	0.3490	0.0004	0.1397	0.0014	0.0328	0.0007
O(4)	0.3473	0.0003	0.6157	0.0015	0.0348	0.0007
O(5)	0.5086	0.0003	0.1226	0.0020	0.2388	0.0007
O(6)	0.5078	0.0003	0.6176	0.0019	0.2347	0.0007
O(7)	0.3642	0.0004	0.1962	0.0007	0.4060	0.0007
O(8)	0.3633	0.0004	0.5533	0.0008	0.4067	0.0008
O(9)	0.3906	0.0003	0.8755	0.0010	0.2767	0.0006

Table 5. Interatomic Distances in Parawollastonite. O(3') is Equivalent by Symmetry to O(3), and O(4') to O(4).

Atoms	distance	$\sigma$		distance	$\sigma$
Ca(1) -O(1)	2.214	0.005	Ca(2) -O(1)	2.494	0.008
Ca(1) -O(2)	2.356	0.005	Ca(2) -O(2)	2.598	0.008
Ca(1) -O(3)	2.392	0.008	Ca(2) -O(4)	2.174	0.005
Ca(1) -O(3')	2.445	0.009	Ca(2) -O(5)	2.318	0.013
Ca(1) -O(4)	2.396	0.009	Ca(2) -O(6)	2.290	0.005
Ca(1) -O(4')	2.407	0.009	Ca(2) -O(8)	2.537	0.006
<hr/> Average	2.368		<hr/> Average	2.402	
Ca(1) -O(9)	2.895				
Ca(3) -O(1)	2.475	0.008	Si(1) -O(3)	1.779	0.007
Ca(3) -O(2)	2.545	0.008	Si(1) -O(5)	1.580	0.006
Ca(3) -O(3)	2.168	0.005	Si(1) -O(7)	1.554	0.005
Ca(3) -O(5)	2.298	0.013	Si(1) -O(9)	1.622	0.007
Ca(3) -O(6)	2.415	0.012	<hr/> Average	1.634	
Ca(3) -O(7)	2.511	0.005			
<hr/> Average	2.402				
Si(2) -O(4)	1.788	0.006	Si(3) -O(1)	1.594	0.005
Si(2) -O(6)	1.577	0.006	Si(3) -O(2)	1.732	0.005
Si(2) -O(8)	1.558	0.006	Si(3) -O(7)	1.637	0.006
Si(2) -O(9)	1.626	0.006	Si(3) -O(8)	1.626	0.007
<hr/> Average	1.637		<hr/> Average	1.647	



Table 6. Bond Angles Between Atoms in Parawollastonite. O(3') is Equivalent by Symmetry to O(3), and O(4') to O(4)

Atoms	angle	Atoms	angle
O(1)-Ca(1)-O(2)	171°12'	O(4)-Ca(2)-O(8)	141°51'
O(3)-Ca(1)-O(4)	93°15'	O(1)-Ca(2)-O(2)	92°27'
O(3)-Ca(1)-O(4)	80°48'	O(1)-Ca(2)-O(6)	80°47'
O(3')-Ca(1)-O(4)	80°01'	O(2)-Ca(2)-O(5)	82°59'
O(3)-Ca(1)-O(4')	104°21'	O(5)-Ca(2)-O(6)	103°37'
O(3)-Ca(1)-O(2)	84°07'	O(1)-Ca(2)-O(4)	88°53'
O(3')-Ca(1)-O(2)	86°33'	O(2)-Ca(2)-O(4)	86°16'
O(4)-Ca(1)-O(2)	83°40'	O(5)-Ca(2)-O(4)	98°06'
O(4')-Ca(1)-O(2)	86°36'	O(6)-Ca(2)-O(4)	94°17'
O(3)-Ca(3)	143°20'	O(3)-Si(1)-O(5)	125°00'
O(1)-Ca(3)-O(2)	93°34'	O(3)-Si(1)-O(7)	108°30'
O(1)-Ca(3)-O(6)	78°47'	O(5)-Si(1)-O(7)	104°25'
O(2)-Ca(3)-O(5)	84°33'	O(3)-Si(1)-O(9)	105°31'
O(5)-Ca(3)-O(6)	103°03'	O(5)-Si(1)-O(9)	106°06'
O(1)-Ca(3)-O(3)	88°34'	O(7)-Si(1)-O(9)	105°59'
O(2)-Ca(3)-O(3)	88°13'		
O(5)-Ca(3)-O(3)	97°57'		
O(6)-Ca(3)-O(3)	91°25'		

Table 6. Continued.

Atoms	angle	Atoms	angle
		0(4)-Si(2)-0(6)	124°07'
		0(4)-Si(2)-0(6)	108°34'
		0(6)-Si(2)-0(8)	104°11'
0(2)-Si(3)-0(7)	112°17'	0(4)-Si(2)-0(9)	104°08'
0(2)-Si(3)-0(8)	112°13'	0(6)-Si(2)-0(9)	109°00'
0(7)-Si(3)-0(8)	107°11'	0(8)-Si(2)-0(9)	105°35'
0(2)-Si(3)-0(1)	129°30'		
0(7)-Si(3)-0(1)	96°39'	Si(1)-0(9)-Si(2)	151°48'
0(8)-Si(3)-0(1)	96°10'	Si(1)-0(7)-Si(3)	135°25'
		Si(2)-0(8)-Si(3)	136°32'

Fig. 1. Projection of the structure of parawollastonite along  $c$ . The double circles are Ca atoms, the full circles  $\bar{Si}$  atoms, and the single circles O atoms.

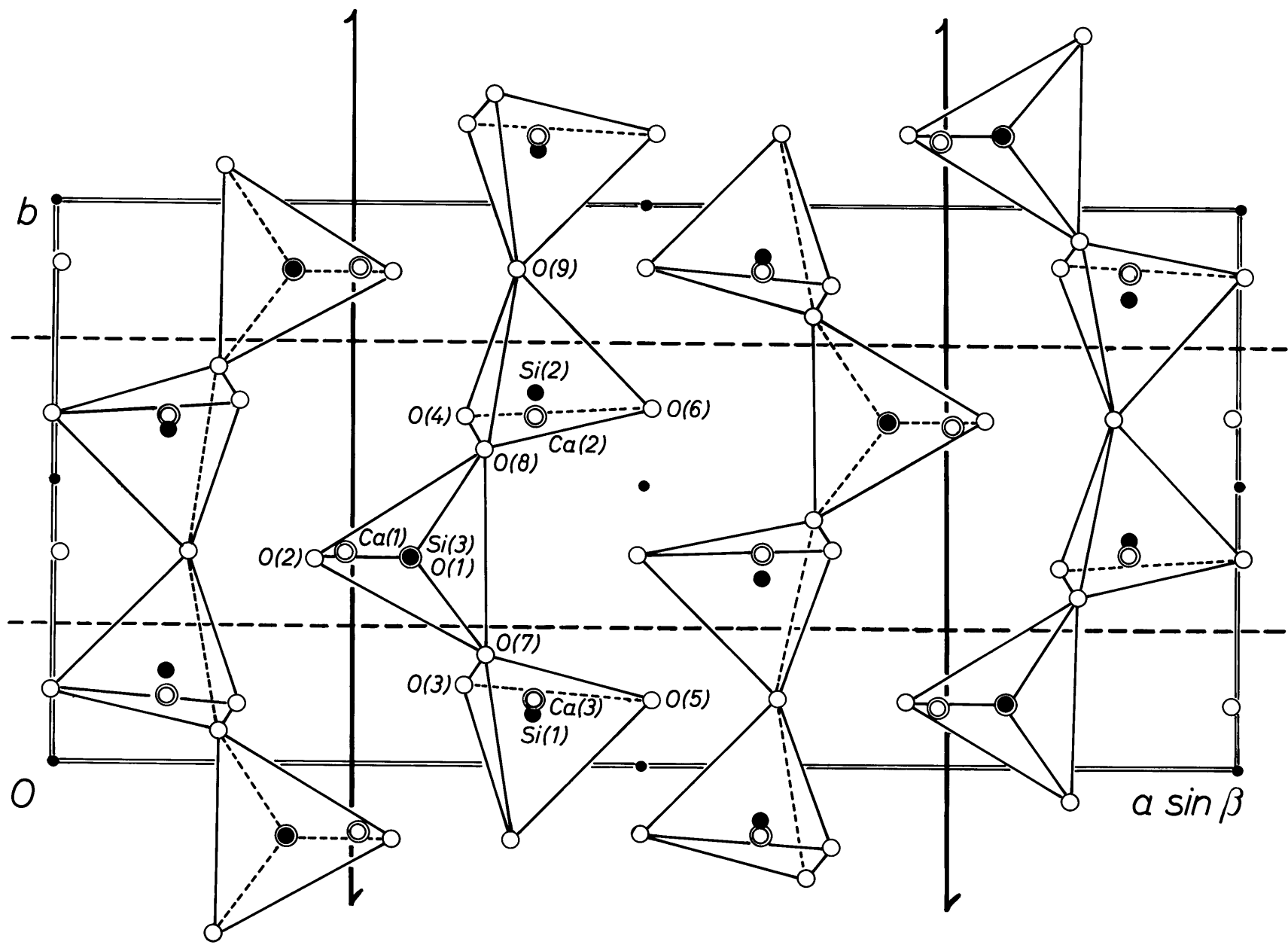


Table 7. Anisotropic Temperature Coefficients  
for Parawollastonite.

Atom	$\beta_{11}$	$\beta_{22}$	$\beta_{33}$	$\beta_{12}$	$\beta_{13}$	$\beta_{23}$
Ca(1) $\sigma$	0.00078 0.00006	0.00337 0.00030	0.00157 0.00029	-0.00001 0.00012	0.00009 0.00009	0.00013 0.00033
Ca(2) $\sigma$	0.00082 0.00007	0.00283 0.00029	0.00335 0.00031	-0.00004 0.00032	0.00003 0.00010	-0.00092 0.00078
Ca(3) $\sigma$	0.00091 0.00007	0.00265 0.00029	0.000336 0.00031	0.00034 0.00032	0.00009 0.00010	0.00024 0.00079
Si(1) $\sigma$	0.00070 0.00010	0.00076 0.00071	0.00257 0.00045	0.00006 0.00016	-0.00013 0.00016	-0.00008 0.00033
Si(2) $\sigma$	0.00072 0.00011	0.00152 0.00073	0.00248 0.00045	-0.00005 0.00016	-0.00010 0.00016	0.00004 0.00032
Si(3) $\sigma$	0.00030 0.00008	0.00368 0.00040	0.00209 0.00040	-0.00003 0.00021	0.00006 0.00013	0.00017 0.00044
O(1) $\sigma$	0.00059 0.00024	0.00428 0.00109	0.00015 0.00010	-0.00017 0.00067	0.00026 0.00034	0.00011 0.00137
O(2) $\sigma$	0.00101 0.00025	0.00422 0.00110	0.00144 0.00095	-0.00007 0.00072	0.00071 0.00031	0.00034 0.00156
O(3) $\sigma$	0.00143 0.00028	0.00143 0.00028	0.00101 0.00112	0.00024 0.00074	-0.00047 0.00041	-0.00053 0.00156
O(4) $\sigma$	0.00126 0.00028	0.00456 0.0017	0.00159 0.00113	0.00007 0.00082	-0.00058 0.00040	-0.00056 0.00173
O(5) $\sigma$	0.00091 0.00027	0.00335 0.00113	0.00720 0.00120	0.00158 0.00104	0.00023 0.00043	-0.00012 0.00241
O(6) $\sigma$	0.00073 0.00026	0.00258 0.00109	0.00698 0.00119	0.00082 0.00100	0.00004 0.00041	0.00126 0.00232
O(7) $\sigma$	0.00141 0.00027	0.00199 0.00111	0.00057 0.00050	0.00082 0.00040	-0.00058 0.00041	0.00001 0.00075
O(8) $\sigma$	0.00114 0.00033	0.00239 0.00116	0.00122 0.00117	-0.00060 0.00045	-0.00050 0.00049	0.00020 0.00089
O(9) $\sigma$	0.00077 0.00025	0.00215 0.00109	0.00362 0.00108	-0.00005 0.00054	0.00095 0.00038	0.00033 0.00114

Table 8, Thermal Parameters for Parawollastonite.

The dimensions are:  $\underline{q}$  in  $\text{\AA}$ ,  $\underline{B}_i$  and  $\underline{B}$  in  $\text{\AA}^2$ .

Atom	$\underline{q}_1$	$\underline{B}_1$	$\underline{q}_2$	$\underline{B}_2$	$\underline{q}_3$	$\underline{B}_3$	Equivalent isotropic $\underline{B}$
Ca(1)	0.097	0.75	0.096	0.72	0.063	0.31	0.63
$\sigma$	0.004	0.06	0.004	0.06	0.006	0.06	0.03
Ca(2)	0.102	0.81	0.082	0.52	0.095	0.71	0.71
$\sigma$	0.004	0.06	0.006	0.08	0.005	0.08	0.04
Ca(3)	0.106	0.89	0.083	0.54	0.092	0.67	0.70
$\sigma$	0.004	0.07	0.006	0.07	0.005	0.07	0.04
Si(1)	0.094	0.70	0.045	0.16	0.078	0.48	0.41
$\sigma$	0.006	0.09	0.021	0.15	0.006	0.08	0.06
Si(2)	0.095	0.72	0.064	0.33	0.077	0.47	0.51
$\sigma$	0.006	0.09	0.015	0.16	0.007	0.08	0.07
Si(3)	0.060	0.28	0.100	0.79	0.073	0.42	0.49
$\sigma$	0.008	0.08	0.005	0.09	0.007	0.08	0.05
O(1)	0.084	0.55	0.108	0.92	0.018	0.02	0.49
$\sigma$	0.017	0.23	0.014	0.23	0.072	0.20	0.12
O(2)	0.110	0.96	0.107	0.90	0.058	0.26	0.71
$\sigma$	0.103	0.23	0.014	0.23	0.020	0.18	0.12
O(3)	0.133	1.40	0.104	0.86	0.048	0.19	0.82
$\sigma$	0.012	0.26	0.016	0.26	0.028	0.22	0.14
O(4)	0.126	1.25	0.111	0.98	0.060	0.28	0.79
$\sigma$	0.013	0.25	0.014	0.25	0.023	0.21	0.14
O(5)	0.120	1.14	0.073	0.42	0.136	1.45	1.00
$\sigma$	0.016	0.31	0.020	0.23	0.011	0.23	0.15
O(6)	0.101	0.81	0.072	0.41	0.134	1.42	0.88
$\sigma$	0.017	0.28	0.021	0.24	0.011	0.24	0.15
O(7)	0.134	1.41	0.071	0.39	0.035	0.10	0.63
$\sigma$	0.012	0.25	0.020	0.23	0.036	0.10	0.13
O(8)	0.121	1.16	0.078	0.48	0.042	0.14	0.59
$\sigma$	0.015	0.29	0.019	0.24	0.038	0.25	0.15
O(9)	0.086	0.58	0.075	0.45	0.104	0.85	0.63
$\sigma$	0.011	0.15	0.018	0.22	0.010	0.16	0.10

The interatomic distances within the  $\text{SiO}_4$  tetrahedra can be separated into two groups: (a) oxygens coordinated by 1 Si and 3 Ca, with an average Si-O distance of 1.723 Å; (b) oxygens coordinated 1 Si and 2 Ca or by Si and 1 Ca, with an average Si-O distance of 1.576 Å. It can be seen that the Si-O distances are considerably larger if the oxygen atoms are coordinated by three Ca. A similar classification was found for wollastonite by Prewitt and Buerger (1963).

The anisotropic temperature coefficients for parawollastonite are found in Table 7. The orientations of the thermal vibration, ellipsoids expressed by the  $\beta_{12}$ ,  $\beta_{13}$ ,  $\beta_{23}$  values, are not well refined. In order to improve these parameters a larger number of observed reflections would be necessary. The thermal parameters are listed in Table 8. The  $q_i$ 's ( $i = 1$  to 3) are the three principal axes of the vibration ellipsoid. A temperature factor  $\underline{B}$  corresponds to each principal axis. The last column in Table 8 lists the average  $\underline{B}$  computed by  $\underline{B} = (\underline{B}_1 + \underline{B}_2 + \underline{B}_3)/3$  which is substantially the usual isotropic temperature factor. The values for parawollastonite are comparable with those for wollastonite published by Buerger and Prewitt (1961).

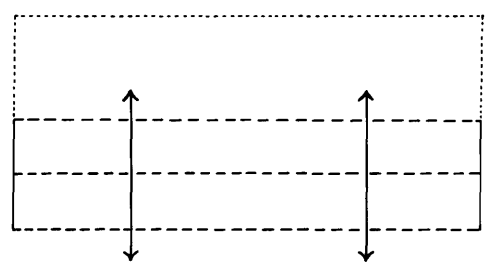
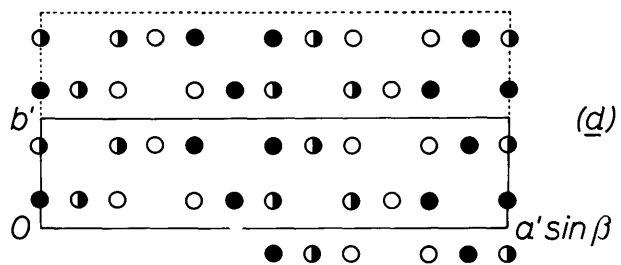
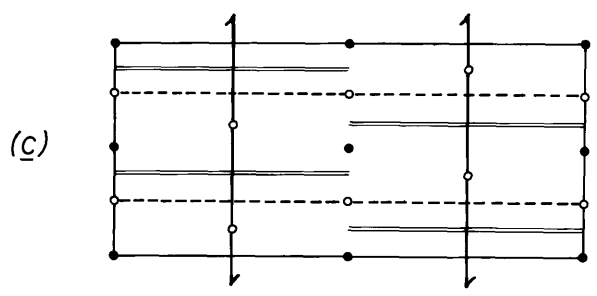
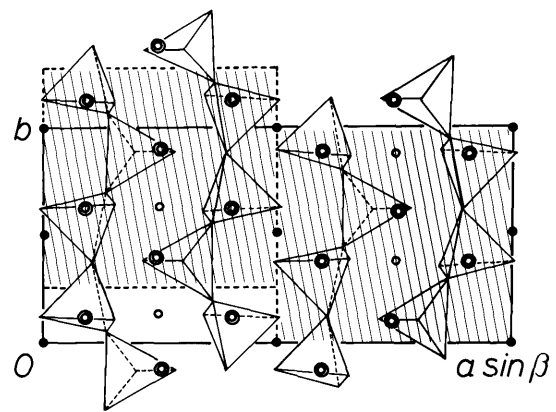
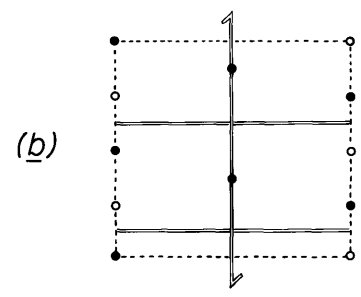
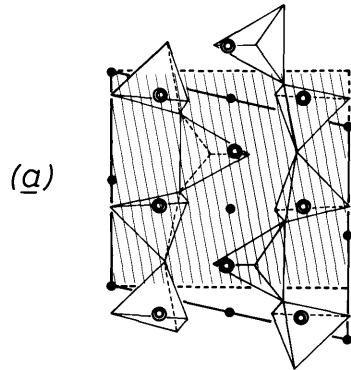
### Pseudosymmetry and Substructure

A close examination of the pseudomonoclinic unit, Fig. 2a reveals that, in addition to the inversion centers which are a remnant of the symmetry of triclinic wollastonite, a set of pseudosymmetry elements is also present. Figure 2b illustrates the following symmetry elements in this pseudomonoclinic unit: inversion centers, pseudomirror planes, and a pseudo  $2_1$  axis. There are also pseudoinversion centers which are generated by the combination of a true inversion center and a pseudomirror plane. All these pseudosymmetry elements mentioned above are only approximately obeyed by the atomic configuration. Figure 2c shows that certain symmetry elements become pseudosymmetry elements, and vice versa, when those units are stacked together to form the parawollastonite structure. The pseudo  $2_1$  axis changes to a true  $2_1$  axis. The combination of the true  $2_1$  axis with a true inversion center gives rise to a glide plane. The former true centers of symmetry on the pseudo  $2_1$  axis become pseudoinversion centers.

This pseudosymmetry suggests that parawollastonite might have a substructure. If small changes in the coordinates of some atoms are introduced in the actual parawollastonite structure an idealized **structure** results which has a distinct substructure. The necessary shifts do not exceed 0.08 of the  $\underline{x}$ ,  $\underline{y}$ , or  $\underline{z}$  coordinates. As seen from Fig. 3, this idealized structure is remarkably close to the actual structure of parawollastonite. Figure 3a shows that the Ca and Si atoms each conform to a substructure which consists of a simple lattice array. Both sets of atoms have very similar  $\underline{x}$  and  $\underline{y}$  coordinates. In respect to the Ca network, the Si atoms are shifted up along the  $\underline{c}$  direction by the amount  $\underline{z} = \frac{1}{2}$ . With the exception of O(7), O(8), and



- Fig. 2. Symmetry in parawollastonite. The pseudomonoclinic units are shaded. Double circles are Ca atoms. Small solid circles are real centers of symmetry, small open circles are pseudocenters. The pseudomirrors and psuedo screw axis are represented by thin double lines.
- (a) Pseudomonoclinic unit.
  - (b) Symmetry in the pseudomonoclinic unit.
  - (c) True and pseudosymmetry in parawollastonite.
  - (d) Symmetry of the subcell as illustrated by the atoms of the substructure.

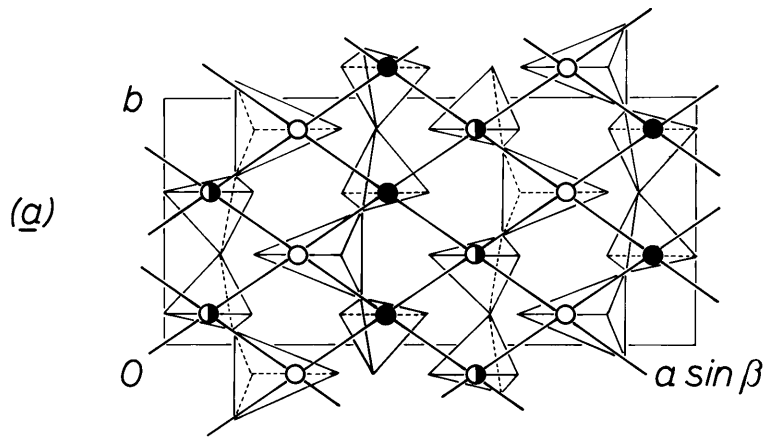


Atoms of the substructure at  
 $z=0$   $z=1/4$   $z=3/4$   
 ○ ● ●

Fig. 3. Projection along  $\underline{c}$  of the idealized parawollastonite structure.

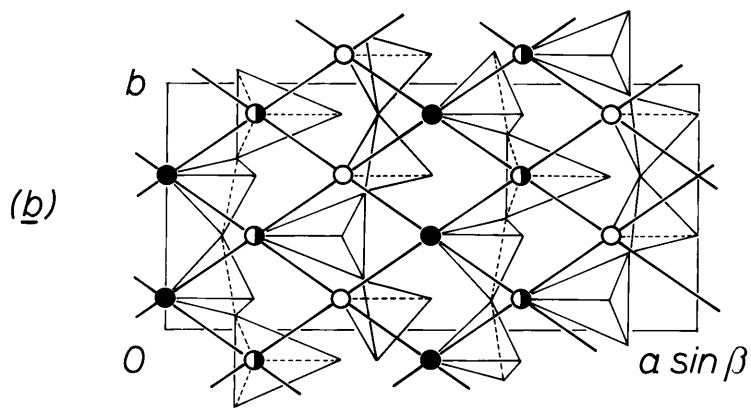
(a) Substructure based on Ca and Si atoms.

(b) and (c) Two substructures based on O atoms.



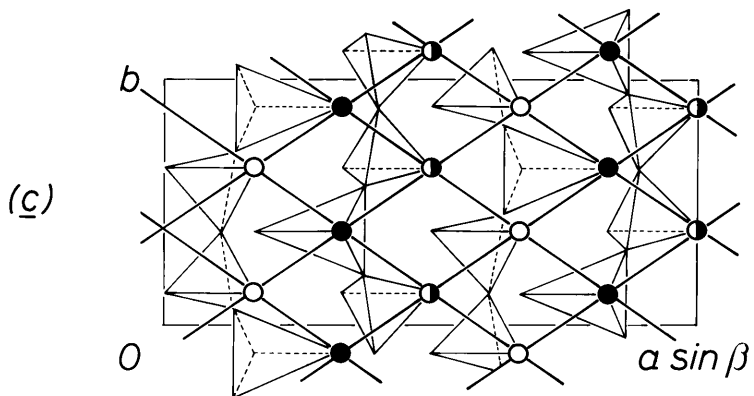
Representing both

- Ca at  $z=0$  and  
Si at  $z=0+1/2=1/2$
- Ca at  $z=1/4$  and  
Si at  $z=1/4+1/2=3/4$
- Ca at  $z=3/4$  and  
Si at  $z=3/4+1/2=1/4$



Oxygen atoms at

- $z=0$
- $z=1/4$
- $z=3/4$



0(9), all oxygens are located on one of two lattice arrays which are between the lattice arrays of the Ca and Si. Figure 2d shows how a  $\underline{C}$ -centered subcell, which is half the volume of the true cell of parawollastonite, is outlined by the positions of the atoms of the substructure. Since the Ca and the Si atoms and the majority of the oxygen atoms conform to this substructure it has a dominant effect on the diffraction pattern. The space group of the subcell is  $\underline{C}2/\underline{a}$ . The glide plane coincides with a glide in  $\underline{P}2_1/\underline{a}$ ; hence no additional absences due to the glide plane are to be expected. The  $\underline{C}$  centering, however, necessitates additional systematic absences of the type  $\underline{h}' + \underline{k}' = 2\underline{n} + 1$ , where  $\underline{h}'$  and  $\underline{k}'$  are indices referred to the subcell. These indices transform to those for the true cell as follows:

$$\underline{h}' = \underline{h}$$

$$\underline{k}' = \underline{k}/2$$

$$\underline{l}' = \underline{l}$$

The same extinction law, expressed in indices referred to the true cell, is  $\underline{h} + \underline{k}/2 = 2\underline{n} + 1$ ; this implies  $2\underline{h} + \underline{k} = 4\underline{n} + 2$ . Since the  $\underline{C}$ -centered subcell is based on an idealized structure, this extinction law is only approximately obeyed, so that reflections with the index combination  $2\underline{h} + \underline{k} = 4\underline{n} + 2$  are not actually absent but have very weak intensities. A sample of those "extinguished reflections" listed on Table 3 indicates clearly that small but measurable intensities have been observed, ruling out the possibility of systematic absences.

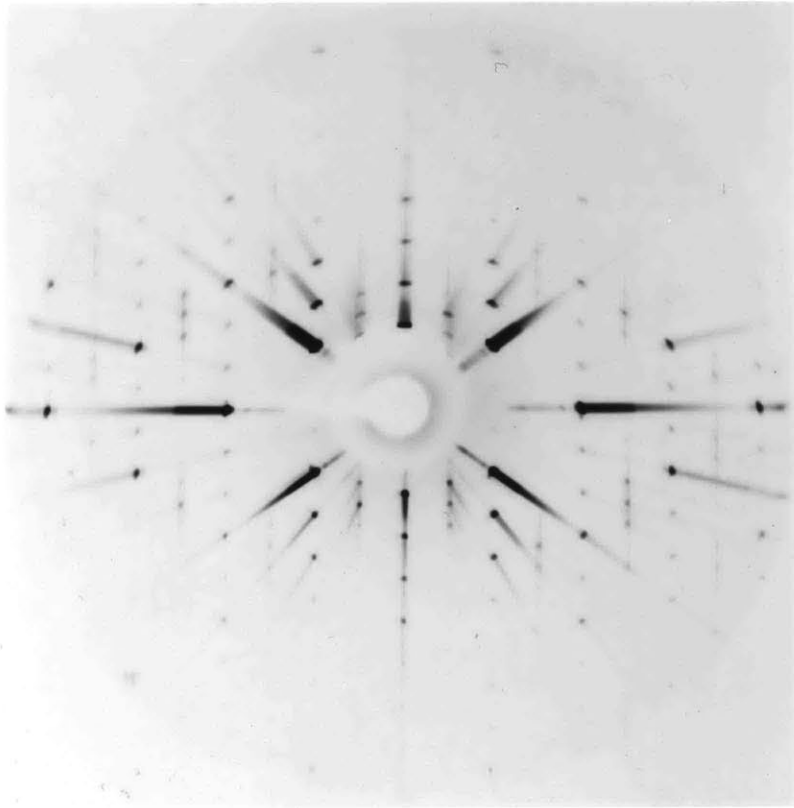
### Disorder in Parawollastonite

Jeffery (1953) investigated wollastonite from Devon, Cornwall. The crystals he used were fibrous and cleaved excessively easily parallel to the direction of the fiber. Weissenberg photographs of odd layers of the index  $k$  made with this material showed disorder streaks along  $a^*$ . Based on this diffraction effect Jeffery concluded that the arrangement of the atoms must be undisturbed parallel the plane (100). He explained the occurrence of streaks only at odd levels of index  $k$  by a relative displacement of neighboring cells by the amount  $b/2$  parallel to (100). Stimulated by these findings, Willis (1958) made an extensive study of diffraction effects caused by stacking faults in wollastonite crystals. In order to produce diffraction patterns of various degrees of disorder he used an optical diffractometer and gratings simulating the structure of wollastonite at several stages of disorder. Willis published optical diffraction patterns of four models, each of them having a different probability of occurrence of displacements. The probability that a given layer or cell is faulted is usually called the faulting parameter  $\alpha$ . It reflects the faulting density in a given specimen. This parameter is normalized so that its limits are 0 and 1; 0 means no stacking fault and 1 represents a structure where each layer is shifted.

Since parawollastonite has a structure closely related to the one for wollastonite, it was natural to assume that similar diffraction effects caused by disorder exist in parawollastonite. In order to check this assumption a fibrous specimen of wollastonite with excellent cleavage was examined. The material originated from Žulova, Moravia in ČSR and was kindly made available by Professor Clifford Frondel, Harvard University. Fig. 4 shows a precession

Fig. 4. Precession photograph showing (hk0) of a disordered parawollastonite from Žulova, Moravia in ČSR.

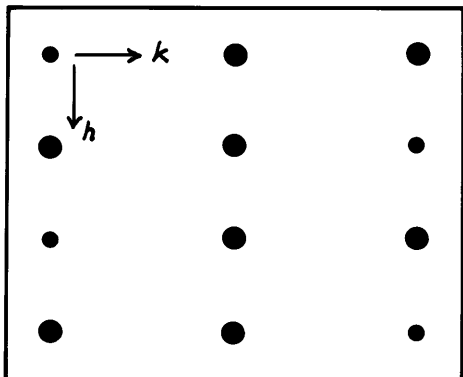
*h*



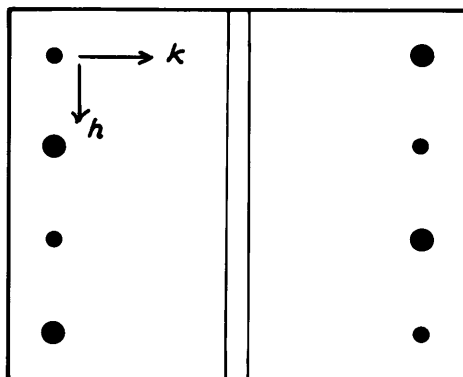
*k*



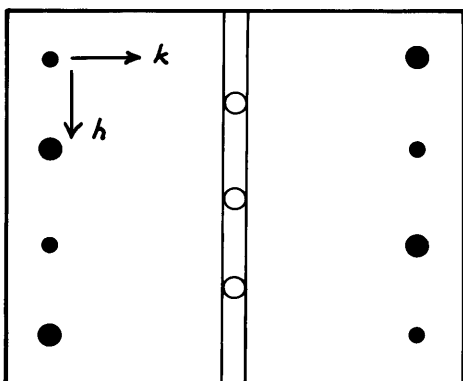
- Fig. 5. Schematic picture of diffraction patterns representing various stages of disorder in parawollastonite. The full circles are reflections not effected by disorder ( $k$  even); the empty circles are diffuse reflections effected by disorder ( $k$  odd). The diameter of the circles symbolizes the relative intensity of the reflections. The double line presents a continuous radiation streak.  $\alpha$  is the faulting parameter.
- a     $\alpha = 0$ , no disorder.
- b     $\alpha = 0.5$ .
- c    Schematic diffraction pattern of disordered parawollastonite from Žulova showing diffuse reflections and continuous radiation streaks.
- d     $\alpha = 0.8$ .



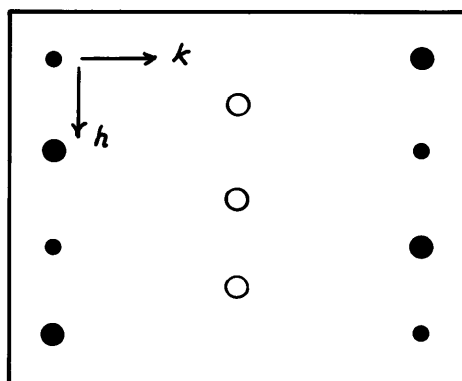
(a)  $d = 0.0$



(b)  $d = 0.5$



(c)



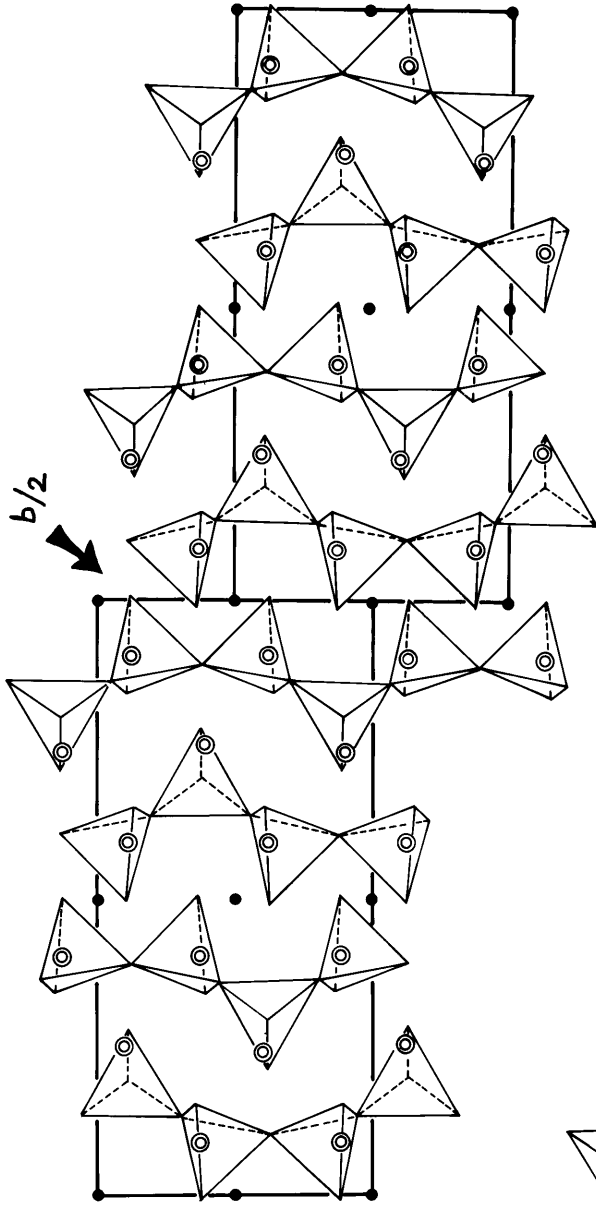
(d)  $d = 0.8$

photograph of the type  $hk0$  having disorder streaks as well as diffuse diffraction spots parallel  $a^*$  at odd levels of index  $k$ . The state of disorder observed in this specimen can be evaluated by a comparison with the optical diffraction patterns made by Willis. Figures 5a, 5b, and 5d show schematically three optical diffraction patterns like the ones published by Willis but adapted to the smaller reciprocal cell of parawollastonite. Fig. 5a represents the diffraction pattern as it is obtained by a completely ordered arrangement of cells in a crystal of parawollastonite. Fig. 5b illustrates the case where the chance of finding the next cell to be displaced is 50%. Fig. 5c is analogous to the precession photograph seen in Fig. 4 of the disordered parawollastonite from Žulova. Fig. 5d represents a diffraction pattern of parawollastonite having a faulting density of  $\alpha = 0.8$ . When the precession photograph of Fig. 4, which is also schematically illustrated in Fig. 5c, is analyzed the following important features can be seen: continuous radiation streaks between several lattice points within a lattice row parallel  $a^*$  and at levels with index  $k$  odd; diffuse reflections located on these streaks, but these diffuse spots are no longer at the positions of the lattice points in a completely ordered crystal, they are located half way between the lattice points of an ordered parawollastonite crystal. Comparing the diffraction pattern of this disordered parawollastonite from Žulova with Figures 5b and 5d, it is readily seen that this sample can be classed somewhere between  $\alpha = 0.5$  and  $\alpha = 0.8$ . This means that the probability of finding a stacking fault after each cell is quite high, possibly in the neighborhood of 70%.

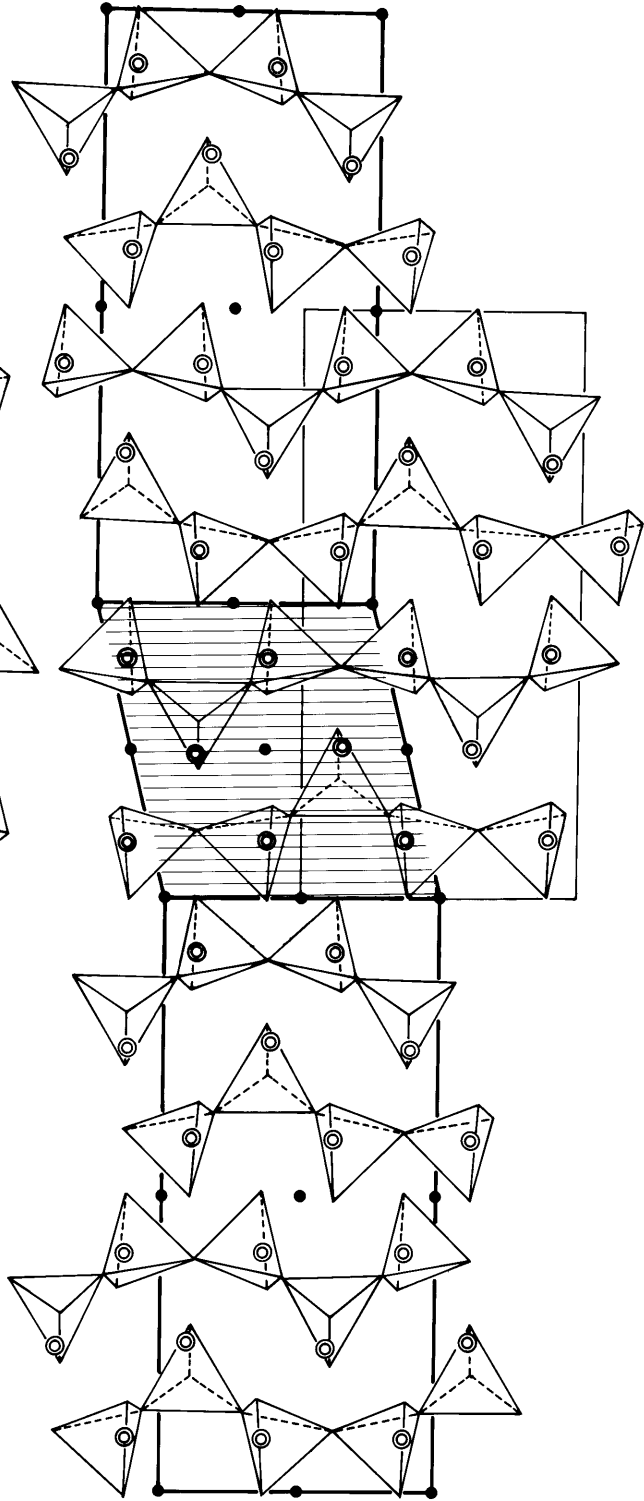
Figure 6 tries to give a structural explanation of the displacements as they occur in disordered parawollastonite. Disorder in parawollastonite can

- Fig. 6. Two interpretations of disorder in parawollastonite.  
The cell of wollastonite is shaded.
- (a) Cells of parawollastonite are displaced in respect to each other by the amount  $\underline{b}/2$  .
  - (b) Intergrowth of parawollastonite giving rise to an almost identical type of disorder as given in the figure above.

(a)



(b)



be interpreted in two ways: first, cells of parawollastonite are displaced in respect to each other by the amount  $b/2$  along (100); second, an intergrowth of wollastonite and parawollastonite occurs parallel to (100). Looking at Fig. 6b, it is evident that this type of intergrowth produces an almost identical situation as is obtained by the displacement illustrated above. A close examination, however, shows that the cell of parawollastonite which appears to be shifted down in Fig. 6b has a set of inversion centers which does not correspond to this cell and its space group symmetry. Nevertheless these centers of symmetry are present in parawollastonite as a set of pseudoinversion centers, a feature discussed in the previous section. The presence of pseudosymmetry means that the arrangement of the atoms differs very little no matter which of the two disorder mechanisms is acting. Thus it seems likely that both types of stacking faults can occur within the same crystal. Jeffery (1953) mentioned that the energy difference between the triclinic and monoclinic forms of wollastonite is so small that it is difficult to ascertain which of the two phases is the low temperature form. Hence if the temperature is close to the inversion point, it is quite feasible that faults occur during growth and that a crystal is formed composed of alternating layers of wollastonite and parawollastonite. This proposal is supported by morphological evidence found by Peacock (1935) on two crystals from Monte Somma, Italy. These specimens were composites of wollastonite and parawollastonite intergrown along the (100) face.

Due to the very strong resemblance in the atomic positions obtained with the two proposed types of stacking faults the difference in the effect on the x-ray diffraction pattern is probably so small that it is impossible to

distinguish a disorder caused by a composite crystal with alternating cells of wollastonite and parawollastonite from a crystal with cells of parawollastonite shifted parallel (100) by the amount  $b/2$ .

Table 9. Observed and Calculated Structure Factors of Parawollastonite.

h	k	l	F <sub>o</sub>	F <sub>c</sub>	h	k	l	F <sub>o</sub>	F <sub>c</sub>	h	k	l	F <sub>o</sub>	F <sub>c</sub>	h	k	l	F <sub>o</sub>	F <sub>c</sub>
5	0	0	0	0.0	10	1	0	-4.9	-3.9	15	1	3	11.9	12.7	6	1	7	-17.8	-14.2
6	0	0	-110.0	-119.6	11	1	0	3.2	5.3	0	1	-4	-56.4	-54.2	6	1	-7	-19.5	19.6
7	0	0	0	0.0	12	1	0	3.9	7.7	0	1	4	56.6	54.2	7	1	7	13.2	13.1
8	0	0	109.0	111.9	13	1	0	-18.4	-17.1	1	1	-4	29.8	27.5	7	1	-7	-22.4	-23.2
9	0	0	0	0.0	14	1	0	-42.6	-41.0	1	1	4	-70.7	-66.5	8	1	7	20.1	21.1
10	0	0	153.0	142.1	15	1	0	39.2	38.6	2	1	-4	14.0	13.6	8	1	-7	-25.8	-25.5
11	0	0	0	0.0	0	1	-1	-20.5	-18.2	2	1	4	-70.4	-65.6	9	1	-7	25.9	25.7
13	0	0	0	0.0	0	1	1	21.0	18.2	3	1	-4	-15.7	-14.3	9	1	7	-36.9	-38.0
14	0	0	-53.2	-50.4	1	1	-1	-14.4	-10.1	3	1	4	47.8	44.6	10	1	-7	21.9	21.9
15	0	0	0	0.0	1	1	1	-27.1	-24.1	4	1	-4	-21.6	-19.3	11	1	-7	-16.6	-17.7
2	0	-1	-28.5	-22.6	2	1	-1	-51.7	-43.1	4	1	4	7.9	6.6	12	1	-7	-11.9	-14.1
2	0	1	-20.4	-23.3	2	1	1	-22.7	-20.8	5	1	-4	25.4	22.0	2	2	0	0	2.7
4	0	-1	59.7	57.4	3	1	-1	72.0	63.4	5	1	4	7.5	5.1	3	2	0	-317.3	-306.8
4	0	1	49.8	50.4	3	1	1	11.6	10.4	6	1	-4	14.5	13.1	4	2	0	2.3	3.9
6	0	-1	-14.2	-9.6	4	1	-1	38.8	52.3	6	1	4	1.7	2.2	5	2	0	119.8	119.2
6	0	1	-82.4	-84.5	4	1	1	17.0	16.1	7	1	-4	-1.5	-1.5	6	2	0	4.5	0.6
8	0	-1	33.5	30.5	5	1	-1	-21.8	-18.4	8	1	4	3.5	3.3	7	2	0	114.5	112.8
8	0	1	95.9	96.6	5	1	1	-17.9	-16.7	8	1	-4	14.2	13.6	8	2	0	12.4	2.8
10	0	-1	-37.8	-36.6	6	1	-1	1.8	0.3	8	1	4	19.2	19.1	9	2	0	67.8	66.4
12	0	-1	123.6	131.0	6	1	1	-42.8	-41.0	9	1	-4	-15.8	-16.4	10	2	0	6.6	3.4
14	0	1	-41.8	-39.8	7	1	-1	8.0	-7.6	9	1	4	-16.7	-16.0	11	2	0	10.6	8.0
0	0	-2	-159.4	-160.7	7	1	1	40.6	38.2	10	1	-4	-9.4	-9.6	12	2	0	3.4	1.5
0	0	2	-159.4	-160.7	8	1	-1	0	-0.5	11	1	-4	6.6	6.3	13	2	0	-69.8	-68.4
2	0	2	-205.6	-193.6	8	1	1	24.6	23.9	12	1	-4	-7.4	-1.2	14	2	0	6.8	0.2
4	0	-2	104.5	106.8	9	1	-1	-18.6	-16.1	12	1	4	-8.6	-9.1	15	2	0	-61.8	-60.4
4	0	2	119.5	129.2	9	1	1	0	2.3	13	1	4	1.8	2.5	0	2	-1	-2.7	-1.1
6	0	-2	99.3	99.6	10	1	-1	-11.7	-9.7	13	1	-4	3.8	5.1	0	2	1	-2.6	-1.1
8	0	-2	24.5	20.7	10	1	1	7.4	5.7	14	1	4	-25.3	-23.3	1	2	-1	-49.5	-39.1
8	0	2	-49.6	-50.5	11	1	-1	-7.0	-6.9	14	1	-4	6.5	8.3	1	2	1	4.9	3.0
12	0	2	-34.2	-33.9	11	1	1	4.4	3.1	15	1	-4	-15.8	-17.0	2	2	-1	3.4	3.0
12	0	-2	-49.2	-47.3	12	1	-1	-23.4	-22.4	15	1	4	26.8	24.7	2	2	1	-2.9	-1.4
14	0	-2	6.2	-1.3	12	1	1	1.3	1.3	0	1	-5	-5.2	-4.3	3	2	-1	-72.9	-67.5
14	0	2	75.4	74.2	13	1	-1	39.8	38.9	0	1	5	5.7	4.3	3	2	1	13.5	13.6
0	0	-3	122.2	114.4	13	1	1	-10.9	-9.1	1	1	-5	12.4	13.4	4	2	-1	0	2.7
0	0	3	123.5	114.4	14	1	-1	39.7	37.9	2	1	-5	8.4	10.2	4	2	1	0	1.2
2	0	-3	-204.3	-207.7	14	1	1	-3.5	-1.8	2	1	5	14.3	13.0	5	2	-1	-57.6	-50.4
2	0	3	29.8	25.4	15	1	-1	-24.2	-24.2	3	1	-5	-8.2	-9.2	6	2	-1	0	-3.6
4	0	-3	64.7	59.9	15	1	1	-16.1	-16.1	3	1	5	-19.9	-17.0	6	2	1	0	0.5
4	0	3	-51.1	-46.9	0	1	-2	-44.7	-40.1	4	1	-5	-16.0	-16.5	7	2	-1	-111.3	-109.7
6	0	-3	-16.6	-16.0	0	1	2	45.3	40.1	4	1	5	-3.6	-2.6	7	2	1	-67.7	-64.2
6	0	3	-42.7	-39.8	1	1	-2	85.8	75.0	5	1	-5	28.9	27.5	9	2	-1	96.3	98.1
8	0	-3	47.0	49.4	1	1	2	-4.2	-3.2	5	1	5	-25.6	-26.0	9	2	1	59.8	55.2
8	0	3	54.3	54.4	2	1	-2	87.9	79.3	6	1	-5	37.0	36.7	10	2	1	0	0.2
10	0	-3	-96.6	-98.7	2	1	2	23.5	20.4	6	1	5	-37.5	-37.7	11	2	-1	-39.2	-39.4
10	0	3	0	-2.2	3	1	-2	-61.7	-55.2	7	1	-5	-42.6	-43.3	11	2	1	-60.6	-58.0
12	0	-3	-12.4	-10.9	3	1	2	-21.1	-17.7	7	1	5	48.3	48.2	12	2	-1	3.7	1.6
12	0	3	35.0	33.8	4	1	-2	-20.1	-19.1	8	1	-5	-40.7	-43.5	12	2	1	0	0.2
2	0	-4	121.9	119.4	4	1	2	8.3	9.9	8	1	5	40.5	40.8	13	2	-1	-19.6	-21.3
2	0	4	-39.8	-36.9	5	1	-2	-14.4	-14.9	9	1	-5	-40.8	-43.5	13	2	1	101.3	102.1
4	0	-4	-69.5	-68.2	5	1	2	8.2	8.9	9	1	5	-19.4	-19.5	14	2	-1	-3.4	-1.2
4	0	4	-39.6	-37.8	6	1	-2	-8.2	-8.9	10	1	-5	-40.9	-42.8	14	2	1	-7.9	-1.0
6	0	-4	-99.5	-99.2	6	1	2	-5.9	-6.5	10	1	5	-21.0	-20.4	15	2	-1	-87.7	-83.9
6	0	4	-23.4	-18.5	7	1	-2	-26.4	-24.7	11	1	-5	25.9	25.0	15	2	1	7.5	7.4
8	0	-4	93.6	97.3	7	1	2	-2.9	-1.9	11	1	5	-40.7	-41.6	0	2	-2	-3.0	-5.2
10	0	-4	91.5	93.7	8	1	-2	-38.8	-36.5	12	1	5	26.0	25.2	0	2	2	-3.9	-5.2
12	0	-4	125.7	138.4	8	1	2	-19.0	-17.6	12	1	-5	-36.3	-35.7	10	2	-2	70.2	66.7
12	0	4	45.5	45.8	9	1	-2	30.9	30.3	13	1	5	-36.5	-36.1	2	2	2	0	-3.1
14	0	-4	-89.1	-89.3	9	1	2	14.5	12.9	13	1	-5	28.5	28.0	2	2	2	0	-3.6
14	0	4	-51.1	-49.3	10	1	-2	9.6	7.1	14	1	5	-29.8	-28.7	3	2	-2	81.3	76.4
0	0	-5	58.5	54.2	10	1	2	-2.9	-4.2	14	1	-5	20.2	18.0	3	2	2	81.9	82.4
0	0	5	57.9	54.2	11	1	-2	9.3	8.9	15	1	-5	-3.5	-4.5	4	2	-2	2.4	0.3
2	0	-5	-28.1	-25.1	11	1	2	10.2	8.9	0	1	-6	-39.8	-38.3	4	2	2	2.6	-1.4
6	0	-5	-33.7	-34.4	12	1	-2	18.3	17.2	0	1	6	39.6	38.3	5	2	-2	115.0	117.1
6	0	5	33.5	36.4	12	1	2	17.6	16.5	1	1	-6	45.5	44.0	5	2	2	65.0	65.9
8	0	-5	35.2	32.6	13	1	-2	-20.0	-19.8	1	1	6	-41.5	-40.2	6	2	-2	-1.9	-2.0
10	0	-5	-22.7	-23.0	13	1	2	-16.6	-15.7	2	1	-6	42.5	41.6	6	2	2	0	-2.4
10	0	5	-60.8	-58.9	14	1	-2	-5.9	-6.0	2	1	6	-36.0	-34.7	8	2	2	0	-3.8
12	0	-5	68.8	64.8	14	1	2	-5.3	-2.6	3	1	-6	-27.8	-28.2	9	2	2	-90.2	-88.7
12	0	5	11.3	8.3	15	1	2	9.8	8.6	3	1	6	39.1	39.0	10	2	2	0	-1.8
14	0	-5	-11.1	-9.1	15	1	-2	3.3	2.7	4	1	-6	-22.6	-23.6	11	2	2	-28.0	-27.1
0	0	-6	-117.5	-117.2	0	1	-3	34.3	29.4	4	1	6	49.2	49.0	11	2	-2	39.3	37.5
0	0	6	-114.7	-117.2	0	1	3	-34.4	-29.4	5	1	-6	16.0	17.2	12	2	2	0	-0.6
2	0	-6	-131.5	-136.6	1	1	-3	-28.0	-24.2	5	1	6	-38.2	-37.9	12	2	-2	-3.8	-1.1
2	0	6	1.7	1.9	1	1	3	15.6	12.1	6	1	-6	12.5	12.6	13	2	-2	121.3	126.2
4	0	-6	66.2	63.5	2	1	-3	11.1	10.1	6	1	6	-22.8	-22.9	13	2	2	109.4	108.2
6	0	-6	95.4	96.2	2	1	3	-12.7	-12.4	7	1	-6	-14.4	-13.5	15	2	-2	-16.7	-13.7
6	0	6	8.8	1.8	3	1	-3	-37.9	-34.2	7	1	6	12.1	12.8	0	2	-3	-1.7	-1.8
8	0	-6	14.5	11.0	3	1	3	48.6	44.5	8	1	6	-8.1	-6.4	0	2	3	-1.7	-1.8
8	0	6	-53.2	-52.6	4	1	-3	-43.3	-40.0	8	1	-6	-6.7	-6.4	1	2	-3	15.8	14.5
12	0	-6	-22.0	-22.8	4	1	3	55.9	52.1	9	1	-6	0	2.2	1	2	3	65.8	61.3
12	0	6	-20.5	-17.4	5	1	-3	-27.9	-26.3	9	1	6	4.6	3.9	2	2	-3	-2.6	-2.0
14	0	-6	-32.9	-32.7	5	1	3	-39.1	-36.9	10	1	6	-8.6	-9.8					



Table 9. Continued.

h	k	l	F <sub>o</sub>	F <sub>c</sub>	h	k	l	F <sub>o</sub>	F <sub>c</sub>	h	k	l	F <sub>o</sub>	F <sub>c</sub>	h	k	l	F <sub>o</sub>	F <sub>c</sub>
13	2	-3	48.1	47.6	8	2	7	- 1.1	- 1.9	10	3	-3	22.3	20.7	1	3	7	27.5	29.3
13	2	3	4.1	3.4	10	2	-7	- 0.8	- 0.4	10	3	3	- 28.6	- 28.5	2	3	-7	- 7.0	- 7.5
14	2	-3	0	- 1.1	11	2	-7	- 11.1	- 7.5	11	3	-3	25.7	25.6	2	3	7	- 20.1	- 22.6
14	2	3	0	- 1.1	2	3	0	1.8	1.4	11	3	3	- 24.5	- 24.4	3	3	-7	6.5	6.4
15	2	-3	25.9	28.9	3	3	0	- 8.7	- 6.9	12	3	-3	- 31.6	- 33.2	3	3	7	- 13.9	- 16.1
15	2	3	- 69.7	- 67.9	4	3	0	6.4	4.3	12	3	3	31.9	32.7	4	3	-7	- 30.9	- 31.9
0	2	-4	1.6	2.9	5	3	0	- 16.5	- 13.1	13	3	-3	- 13.7	- 14.3	4	3	7	2.2	4.2
0	2	4	1.4	2.9	6	3	0	42.8	38.5	13	3	3	17.8	18.1	5	3	-7	- 49.2	- 51.1
1	2	-4	- 5.0	- 1.8	7	3	0	61.9	57.8	14	3	-3	- 8.2	- 8.1	5	3	7	0.7	2.3
1	2	4	- 78.2	- 77.1	8	3	0	- 42.8	- 40.4	14	3	3	- 4.9	- 5.8	6	3	-7	46.0	46.9
2	2	-4	0	2.0	9	3	0	- 4.0	- 0.2	15	3	-3	- 13.2	- 13.3	6	3	7	- 17.3	- 18.0
2	2	4	0.9	0.8	10	3	0	- 35.1	- 32.6	15	3	3	5.6	4.3	7	3	-7	24.4	25.0
3	2	-4	- 104.8	- 102.0	11	3	0	- 59.5	- 57.2	0	3	-4	- 53.0	- 50.5	7	3	7	- 19.7	- 19.0
4	2	-4	0	0.3	12	3	0	47.9	45.7	0	3	4	51.8	50.5	8	3	-7	- 4.2	- 4.9
4	2	4	0	1.9	13	3	0	16.1	14.5	1	3	-4	- 65.4	- 61.4	9	3	-7	3.8	3.6
6	2	-4	0	- 0.4	14	3	0	- 4.9	- 3.4	1	3	4	19.7	18.3	10	3	-7	8.5	8.1
6	2	4	0	- 0.5	15	3	0	- 2.0	- 2.0	2	3	-4	57.8	54.0	2	4	0	31.5	28.2
7	2	-4	87.4	87.0	0	3	-1	- 6.3	- 3.2	2	3	4	- 3.8	- 4.0	3	4	0	- 2.0	- 3.8
7	2	4	48.5	44.4	0	3	1	6.6	3.2	3	3	-4	27.8	24.5	4	4	0	38.5	35.2
8	2	-4	0	2.7	1	3	-1	- 15.9	- 12.6	3	3	4	- 11.7	- 11.9	5	4	0	0	- 0.3
8	2	4	0	1.8	1	3	1	- 5.0	- 3.5	4	3	-4	1.3	2.5	6	4	0	98.0	97.8
9	2	-4	69.6	69.4	2	3	-1	14.6	13.2	4	3	4	29.6	28.3	7	4	0	1.5	1.4
10	2	-4	1.8	3.2	2	3	1	- 3.5	- 4.0	5	3	-4	4.1	5.0	8	4	0	- 55.8	- 52.7
10	2	4	2.7	2.3	3	3	-1	- 6.6	- 4.0	5	3	4	50.0	49.1	9	4	0	4.0	1.2
11	2	-4	- 8.6	- 10.2	3	3	1	- 11.5	- 12.3	6	3	-4	5.6	6.8	10	4	0	- 109.2	- 114.1
11	2	4	- 69.2	- 63.4	4	3	-1	43.3	38.7	6	3	4	- 41.4	- 41.3	11	4	0	- 1.9	- 2.6
12	2	-4	0	0.2	4	3	1	17.1	18.0	7	3	-4	14.2	14.0	12	4	0	- 60.4	- 59.6
12	2	4	0	1.1	5	3	-1	67.9	60.6	7	3	4	- 1.7	- 3.7	13	4	0	- 4.1	- 2.0
13	2	-4	- 43.5	- 39.2	5	3	1	19.7	19.0	8	3	-4	- 2.0	- 2.3	14	4	0	55.0	55.2
14	2	-4	0	- 1.1	6	3	-1	- 69.4	- 64.9	8	3	4	- 18.3	- 18.4	15	4	0	- 43.6	- 36.6
14	2	4	0	- 0.4	6	3	1	- 18.7	- 16.7	9	3	-4	17.8	18.0	0	4	-1	- 43.2	- 36.6
15	2	-4	- 91.1	- 90.9	7	3	-1	- 30.7	- 29.1	9	3	4	- 24.1	- 25.4	0	4	1	2.0	0.8
15	2	4	10.6	8.2	7	3	1	- 30.7	- 28.0	10	3	-4	- 26.5	- 26.7	1	4	-1	1.7	3.1
0	2	-5	- 0.7	- 0.3	8	3	-1	- 17.2	- 13.5	10	3	4	16.6	17.2	1	4	1	- 24.2	- 23.1
0	2	5	0	- 0.3	8	3	1	45.2	42.2	11	3	-4	- 20.5	- 20.7	2	4	-1	60.8	60.9
1	2	-5	- 13.8	- 12.0	9	3	-1	- 34.5	- 33.3	11	3	4	- 14.1	- 12.0	3	4	-1	- 0.6	- 3.5
1	2	5	- 16.3	- 19.1	9	3	1	32.9	30.7	12	3	-4	- 3.9	- 4.3	3	4	1	3.0	3.8
2	2	-5	0.9	2.2	10	3	-1	38.5	37.5	12	3	4	21.9	19.8	4	4	-1	- 25.6	- 25.7
2	2	5	0	- 0.7	10	3	1	- 16.8	- 16.0	13	3	-4	- 27.7	- 29.6	4	4	1	7.0	2.1
3	2	-5	- 82.2	- 80.8	11	3	-1	20.0	19.5	13	3	4	16.3	14.3	5	4	-1	- 1.4	- 7.9
3	2	5	15.5	12.3	11	3	1	4.8	5.9	14	3	-4	30.7	32.0	5	4	1	1.3	3.4
4	2	-5	1.7	2.7	12	3	-1	0	1.9	14	3	4	- 18.5	- 18.7	5	4	-1	31.2	31.8
4	2	5	0	1.4	12	3	1	- 31.4	- 31.4	15	3	-4	18.0	18.9	6	4	-1	25.9	21.4
5	2	-5	26.4	26.7	13	3	-1	0	- 2.1	0	3	-5	13.0	11.3	6	4	1	- 2.2	- 3.7
5	2	5	47.3	45.6	13	3	1	- 23.7	- 23.5	0	3	5	- 12.9	- 11.3	7	4	-1	0	2.1
6	2	-5	- 1.4	- 1.4	14	3	-1	16.5	17.8	1	3	-5	- 3.1	- 2.7	7	4	1	- 42.4	- 39.9
6	2	5	0	1.9	14	3	1	3.0	4.1	1	3	5	- 13.2	- 10.1	8	4	-1	- 98.3	- 99.1
7	2	-5	- 74.8	- 71.7	15	3	-1	- 27.1	- 27.3	2	3	-5	8.1	9.8	9	4	-1	4.8	2.4
7	2	5	37.5	40.0	15	3	1	- 9.8	- 8.4	2	3	5	- 7.7	- 9.8	9	4	1	3.3	3.5
8	2	-5	0	- 0.6	0	3	-2	11.2	8.9	3	3	-5	9.5	10.8	10	4	-1	54.7	52.7
8	2	5	2.1	0.8	0	3	2	- 10.7	- 8.9	3	3	5	- 19.2	- 20.9	10	4	1	108.8	111.0
9	2	-5	63.4	61.3	1	3	-2	21.0	19.3	4	3	-5	- 4.5	- 6.2	11	4	-1	0	- 3.9
9	2	5	- 20.7	- 24.5	1	3	2	24.1	23.2	4	3	5	23.4	24.9	11	4	1	- 95.3	- 95.3
10	2	-5	0	0.6	2	3	-2	4.2	2.8	5	3	-5	- 3.2	- 5.0	12	4	-1	- 22.7	- 20.8
10	2	5	0	0.1	2	3	2	- 47.2	- 47.3	5	3	5	16.1	16.2	12	4	1	- 4.7	- 5.0
11	2	-5	8.6	6.2	3	3	-2	47.4	45.7	6	3	-5	21.2	22.0	13	4	-1	0	5.2
11	2	5	- 25.4	- 23.3	3	3	2	- 40.0	- 40.6	6	3	5	5.2	5.5	13	4	1	7.1	5.2
12	2	-5	0	1.8	4	3	-2	- 84.3	- 77.4	7	3	-5	48.8	49.7	14	4	-1	32.4	32.8
12	2	5	0	0.8	4	3	2	19.0	19.7	7	3	5	- 2.6	- 2.3	14	4	1	0	- 3.2
13	2	-5	- 34.5	- 36.6	5	3	-2	- 75.5	- 71.2	8	3	-5	- 67.6	- 69.7	15	4	-1	1.3	4.1
13	2	5	0	0.7	5	3	2	- 14.4	- 13.0	8	3	5	21.9	21.7	15	4	1	113.6	103.0
15	2	-5	- 43.6	- 46.5	6	3	-2	39.2	36.3	9	3	-5	- 63.2	- 65.1	0	4	-2	2.7	3.7
0	2	-6	- 0.5	- 2.0	6	3	2	25.5	25.0	9	3	5	37.2	36.4	1	4	-2	0	5.6
1	2	-6	- 10.9	- 9.1	7	3	-2	- 1.4	- 2.5	10	3	-5	40.7	43.7	2	4	2	95.1	93.4
2	2	-6	0	0.2	7	3	2	10.7	9.4	10	3	5	- 57.1	- 57.7	3	4	2	0	1.7
2	2	6	0	- 1.9	8	3	-2	15.1	14.5	11	3	-5	13.4	15.0	3	4	-2	0	3.2
3	2	-6	31.1	27.8	8	3	2	- 9.9	- 8.9	11	3	5	- 50.8	- 51.2	4	4	2	- 101.2	- 97.2
4	2	-6	0	0.4	9	3	-2	4.7	4.0	12	3	-5	- 4.4	- 1.8	4	4	-2	- 101.5	- 106.2
4	2	6	0	1.0	9	3	2	- 7.1	- 6.4	12	3	5	25.8	26.5	5	4	2	0	- 2.0
5	2	-6	63.8	64.0	10	3	-2	7.8	8.8	13	3	-5	- 8.4	- 8.0	5	4	-2	0	- 0.1
5	2	6	- 26.3	- 24.6	10	3	2	7.2	6.0	14	3	-5	27.0	27.1	5	4	2	- 89.3	- 87.4
6	2	-6	- 2.2	- 0.7	11	3	-2	15.6	16.1	15	3	-5	31.2	29.6	6	4	-2	- 51.6	- 52.6
7	2	-6	- 92.9	- 94.7	11	3	2	9.1	10.1	0	3	-6	- 26.6	- 26.9	6	4	2	- 1.7	- 2.4
7	2	6	- 94.5	- 98.4	12	3	-2	- 3.2	- 3.6	0	3	6	26.6	26.9	7	4	-2	- 1.3	- 2.0
8	2	-6	- 1.7	- 0.9	12	3	2	8.0	8.0	1	3	-6	- 27.1	- 27.2	8	4	-2	9.5	10.4
8	2	6	0	- 1.1	13	3	-2	18.0	20.0	1	3	6	41.0	41.3	8	4	2	31.8	32.0
9	2	-6	- 68.6	- 68.2	13	3	2	28.9	29.8	2	3	-6	41.0	41.7	9	4	-2	0	- 0.2
9	2	6	- 7.2	- 7.7	14	3	-2	- 22.1	- 22.9	2	3	6	- 48.7	- 48.2	9	4	2	0	2.1
10	2	-6	- 1.3	- 1.3	14	3	2	- 33.7	- 32.9	3	3	-6	46.7	48.0	10	4	-2	129.3	140.6
10	2	6	0	- 1.1	15	3	-2	- 13.8	- 12.2	3	3	6	- 42.1	- 41.6	11	4	-2	0	2.9
11	2	-6	- 44.6	- 43.9	15	3	2	- 29.4	- 28.3	4	3	-6	- 46.4	- 47.7	11				

Table 9. Continued.

h	k	l	F <sub>o</sub>	F <sub>c</sub>	h	k	l	F <sub>o</sub>	F <sub>c</sub>	h	k	l	F <sub>o</sub>	F <sub>c</sub>	h	k	l	F <sub>o</sub>	F <sub>c</sub>
5	4	3	- 2.3	- 5.9	4	4	7	2.0	1.7	11	5	-3	14.3	14.7	8	6	-1	0.6	1.7
6	4	-3	46.1	43.3	5	4	7	0	- 2.9	11	5	3	- 26.2	- 27.5	9	6	-1	0	2.4
6	4	3	22.3	20.4	5	4	-7	1.4	3.4	12	5	-3	7.3	4.8	9	6	-1	- 63.3	- 64.8
7	4	-3	0	1.0	6	4	-7	- 4.4	- 6.0	12	5	3	- 9.0	- 9.2	10	6	-1	0	1.2
7	4	3	0	- 3.1	7	4	-7	0	1.6	13	5	-3	- 5.7	- 3.8	10	6	-1	- 1.7	- 1.6
8	4	-3	- 67.3	- 65.5	8	4	-7	- 12.5	- 12.3	14	5	-3	- 14.8	- 13.3	11	6	-1	58.7	57.9
8	4	3	- 14.6	- 11.6	2	5	0	14.4	16.3	0	5	-4	26.9	25.4	11	6	-1	17.4	16.0
9	4	-3	0	2.8	3	5	0	22.4	21.6	0	5	4	- 26.6	- 25.4	12	6	-1	- 1.8	- 0.8
9	4	3	0	1.3	4	5	0	60.8	61.5	1	5	-4	6.7	7.6	12	6	-1	- 2.2	- 3.7
10	4	-3	54.6	50.1	5	5	0	- 64.6	- 64.4	1	5	4	61.5	60.7	13	6	-1	- 82.1	- 84.7
10	4	3	16.1	16.4	6	5	0	- 21.7	- 20.8	2	5	4	73.0	73.5	13	6	-1	- 12.8	- 10.1
11	4	-3	0	- 0.3	7	5	0	- 24.3	- 24.4	3	5	-4	21.5	20.1	0	6	-2	0	7.3
11	4	3	0	- 3.0	8	5	0	- 46.1	- 47.0	3	5	4	- 30.9	- 50.1	0	6	2	0	7.3
12	4	-3	24.3	24.6	9	5	0	29.8	31.1	4	5	-4	44.9	42.1	1	6	-2	- 42.4	- 37.7
12	4	3	- 56.1	- 57.9	10	5	0	- 10.6	- 9.6	4	5	4	2.7	3.9	2	6	-2	0	4.2
13	4	-3	0	3.6	11	5	0	26.8	25.8	5	5	-4	- 41.8	- 40.2	2	6	2	1.9	6.3
13	4	3	0	- 3.3	12	5	0	19.1	17.1	5	5	4	- 30.4	- 31.1	3	6	-2	- 59.3	- 56.2
14	4	-3	31.1	29.9	13	5	0	14.5	14.6	6	5	-4	- 9.0	- 8.2	3	6	2	- 7.7	- 7.2
14	4	3	16.1	15.5	14	5	0	48.2	50.2	6	5	4	- 20.3	- 21.7	4	6	-2	- 2.0	- 1.6
15	4	-3	2.7	4.5	15	5	0	- 48.7	- 49.0	7	5	-4	- 20.9	- 20.0	4	6	2	- 2.6	- 3.1
1	4	4	0	2.3	0	5	-1	30.2	28.8	7	5	4	- 5.6	- 6.4	5	6	-2	- 53.9	- 50.4
1	4	4	0	- 1.2	0	5	1	- 29.4	- 28.8	8	5	-4	- 29.1	- 28.4	6	6	2	3.0	2.1
2	4	-4	- 62.5	- 57.5	1	5	-1	- 3.0	- 0.7	8	5	4	- 36.3	- 37.2	6	6	-2	0	2.4
2	4	4	20.0	15.4	1	5	1	26.8	26.3	9	5	-4	14.6	14.9	7	6	2	71.5	73.2
3	4	-4	0	- 2.4	2	5	-1	39.5	38.0	9	5	4	34.4	35.3	7	6	-2	104.1	105.3
3	4	4	- 1.6	- 3.6	2	5	1	6.7	5.5	10	5	-4	- 7.8	- 9.2	8	6	-2	0	5.2
4	4	-4	40.3	39.6	3	5	-1	12.9	15.2	11	5	-4	12.6	13.8	8	6	2	0	6.0
4	4	4	64.3	62.6	4	5	-1	- 41.6	- 40.6	11	5	4	16.7	16.9	9	6	2	27.8	27.7
5	4	-4	0	- 0.3	4	5	1	0	4.0	12	5	-4	5.0	5.4	9	6	-2	45.8	43.5
5	4	4	- 2.4	- 0.5	5	5	-1	- 4.0	- 3.8	13	5	-4	9.1	8.8	10	6	2	0	3.1
6	4	-4	52.7	48.2	5	5	1	32.4	33.0	0	5	-5	16.3	15.7	10	6	-2	0	5.4
6	4	4	111.2	114.0	6	5	1	51.4	51.7	0	5	5	- 16.2	- 15.7	11	6	2	- 15.4	- 14.9
7	4	-4	0.4	4.9	6	5	-1	- 25.9	- 27.1	1	5	-5	- 8.5	- 11.2	11	6	-2	- 3.1	- 2.4
7	4	4	0	- 1.0	7	5	-1	18.1	18.8	1	5	5	5.3	4.9	12	6	2	0	2.2
8	4	-4	6.7	3.2	7	5	1	- 47.3	- 46.7	2	5	-5	6.4	5.4	12	6	-2	2.0	2.3
8	4	4	- 117.6	- 124.5	8	5	-1	- 11.3	- 8.7	2	5	5	- 10.5	- 11.2	13	6	-2	- 69.9	- 69.4
9	4	-4	2.5	2.1	8	5	1	- 15.5	- 14.8	3	5	-5	- 5.6	- 5.5	0	6	-3	4.4	2.2
9	4	4	2.3	0.6	9	5	-1	37.4	36.3	3	5	5	30.3	30.8	0	6	3	0	2.2
10	4	-4	- 35.1	- 34.4	9	5	1	- 17.6	- 18.4	4	5	-5	14.4	14.9	1	6	-3	- 7.9	- 6.0
10	4	4	- 72.7	- 69.9	10	5	-1	25.3	26.6	4	5	5	18.6	18.6	1	6	3	- 38.5	- 37.2
11	4	-4	0	- 3.2	11	5	-1	7.0	5.8	5	5	-5	- 37.5	- 38.6	2	6	-3	2.5	4.1
11	4	4	- 1.2	- 3.1	11	5	1	- 2.2	- 1.5	5	5	5	18.4	20.3	3	6	3	21.1	26.6
12	4	-4	- 103.1	- 104.7	12	5	-1	33.3	33.2	6	5	-5	- 43.9	- 44.2	3	6	3	51.2	48.6
12	4	4	- 17.6	- 18.9	12	5	1	- 16.2	- 16.7	6	5	5	45.0	47.5	4	6	3	- 2.3	- 0.8
13	4	-4	0	- 2.7	13	5	-1	- 51.1	- 50.7	7	5	-5	32.5	33.6	4	6	-3	- 3.0	- 1.0
14	4	-4	67.1	66.6	13	5	1	25.4	25.3	8	5	-5	14.1	16.4	5	6	3	45.6	47.7
0	4	-5	- 13.8	- 10.7	14	5	-1	- 33.4	- 34.0	9	5	-5	- 12.7	- 15.0	5	6	-3	- 119.9	- 124.2
0	4	5	- 12.0	- 10.7	14	5	1	6.5	6.7	10	5	-5	- 24.4	- 24.9	6	6	-3	0	1.6
1	4	-5	5.1	1.9	15	5	-1	8.1	8.0	11	5	-5	42.6	43.4	6	6	3	1.9	4.8
1	4	5	0	0.8	15	5	1	24.2	25.5	12	5	-5	45.4	46.2	7	6	3	31.7	35.9
2	4	-5	16.1	16.4	0	5	-2	38.5	36.0	0	5	-6	39.0	39.9	7	6	-3	24.5	20.4
2	4	5	10.5	9.1	0	5	2	- 37.8	- 36.0	0	5	6	- 39.7	- 39.9	8	6	-3	- 3.4	- 3.3
3	4	-5	0	- 3.5	1	5	-2	- 18.1	- 17.6	1	5	-6	- 30.0	- 32.7	8	6	3	0	2.7
3	4	5	2.5	3.7	2	5	2	- 47.4	- 46.4	1	5	6	24.7	25.1	9	6	-3	- 6.9	- 4.1
4	4	-5	- 91.2	- 87.5	3	5	-2	41.0	38.6	2	5	-6	- 38.4	- 38.6	9	6	3	- 35.4	- 37.4
4	4	5	24.3	26.0	3	5	2	33.6	33.1	2	5	6	7.0	7.2	10	6	3	0	- 0.1
5	4	-5	- 1.5	- 4.0	4	5	-2	- 13.2	- 14.4	3	5	-6	9.9	10.2	10	6	-3	1.5	2.3
5	4	5	2.4	2.3	4	5	2	- 13.9	- 15.5	3	5	6	- 16.2	- 17.0	11	6	3	- 6.0	- 8.5
6	4	-5	42.0	41.0	5	5	-2	27.3	27.2	4	5	-6	- 3.9	- 3.9	11	6	-3	44.7	44.6
6	4	5	- 35.1	- 37.7	5	5	2	34.0	36.6	4	5	6	- 40.3	- 43.5	12	6	-3	0.8	3.0
7	4	-5	- 0.9	- 2.1	6	5	-2	1.0	1.2	5	5	-6	- 4.3	- 5.8	0	6	-4	0	- 5.6
7	4	5	1.3	0.9	6	5	2	20.4	21.4	5	5	6	49.1	53.3	0	6	4	0	+ 5.6
8	4	-5	- 5.1	- 3.8	7	5	-2	36.2	35.3	6	5	6	34.9	38.0	1	6	4	30.0	30.2
8	4	5	- 24.8	- 22.8	7	5	2	8.4	7.3	6	5	-6	33.6	34.7	1	6	-4	19.7	22.3
9	4	-5	2.7	1.6	8	5	-2	47.0	47.4	7	5	-6	- 10.7	- 11.7	2	6	4	- 2.4	- 0.6
9	4	5	1.1	1.1	8	5	2	32.4	32.7	8	5	-6	21.0	21.1	2	6	-4	- 1.5	- 4.2
10	4	-5	18.4	18.7	9	5	-2	- 28.0	- 28.4	9	5	-6	4.8	5.2	3	6	4	120.5	127.7
10	4	5	46.5	44.5	9	5	2	- 25.6	- 24.4	0	5	-7	3.6	2.3	3	6	-4	49.1	46.7
11	4	-5	0	- 1.6	10	5	-2	9.1	8.5	0	5	7	- 2.1	- 2.3	4	6	-4	- 2.8	- 0.5
11	4	5	0	0.8	10	5	2	6.7	8.3	1	5	-7	- 13.8	- 15.8	4	6	4	0	- 2.9
12	4	-5	- 69.2	- 65.5	11	5	-2	- 29.8	- 30.4	1	5	7	- 8.2	- 7.2	5	6	-4	15.2	13.6
0	4	-6	70.6	69.1	11	5	2	- 22.8	- 24.4	2	5	-7	- 33.4	- 36.5	5	6	4	- 85.3	- 87.8
0	4	6	70.6	69.1	12	5	-2	- 24.2	- 24.2	4	5	-7	17.7	18.4	6	6	-4	2.5	1.7
1	4	-6	0	1.6	12	5	2	- 26.1	- 26.9	2	6	0	- 1.4	- 3.0	6	6	4	0.2	1.0
1	4	6	0	3.0	13	5	2	9.5	9.3	4	6	0	- 0.7	- 2.8	7	6	4	- 29.7	- 31.2
2	4	-6	92.2	93.5	14	5	-2	- 15.4	- 14.9	5	6	0	- 37.8	- 34.6	7	6	-4	- 42.1	- 40.9
2	4	6	11.4	13.4	14	5	2	- 15.3	- 17.6	6	6	0	0	0.9	8	6	4	0	- 3.9
3	4	-6	0	0.5	15	5	-2	10.2	9.8	7	6	0	- 47.0	- 45.3	8	6	-4	0	- 4.1
3	4	6	0	3.3	0	5	-3	- 50.0	- 47.4	8	6	0	- 2.4	- 5.7	9	6	4	- 30.7	- 29.8
4	4	-6	- 32.5	- 32.4	0	5	3	48.4	47.8	9	6	0	- 52.9	- 52.4	9	6	-4	- 64.5	- 64.3
4	4	6	- 81.7	- 82.5	1	5	3	28.6	26.0	10	6	0	- 3.1	- 7.5	11	6	-4	7.4	7.4
5																			

Table 9. Continued.

h	k	l	F <sub>o</sub>	F <sub>c</sub>	h	k	l	F <sub>o</sub>	F <sub>c</sub>	h	k	l	F <sub>o</sub>	F <sub>c</sub>	h	k	l	F <sub>o</sub>	F <sub>c</sub>
1	6	6	-65.7	-67.1	3	7	1	36.6	38.8	6	7	-2	-18.9	-17.4	7	7	-3	-11.6	-19.5
1	6	-6	11.1	10.6	4	7	-1	-10.4	-9.1	6	7	2	-28.5	-28.9	7	7	3	35.5	35.5
2	6	6	0	3.3	4	7	1	-34.0	-35.5	7	7	-2	13.0	14.2	8	7	-3	-1.6	-0.9
2	6	-6	0	1.0	5	7	-1	-28.8	-28.3	7	7	2	3.3	6.3	8	7	3	-22.6	-21.1
3	6	-6	-45.5	-45.8	5	7	1	-12.3	-10.7	8	7	-2	-16.8	-17.2	9	7	-3	-3.5	-5.6
4	6	-6	0	-1.6	6	7	-1	38.7	38.8	8	7	2	-16.3	-18.1	0	7	-4	50.2	50.2
5	6	-6	-41.9	-43.9	7	7	-1	16.7	17.6	9	7	-2	0	1.5	0	7	4	-49.2	-50.2
3	7	0	-14.0	-13.2	7	7	1	-4.7	-5.4	9	7	2	-13.4	-14.4	1	7	-4	55.1	56.7
4	7	0	-11.4	-14.1	8	7	-1	-13.9	-14.8	10	7	-2	-19.4	-21.2	1	7	4	-17.2	-15.9
5	7	0	-17.4	-19.8	8	7	1	-18.6	-17.4	0	7	-3	-23.0	-24.9	2	7	-4	-39.4	-39.5
6	7	0	-6.1	-5.2	9	7	-1	-24.8	-25.7	0	7	3	-22.3	-24.9	2	7	4	0	-3.3
7	7	0	-36.6	-36.1	9	7	1	-25.7	-25.9	1	7	-3	1.6	0.9	3	7	4	0	-1.2
8	7	0	40.4	39.7	10	7	-1	-23.2	-24.2	1	7	3	-26.6	-27.8	4	7	-4	-24.4	-27.0
9	7	0	13.6	13.7	10	7	1	24.9	24.7	2	7	-3	24.8	23.9	4	7	4	-16.7	-17.8
10	7	0	17.5	17.9	0	7	-2	8.2	6.8	2	7	3	11.6	11.9	5	7	-4	-18.3	-19.1
11	7	0	40.8	42.9	0	7	2	-7.4	-6.8	3	7	-3	27.5	27.2	6	7	-4	-9.4	-10.8
0	7	-1	-25.2	-23.7	2	7	-2	6.9	9.0	3	7	3	-4.4	-5.9	7	7	-4	-30.7	-31.7
0	7	1	24.5	23.7	2	7	2	45.8	47.3	4	7	-3	-9.1	-8.3	0	7	5	13.6	14.6
1	7	1	8.0	8.7	3	7	-2	-20.8	-20.0	4	7	3	7.6	6.1	0	7	-5	-13.9	-14.6
1	7	-1	-17.1	-16.9	3	7	2	21.7	22.4	5	7	-3	21.3	22.3	1	7	-5	7.2	7.7
2	7	-1	2.3	2.0	4	7	-2	50.7	50.5	5	7	3	-10.1	-9.7	2	7	-5	-21.1	-23.9
2	7	1	20.9	21.4	5	7	-2	47.3	46.5	6	7	-3	-33.2	-33.6					
3	7	-1	-4.0	-7.0	5	7	2	35.2	36.3	6	7	3	35.8	36.6					

## CHAPTER II

## HIGH-PRESSURE PHASE OF CALCIUM METASILICATE

## Introduction

The first attempt to synthesize calcium metasilicate at high temperatures was made by Bourgeois (1882). An examination with the microscope indicated that the crystalline material he had obtained was monoclinic with a very small optic axial angle. He reported that this finding is quite different from the axial angle known for wollastonite. In continuing the examination he measured a density of 2.7 g/cc on the same material. Compared with the density of wollastonite,  $\rho = 2.88$  g/cc, the new value is significantly lower. Hence Bourgeois concluded that his synthetic product must be a new phase of calcium metasilicate. Dölter (1886) repeated the experiment as outlined by the French scientist. He found small, round or sometimes hexagonal looking crystals. He also measured the density and found a much higher value,  $\rho = 2.90$  g/cc, than Bourgeois. His crystals grew at a temperature  $1200^\circ\text{C}$ . Based on an optic examination Dölter suggested that this specimen is orthorhombic with an optic axial angle so small that the interference figure resembles those of hexagonal substances. Several years later this phase was named pseudowollastonite by Allen, White, and Wright (1906). These authors performed extensive experiments on the phase transformation between wollastonite and pseudowollastonite. The inversion of the low-temperature phase wollastonite to the high-temperature phase pseudowollastonite was determined to take place about  $1180^\circ\text{C}$ . By adding some  $\text{Ca}(\text{VO}_3)_2$ , Allen, White, and Wright were able to make the transformation reversible for the first time. With the availability of x-ray

diffraction methods the wollastonite group was reinvestigated. Warren (1931) determined the symmetry of wollastonite to be triclinic. Peacock (1935) proved the existence of a second low-temperature modification of  $\text{CaSiO}_3$ , namely parawollastonite. The first structure proposal for a phase of  $\text{CaSiO}_3$  was made by Barnik (1936). He suggested  $\text{Si}_3\text{O}_9$  rings as the principal structural feature for parawollastonite. This proposal was rejected by many crystal-structure analysts. It is interesting to remark at this place that many years later a structure proposal containing  $\text{Si}_3\text{O}_9$  rings has been accepted as the correct one for pseudowollastonite. Meanwhile other modifications of  $\text{CaSiO}_3$  or chemically similar compounds were studied in none of which rings have been revealed.

In this context Jeffrey and Heller (1953) made a preliminary x-ray investigation of a high-temperature phase of  $\text{CaSiO}_3$  known as pseudowollastonite. With oscillation, rotation, and Weissenberg photographs these authors were able to determine the symmetry to be pseudo-hexagonal which might well allow for  $\text{Si}_3\text{O}_9$  rings. Unfortunately the crystals were not good enough to proceed with a detailed structure determination. In the meantime Barnik's ring proposal for monoclinic wollastonite was proven incorrect by Mamedov and Belov (1956). The Russian authors found  $\text{Si}_3\text{O}_9$  chains to be the basic structural feature in wollastonite. Considering the limited results given by Jeffrey and Heller for pseudowollastonite, Hilmer (1963) tried to avoid the difficulty encountered by bad crystalline material through solving a structurally analogous compound. Liebau (1960) suggested that  $\text{SrGeO}_3$ , as well as  $\text{SrSiO}_3$ , and the low-temperature phase of  $\text{BaGeO}_3$  were structural analogs of pseudowollastonite. Hilmer selected  $\text{SrGeO}_3$  and succeeded in determining the structure in which she found  $\text{Ge}_3\text{O}_9$  rings. On the basis of this investigation Hilmer suggested that the results obtained with  $\text{SrGeO}_3$

also apply to the structure of pseudowollastonite. Encouraged by these findings, the present project was undertaken to examine a high-pressure, high-temperature polymorph of calcium metasilicate with the hope of answering the following two questions: first, what is the arrangement of the silicon-oxygen tetrahedra and, second, is there any relation to the structure proposed by Hilmer for pseudowollastonite.

## Material

The specimen used in this investigation was synthesized by Dr. R.D. Shannon (Central Research Department, E. I. du Pont de Nemours and Co.) and was kindly made available by Dr. Charles T. Prewitt. The crystals were made from  $\text{CaSiO}_3$  glass at 65 kilobars and approximately  $1300^\circ\text{C}$ . A density of 3.05 g/cc was determined by the immersion method using a mixture of methylene iodide ( $\rho = 3.32$  g/cc) and methyl iodide ( $\rho = 2.28$  g/cc). This density is considerably higher than the value of 2.88 g/cc found for wollastonite or 2.92 g/cc for pseudowollastonite.

A Guinier powder photograph of high-pressure  $\text{CaSiO}_3$  is illustrated in Fig. 7 and compared with one made of pseudowollastonite. It is of interest to point out that the strong lines in both compounds match with each other in intensity and  $d$  values. Based on this observation the existence of significant structural relations between the two phases is quite probable. According to Buckner and Roy (1955) pseudowollastonite is stable at temperatures above  $1120^\circ\text{C}$ . They made hydrothermal phase equilibria studies of the system  $\text{CaSiO}_3 - \text{H}_2\text{O}$  at pressures ranging from 7 to 68 kilobars. However, Buckner and Roy did not indicate any exact information about the upper limit of pressure in the  $p$ - $T$  stability field of pseudowollastonite. Possibly this limit is similar to the one reported for wollastonite. Buckner, Roy, and Roy (1960) found wollastonite to be stable at pressures of 35 kilobars. Judging from this limited  $p$ - $T$  data available for the  $\text{CaSiO}_3$  system, the present compound might well be a high-pressure modification of the high-temperature phase pseudowollastonite.

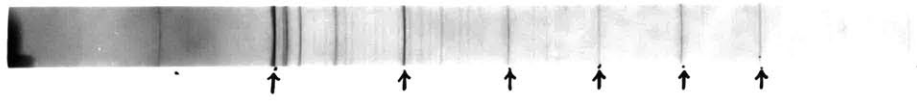
The pressure and temperature conditions mentioned above for high-pressure  $\text{CaSiO}_3$  are within the stability field of another new phase of  $\text{CaSiO}_3$  observed

Fig. 7. Guinier powder photograph using  $\text{CuK}\alpha$  radiation. The lines indicated with an arrow are common to both structures.

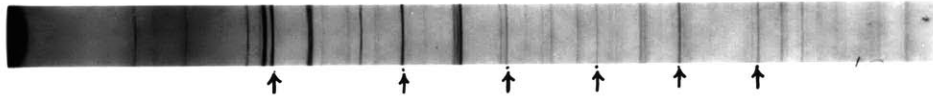
(a) High-pressure  $\text{CaSiO}_3$ .

(b) Pseudowollastonite





(a)

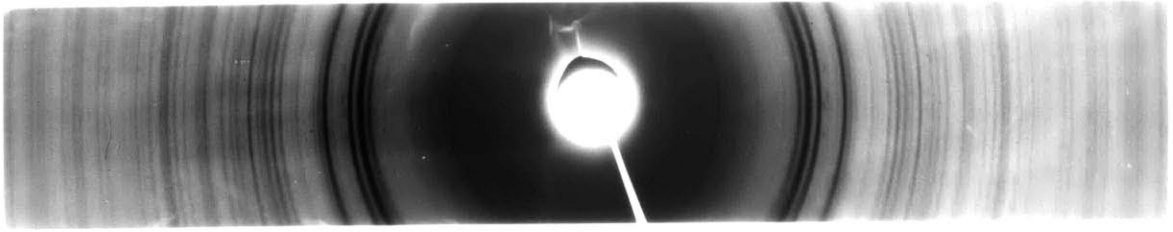


(b)

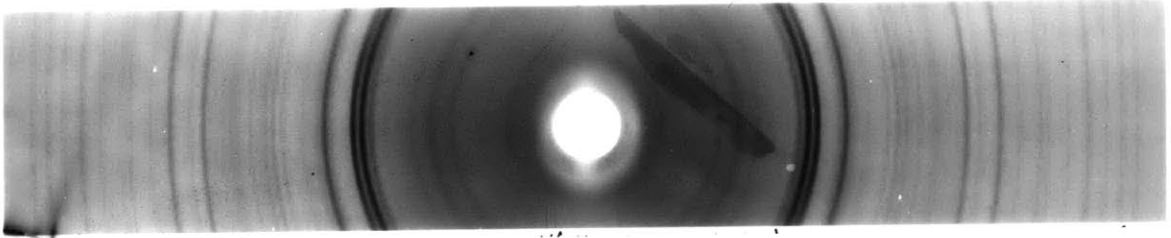
Fig. 8. Powder photograph with  $\text{CuK}\alpha$  radiation.

(a) High-pressure  $\text{CaSiO}_3$ .

(b) Ringwood and Major's high-pressure phase of  $\text{CaSiO}_3$ .



(a)



(b)

by Ringwood and Major (1967). These two Australian scientists report that wollastonite is stable up to 30 kilobars. Above this pressure they observed a new phase which is characterized by a higher density than wollastonite and a powder pattern very similar to the one made from this sample. Fig. 8 compares the powder photographs of both substances. Ringwood and Major found their phase to be stable up to pressures well above 100 kilobars. The strong similarity in stability field, powder pattern, and density suggests a close structural resemblance if not actual identity of these two phases.

### X-ray Diffraction Experiment

Precession photographs showed triclinic symmetry, indicating one of the two space groups  $\bar{P}1$  and  $P1$ . The choice of  $\bar{P}1$  as the correct space group was based on a statistical analysis of the  $F_{\text{obs}}$ . According to Karle and Hauptman (1958), centrosymmetric structures have theoretical statistical averages of their normalized structure factors,  $\bar{E}$ , as listed in Table 10. This table also shows the close resemblance of the observed values for the  $\text{CaSiO}_3$  phase, examined in this investigation, with the theoretical values for a centrosymmetric structure. In order to appraise the significance of the agreement between the observed and theoretical values, also the theoretical values for an acentric structure, as established by Karle and Karle (1966), are given in the last column.

A set of back-reflection Weissenberg photographs was used to determine precise lattice constants. These film data were refined by the least-squares method. The cell dimensions are given in Table 11.

Most of the crystals of this high-pressure phase were either too small or of too poor quality to be used for intensity measurement. Finally, after examining about 40 specimens, a suitable crystal with a volume of  $0.0005 \text{ mm}^3$  was found. Nickel-filtered  $\text{CuK}\alpha$  radiation was used to measure 1051 reflections with an equi-inclination single-crystal diffractometer. The diffracted x-ray beam was recorded by a proportional counter connected with a pulse-height discriminator. The integrated intensities were corrected for Lorentz and polarization factors as well as for absorption. The observed structure factors are listed in Table 18.

Table 10. Theoretical and Observed Statistical Averages  
of Normalized Structure Factors for High-Pressure  
 $\text{CaSiO}_3$ .

Nature of Average	Expected for Centrosymmetric Structures	Observed	Expected for Acentric Structures
$\langle E \rangle$	0.798	0.785	0.89
$\langle  E ^2 - 1 \rangle$	0.968	0.992	0.74
$\langle E^2 \rangle$	1.0	1.0	1.0

Table 11. Symmetry and Cell Data for the High-Pressure Polymorph of  $\text{CaSiO}_3$ .

Space group	$\underline{P} \bar{1}$
Cell dimensions:	$\underline{a} = 6.695 \pm 0.005 \text{ \AA}$ $\underline{b} = 9.257 \pm 0.007 \text{ \AA}$ $\underline{c} = 6.666 \pm 0.006 \text{ \AA}$ $\alpha = 86^\circ 38' \pm 3'$ $\beta = 76^\circ 08' \pm 3'$ $\gamma = 70^\circ 23' \pm 2'$
Density observed:	3.05 g/cc
Density calculated:	3.06 g/cc for $\underline{Z} = 6 \text{ CaSiO}_3$
Density of wollastonite:	2.88 g/cc

### Structure Determination and Refinement

A three-dimensional Patterson function was computed. In order to interpret it, all its maxima were projected along the  $\underline{a}$  axis. A careful investigation of this map showed that the strong peaks outline a subcell with one third of the volume of the original cell. The transformation of the original cell vectors to those for the subcell is as follows:

$$\begin{aligned}\underline{a}' &= \underline{a} \\ \underline{b}' &= \frac{1}{3}\underline{b} - \frac{1}{3}\underline{c} \\ \underline{c}' &= \underline{c}\end{aligned}$$

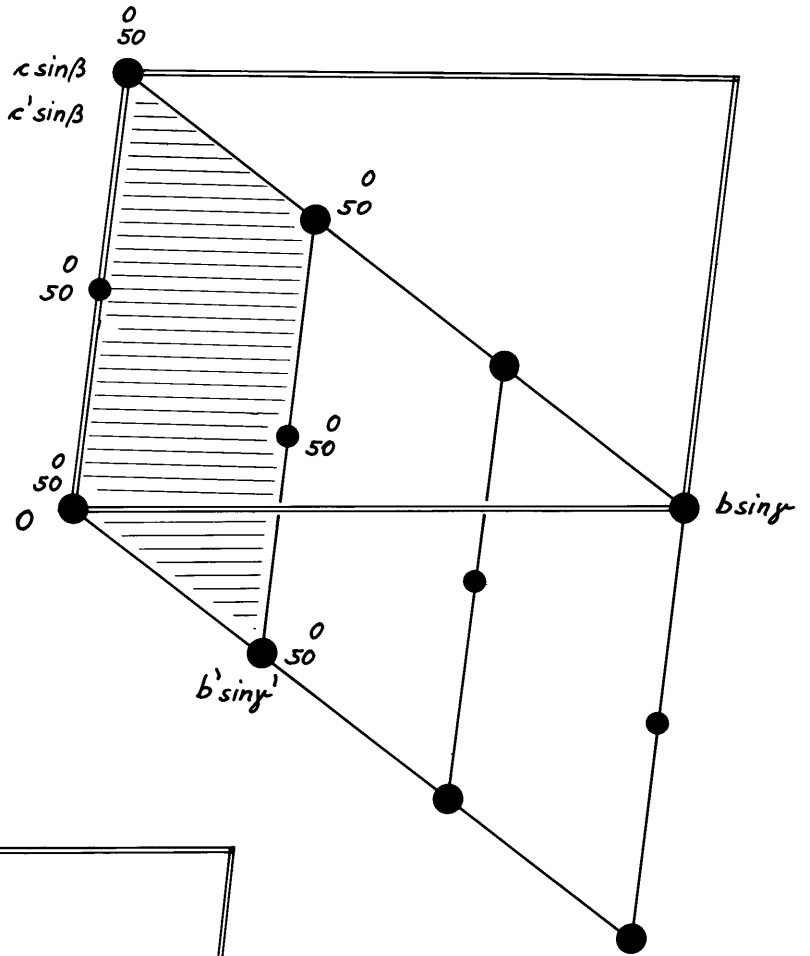
About 300 reflections with indices  $\underline{h} \ \underline{k} \ \underline{l}$  corresponding to the subcell were selected from the full data deck. These 300 strong reflections were used to compute a Patterson function which projected along  $\underline{a}$ , is shown schematically in Fig. 9a. Figure 9b illustrates a substructure model containing two possible locations of heavy atoms which are derived from the Patterson map seen in Fig. 9a. If three of these substructure cells are arranged in such a way that they cover the same volume as the true cell of high-pressure  $\text{CaSiO}_3$ , six independent positions for the metal atoms are obtained. These six atomic positions were tested on a set of reflection amplitudes with  $|F_{\text{obs}}| > 30$ , which represents roughly half of the whole reflection set. The structure-factor computation yielded an  $R$  value of 44%, thus warranting considering this proposal as a possible candidate for the structure of this high-pressure phase of  $\text{CaSiO}_3$ .

Further evidence supporting the above mentioned findings was obtained by reiterative application of Sayre's (1952) equation. This was performed with an IBM 7094 program REL written by R.E. Long, University of California, Los Angeles. In his program R.E. Long uses a modified version of Sayre's



- Fig. 9. Schematic presentation of the substructure of high-pressure  $\text{CaSiO}_3$ . The subcell is shaded, the true cell is outlined by double lines. The numbers give the height  $\underline{x}$  in hundredths.
- (a) Idealized substructure Patterson projected along a, showing only the high peaks.
- (b) Idealized substructure as a model derived from the Patterson map shown in Fig. 9a.

(a)



(b)

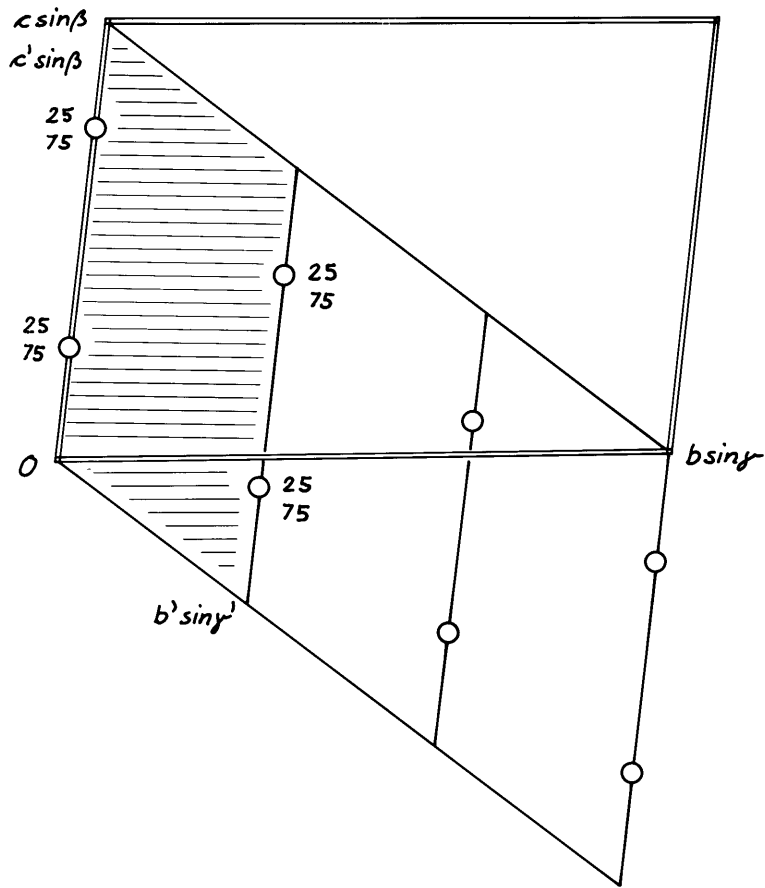
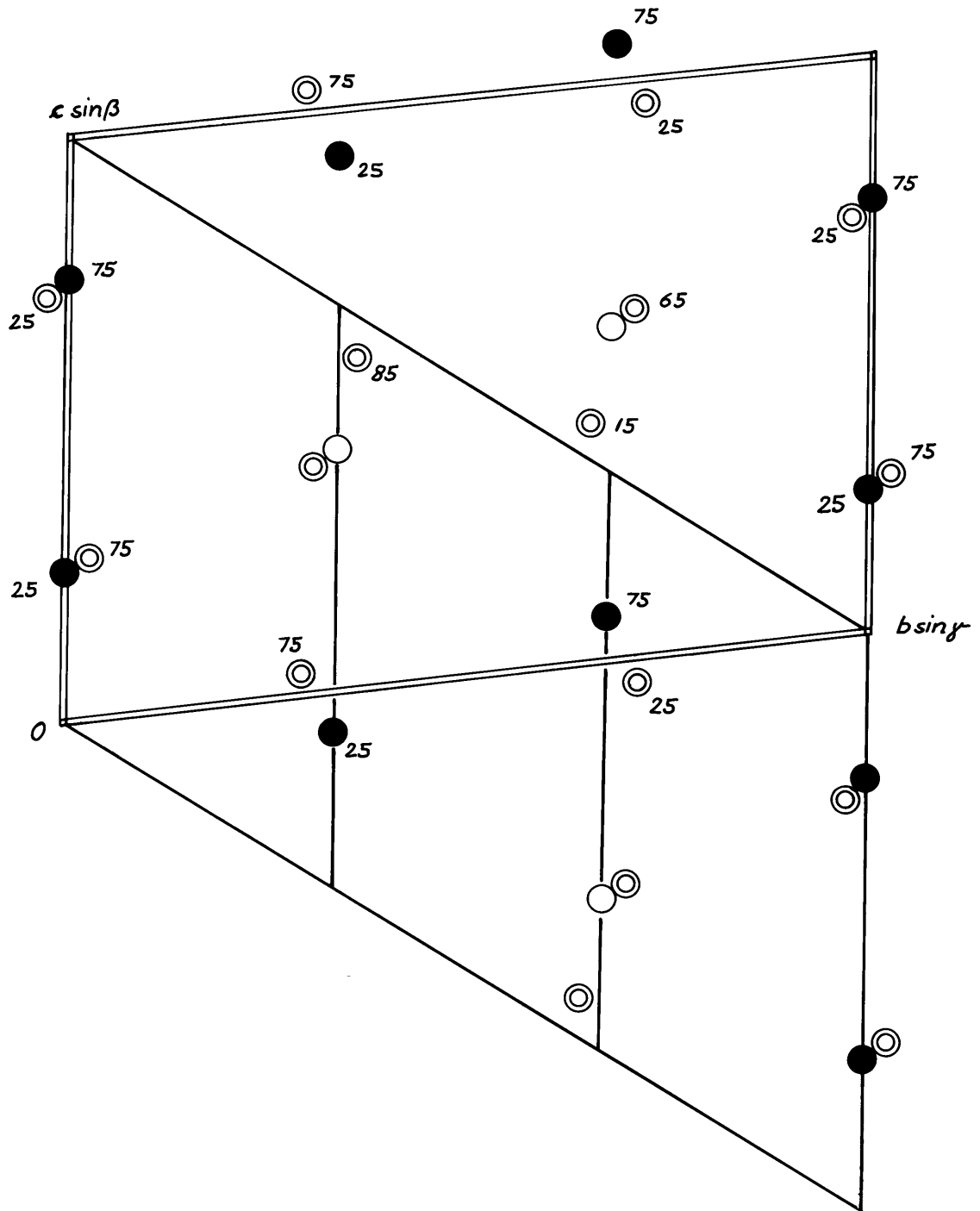


Fig. 10. Comparison of the atomic positions suggested by the substructure with the actual locations of the Ca and Si atoms in high-pressure  $\text{CaSiO}_3$ . The black full circles represent atoms with no deviation from the predicted position. The double circles represent atoms which do not quite correspond to the positions derived from the substructure (empty circles). The numbers give the height  $\underline{x}$  in hundredths. The true cell is outlined by double lines.



equation which was published by Hauptman and Karle (1953) and named the  $\Sigma_2$  equation:

$$\text{sign}(\underline{E}_A) = \text{sign}\left(\sum_{A=B+C} \underline{E}_B \underline{E}_C\right)$$

$\underline{A}$ ,  $\underline{B}$ , and  $\underline{C}$  are the indices  $hkl$  for the normalized structure factors  $\underline{E}_A$ ,  $\underline{E}_B$ , and  $\underline{E}_C$ . The sign determination was carried out as follows: A starting set of 7 reflections is chosen which have a high value of  $\underline{E}$  and indices which allow a large number of index combinations in the equation mentioned above. The first 3 reflections used for the origin determination have to be linearly independent. Therefore the parity  $\underline{g} \underline{g} \underline{g}$  ( $\underline{g}$  stands for even and  $\underline{u}$  for odd), in their indices has to be avoided. Furthermore, the parity of each of the 3 reflections must be different from one another. The signs for the origin determination may be chosen arbitrarily. The remaining 4 reflections may have any combination of + and - signs thus 16 combinations are obtained. The origin reflections, which remain unchanged throughout the whole procedure, and one of the 16 combinations form a starting set for a specific model of signs for all the remaining reflections included in the program. For each of these 16 starting sets Sayre's equation predicts additional signs which are used to determine more signs and to redetermine those already specified. This procedure is reiterated until there are no changes or new signs predicted. Hence the model corresponding to such a starting set is said to be consistent. In order to appraise the quality of a model, R.E. Long introduced a consistency index  $\underline{C}$  :

$$\underline{C} = \frac{\langle |E_A| \sum_{A=B+C} E_B E_C \rangle}{\langle |E_A| \sum_{A=B+C} |E_B| |E_C| \rangle}$$

Table 12. Summary of the Sixteen Models Obtained by Application of R.E. Long's sign Determination Program for High-Pressure  $\text{CaSiO}_3$ .

Models	Number of cycles	Consistency index	Starting set for Model 12		
			$\underline{h}$ $\underline{k}$ $\underline{l}$	$\underline{E}$	Parity
1	-	-	0 3 0	2.61	$\underline{g}$ $\underline{u}$ $\underline{g}$
2	12	0.918	3 5 0	2.37	$\underline{u}$ $\underline{u}$ $\underline{g}$
3	17	0.519	2 2 1	1.88	$\underline{g}$ $\underline{g}$ $\underline{u}$
4	17	0.552			
5	7	0.819	0 3 $\bar{6}$	-3.72	$\underline{g}$ $\underline{u}$ $\underline{g}$
6	7	0.814	2 1 $\bar{2}$	2.32	$\underline{g}$ $\underline{u}$ $\underline{g}$
7	11	0.688	4 5 2	-2.98	$\underline{g}$ $\underline{u}$ $\underline{g}$
8	17	0.616	$\bar{4}$ 5 2	-3.37	$\underline{g}$ $\underline{u}$ $\underline{g}$
9	15	0.568			
10	15	0.557			
11	7	0.903			
12	6	0.971			
13	17	0.633			
14	13	0.707			
15	8	0.813			
16	7	0.825			

This index expresses the average change in sign within a given set of reflections and is normalized so that its limits are 0 and 1. Usually the true solution has a consistency index approaching the upper limit and a small number of cycles required to reach consistency.

The sign determination was carried out on 181 reflections which had a normalized structure factor  $|E| > 1.4$ . A study of these models revealed that the one with the highest consistency index of 0.971 and the lowest number of cycles was almost identical with the proposal obtained by analysis of the Patterson map of the subcell. Table 12 lists the consistency index and the number of cycles for all 16 models and in addition it gives the starting set of the best model.

Accordingly a fourier synthesis based on the six positions of the metal atoms was computed. This function produced additional peaks which could be interpreted as the locations of the nine oxygens. Employing the positional parameters of the six metal atoms and the nine oxygens, a structure-factor computation gave an  $R$  value of 30% suggesting that the preliminary atomic coordinates were probably correct.

Figure 10 illustrates the close resemblance of the proposed arrangement of the metal atoms to the actual location of these atoms as obtained during a later stage of the investigation. A preliminary cycle of least-squares refinement of these positional parameters using equal weights and an overall isotropic temperature factor of  $B = 1.0 \text{ \AA}^2$  decreased the  $R$  value from 30% to 20%. In continuing the refinement, a weighting scheme was introduced based on a weighting factor  $w = |F_{\text{obs}}|$ , described by de Vries (1965). Allowing all parameters to vary, the best  $R$  value with isotropic temperature factors was

9.4% and with anisotropic thermal parameters, 6.5% (unweighted) and 5.4% (weighted).



### Discussion of the Structure

The basic structural features of this high-pressure phase of  $\text{CaSiO}_3$  are Ca-O layers and  $\text{Si}_3\text{O}_9$  rings. The layers contain two types of Ca atoms, one coordinated by six oxygens the other by eight oxygens. The  $\text{Si}_3\text{O}_9$  rings are located between these layers. The third type of Ca atom, also coordinated by six oxygens, connects neighboring layers, thus sharing the space with the  $\text{Si}_3\text{O}_9$  rings. The rings are seen projected along  $\underline{a}$  in Fig. 11. The Ca layers and their orientation in respect to the cell of high-pressure  $\text{CaSiO}_3$  are illustrated in Fig. 16.

All atoms in this structure occupy the general position  $2i$  in space group  $\overline{P}1$ . The refined coordinators are listed in Table 13. Table 14 gives the interatomic distances and Table 15 the bond angles between atoms.

The cell of high-pressure  $\text{CaSiO}_3$  contains three Ca-O layers as seen in Fig. 16. The Ca atoms define planes parallel to (111) which intersect the axes at  $\frac{1}{2}$ . A view normal to the Ca-O layer is illustrated in Fig. 12. If the Ca(2) octahedra, which are not located within the layer, are neglected, Fig. 12 shows that the layer is composed of oxygen polyhedra around Ca(1) and Ca(3) which share edges with each other. These polyhedra do not fill all the space of the layer, which has large voids. The Ca(2) octahedra, shown cross-hatched in Fig. 12, are above and below the layer. Ca(1) is coordinated by eight oxygens forming a distorted scalenohedron. The largest Ca-O distance within this polyhedron is  $2.725\text{\AA}$ , which lies between similar unusually large Ca-O distances found by Prewitt and Buerger (1963) for wollastonite:  $\text{Ca}_3\text{-O}_9 = 2.642\text{\AA}$ ; and by Trojer (1968) for parawollastonite:  $\text{Ca(1)-O(9)} = 2.895\text{\AA}$ . Ca(3) has octahedral coordination with an average Ca-O distance of  $2.375\text{\AA}$ .

7

Fig. 11. Projection along  $\underline{a}$  of the structure of high-pressure  $\text{CaSiO}_3$ . The double circles are Ca atoms, the full circles Si atoms, and the single circles O atoms.

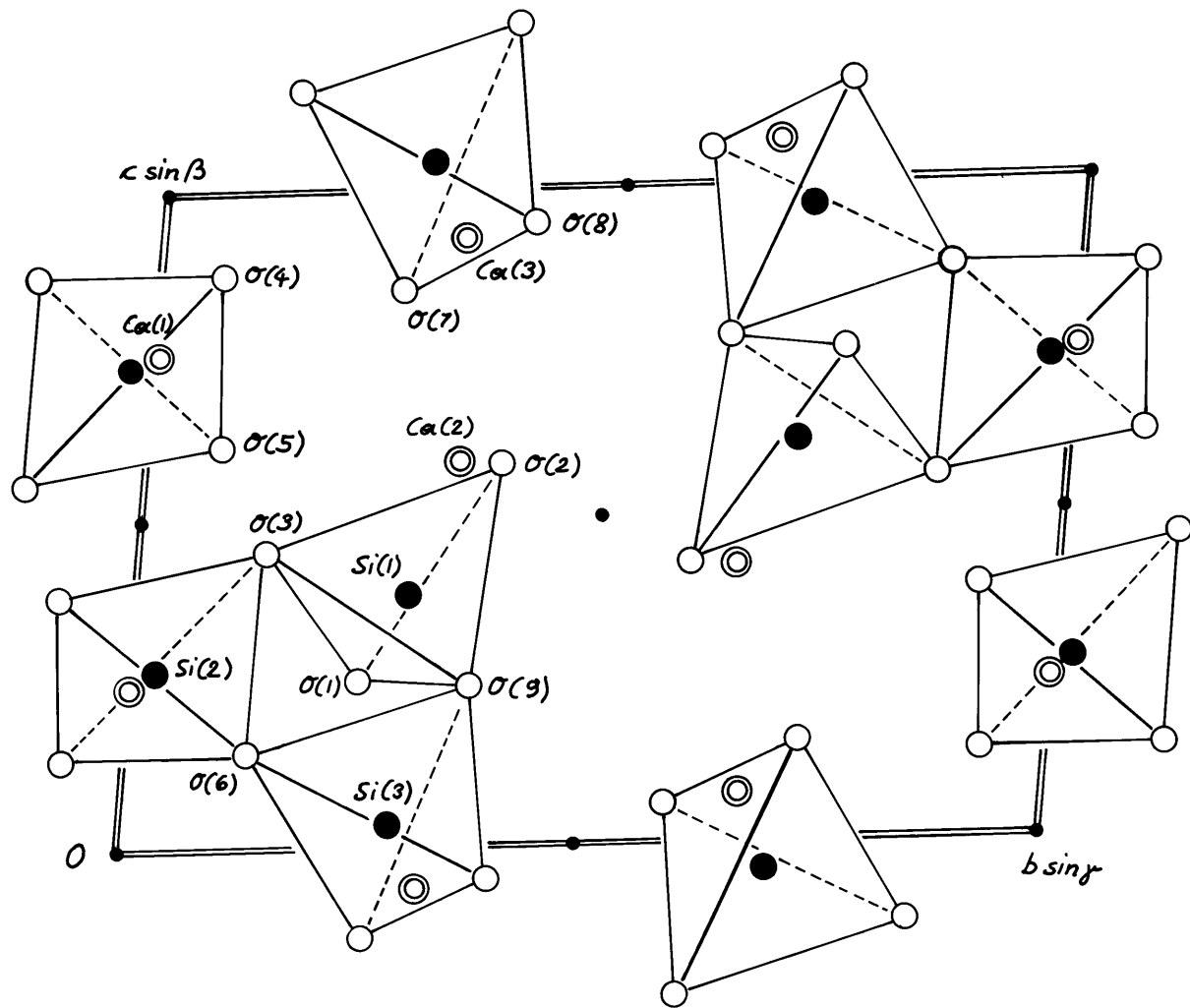


Table 13. Atomic Coordinates for the High-Pressure Polymorph  
of  $\text{CaSiO}_3$ .

Atom	$\underline{x}$	$\sigma(\underline{x})$	$\underline{y}$	$\sigma(\underline{y})$	$\underline{z}$	$\sigma(\underline{z})$
Ca(1)	0.7441	0.0003	0.0002	0.0003	0.7623	0.0003
Ca(2)	0.8789	0.0003	0.3513	0.0003	0.5846	0.0003
Ca(3)	0.2443	0.0003	0.3356	0.0003	0.9245	0.0003
Si(1)	0.3684	0.0004	0.2951	0.0004	0.3916	0.0004
Si(2)	0.7583	0.0004	0.0162	0.0004	0.2701	0.0004
Si(3)	0.7218	0.0004	0.3009	0.0004	0.0416	0.0004
O(1)	0.2150	0.0010	0.2564	0.0009	0.2656	0.0009
O(2)	0.2140	0.0009	0.4055	0.0008	0.5843	0.0009
O(3)	0.5556	0.0010	0.1359	0.0009	0.4518	0.0009
O(4)	0.3391	0.0010	0.0612	0.0009	0.8715	0.0010
O(5)	0.0629	0.0010	0.0932	0.0009	0.6140	0.0010
O(6)	0.8661	0.0010	0.1386	0.0009	0.1353	0.0010
O(7)	0.6282	0.0010	0.2629	0.0009	0.8591	0.0009
O(8)	0.8650	0.0010	0.4031	0.0009	0.9540	0.0010
O(9)	0.5154	0.0010	0.3853	0.0009	0.2426	0.0009

Each layer is connected with the neighboring layers both by  $\text{Si}_3\text{O}_9$  rings and by two Ca(2) octahedra which are located above and below each layer. In Fig. 13, centrosymmetrically related parts of two neighboring layers are shown. The polyhedra to the right (dark shading) are part of the same layer illustrated in Fig. 12. The polyhedra to the left (light shading) belong to the centrosymmetrical layer below. A pair of Ca(2) octahedra (cross-hatched) links those two layers. This connection can be described as follows: The Ca(2) octahedron on the right shares two edges with two Ca(1) polyhedra belonging to the layer above. The same octahedron also shares corners with two Ca(3) octahedra of the layer above and shares a corner with one Ca(3) octahedron in the layer below. The other Ca(2) octahedron on the left is linked up in a centrosymmetrical way. The two Ca(2) octahedra themselves share an edge with each other. The coordination octahedron around Ca(2) is highly distorted so that the average Ca-O distance,  $2.467 \text{ \AA}$ , is larger than the one for the more regular Ca(3) coordination polyhedron which has an average Ca-O distance of  $2.375 \text{ \AA}$ .

As pointed out before, the Ca(1) and Ca(3) polyhedra form an incomplete layer. In Fig. 12 the Ca(2) octahedra, actually located above and below the layer, are projected onto the layer. As seen in this figure, these octahedra fit the voids of the layer very well. Thus it is geometrically possible to obtain a layer of linked polyhedra by stuffing the Ca(2) octahedra next to Ca(3). Only minor distortions of the Ca(2) octahedra would be necessary to make them share edges with their neighboring polyhedra. The result would be a distorted but complete layer composed of oxygen octahedra and scalenohedra sharing edges with each other.

Fig. 12. The Ca-O layer in high-pressure  $\text{CaSiO}_3$ . The Ca(1) and Ca(3) polyhedra within the layer have dark shading. The Ca(2) octahedra (cross-hatched), actually above and below the layer, are projected onto the layer.

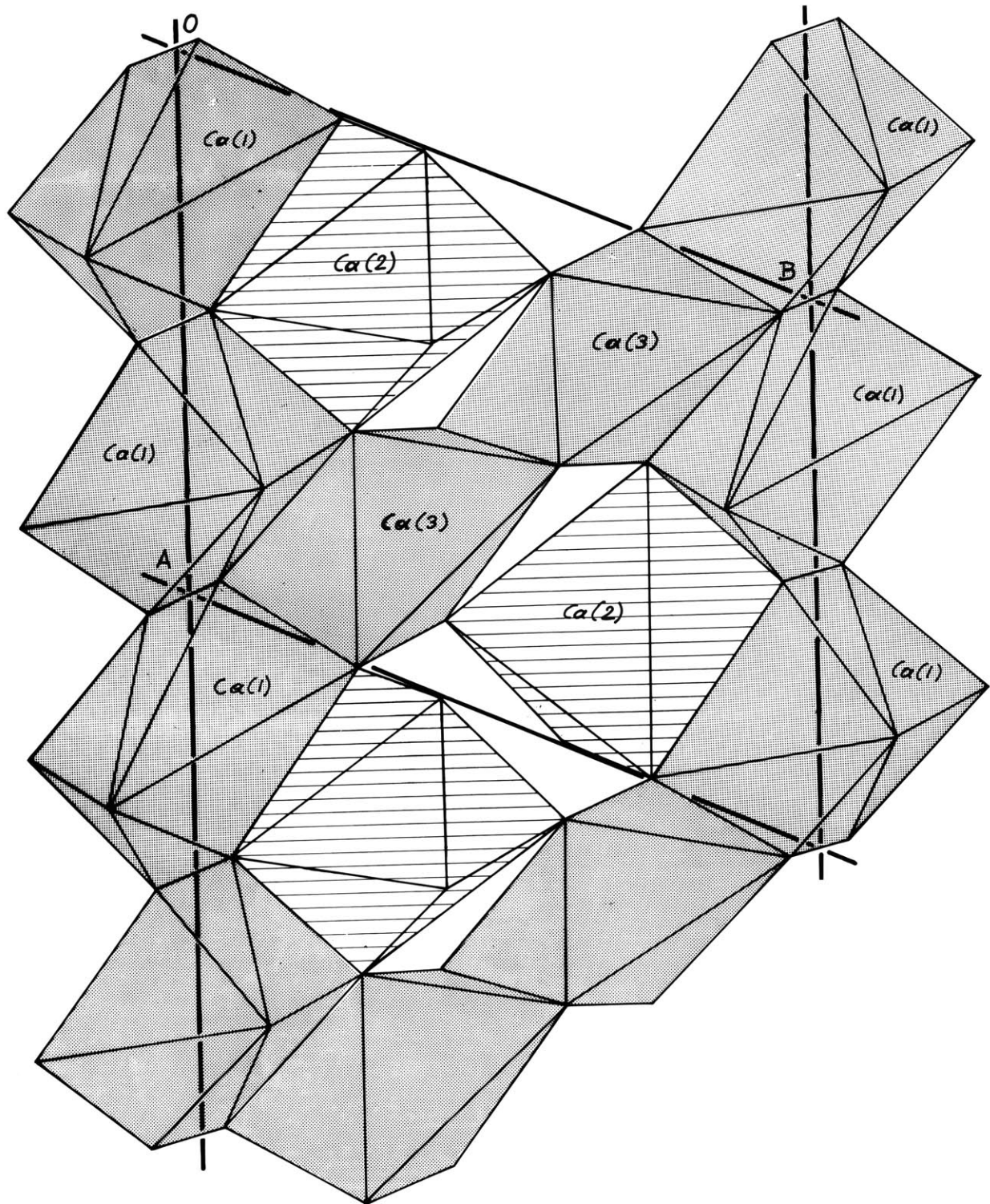


Fig. 13. Graphic presentation of the Ca(2) octahedra connecting two sections of neighboring layers in high-pressure  $\text{CaSiO}_3$ . The polyhedra to the right with dark shading belong to the same layer illustrated in Fig. 12. The polyhedra to the left have light shading and belong to the layer below. The Ca(2) octahedra are cross-hatched.



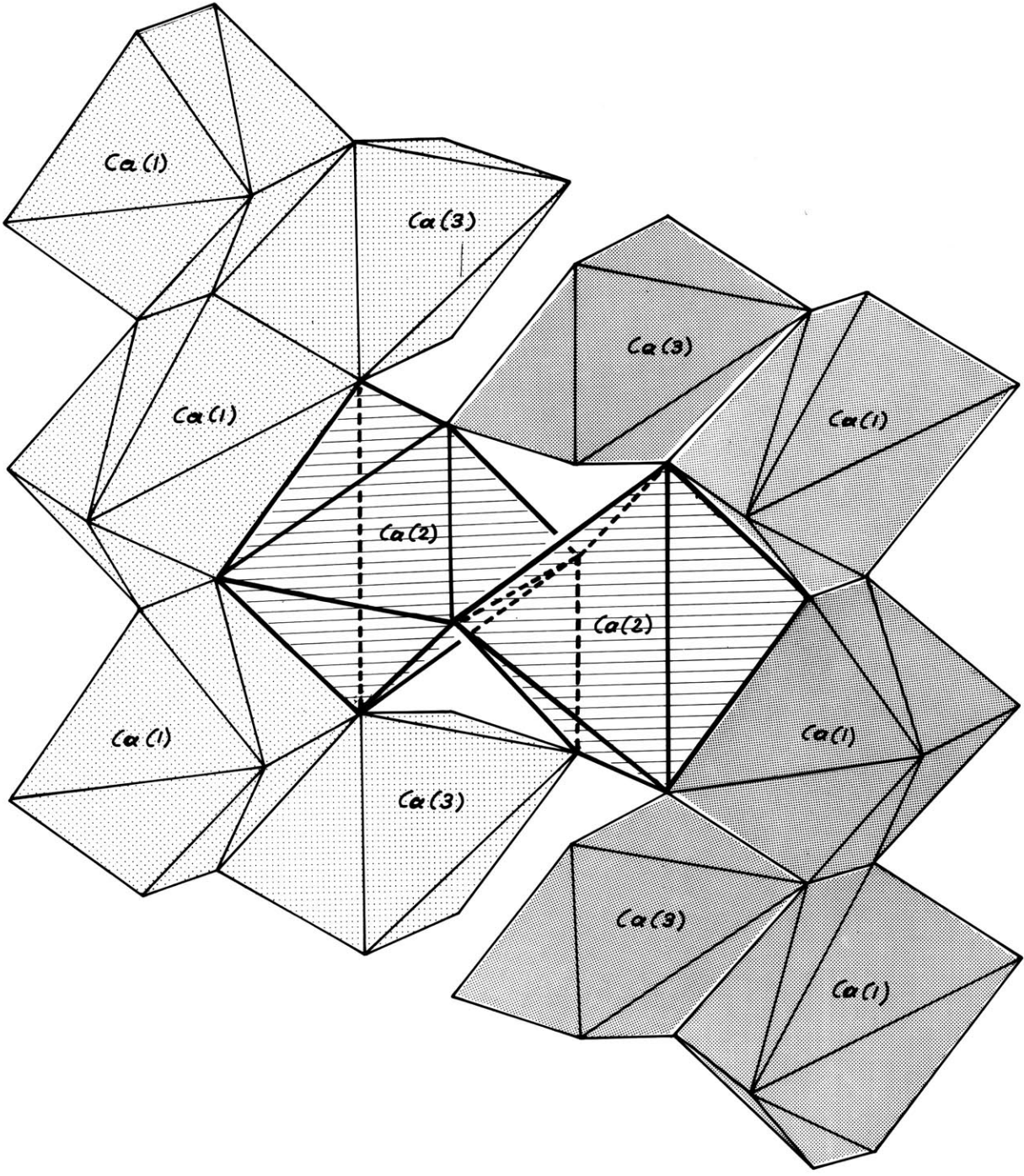


Fig. 14. Schematic projection of the structure of high-pressure  $\text{CaSiO}_3$  parallel (101). The  $\text{Si}_3\text{O}_9$  rings and the Ca(2) octahedra are located between the layers composed of Ca(1) and Ca(3). The layers are cross-hatched, the Ca(2) octahedra have light shading, and the rings have dark shading.  $\delta$  is the acute angle between the planes (100) and (101).

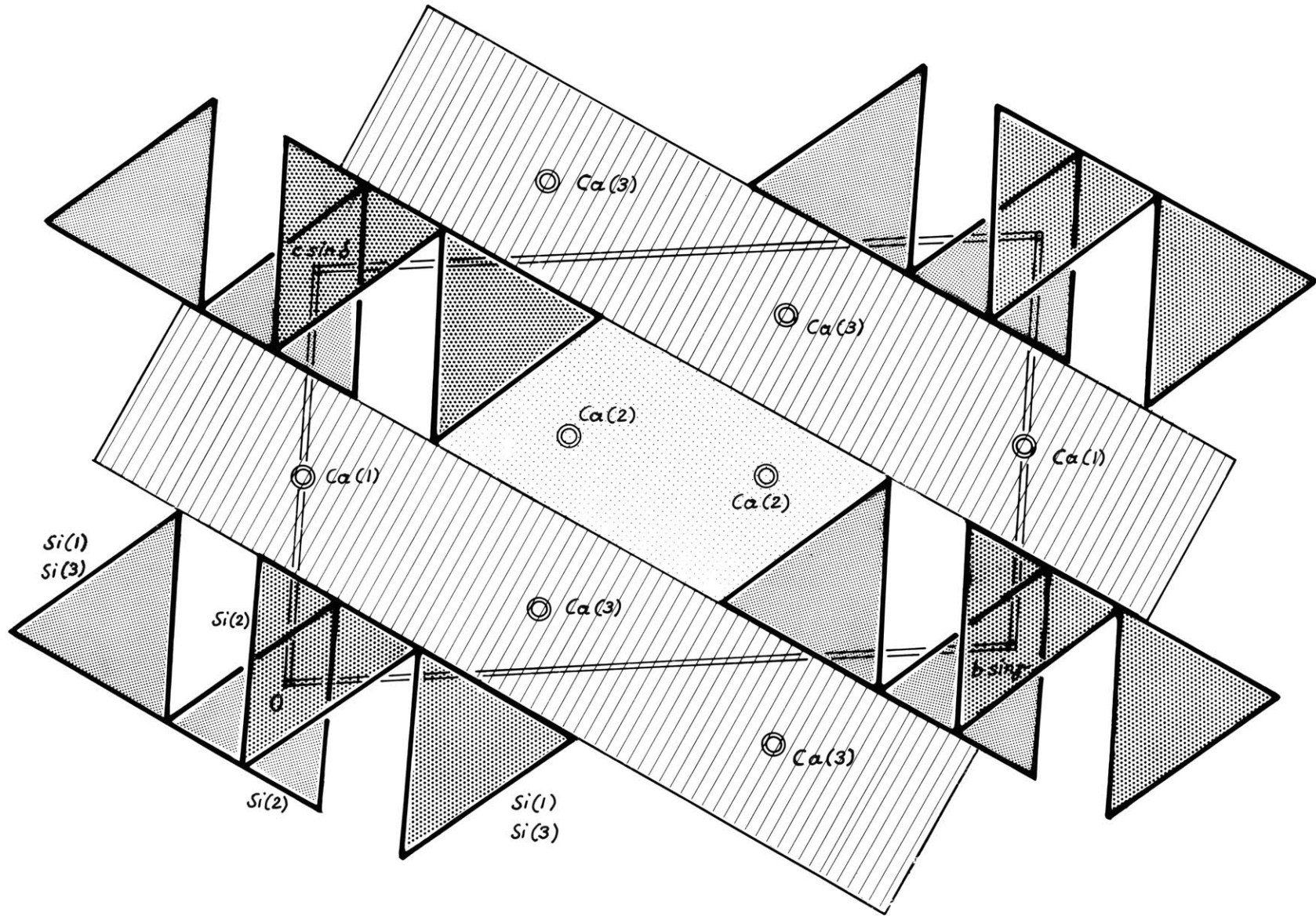
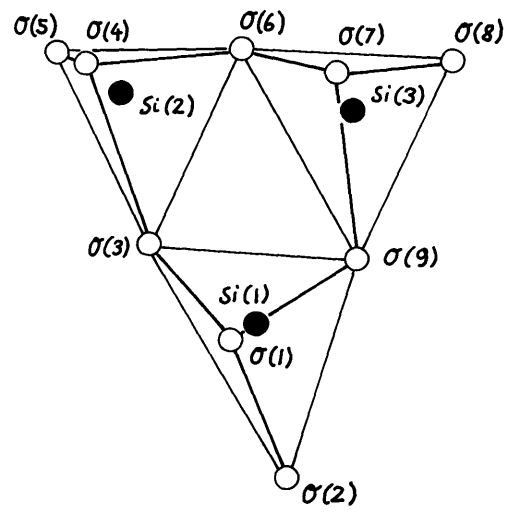
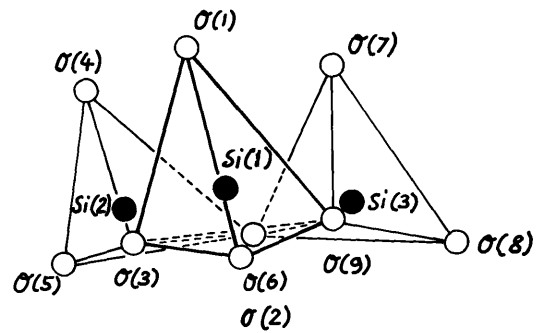


Fig. 15. A silicon-oxygen ring in high-pressure  $\text{CaSiO}_3$  .  
(a) Projected in direction normal to the Ca plane.  
(b) Viewed parallel to the Ca plane.



(a)



(b)

Fig. 16. The orientation of the Ca planes in the reduced cell of high-pressure  $\text{CaSiO}_3$ . The Ca planes are shaded.

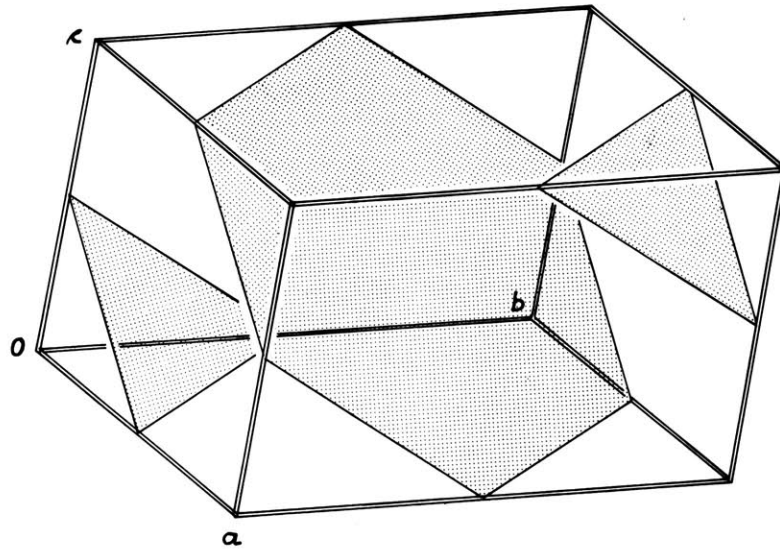


Table 14. Interatomic distances for high-pressure  $\text{CaSiO}_3$ , distances.  
 Atoms with a Primed Number are Equivalent by Symmetry to  
 Atoms of the same Number without Primes.

Atoms	distance	$\sigma$
Ca(1)-0(1')	2.314 Å	0.009 Å
Ca(1)-0(3)	2.709	0.007
Ca(1)-0(4)	2.506	0.007
Ca(1)-0(5)	2.446	0.007
Ca(1)-0(5')	2.529	0.007
Ca(1)-0(5'')	2.580	0.007
Ca(1)-0(6')	2.725	0.007
<u>Ca(1)-0(7)</u>	<u>2.368</u>	0.008
Average	2.630	
Ca(3)-0(1)	2.329	0.007
Ca(3)	2.358	0.006
Ca(3)-0(4)	2.426	0.009
Ca(3)-0(7)	2.364	0.006
Ca(3)-0(8)	2.363	0.007
<u>Ca(3)-0(8')</u>	<u>2.409</u>	0.008
Average	2.375	
Si(1)-0(1)	1.607	0.007
Si(1)-0(2)	1.603	0.007
Si(1)-0(3)	1.683	0.008
<u>Si(1)-0(9)</u>	<u>1.626</u>	0.007
Average	1.630	



Table 14. Continued.

Atoms	distance	$\sigma$
Ca(2)-O(1'')	2.637 Å	0.006 Å
Ca(2)-O(2')	2.412	0.007
Ca(2)-O(2'')	2.458	0.006
Ca(2)-O(5')	2.314	0.008
Ca(2)-O(7)	2.472	0.007
<u>Ca(2)-O(8)</u>	<u>2.510</u>	0.007
Average	2.467	
Si(2)-O(3)	1.701	0.007
Si(2)-O(4''')	1.589	0.007
Si(2)-O(5'')	1.609	0.007
<u>Si(2)-O(6)</u>	<u>1.652</u>	0.008
Average	1.638	
Si(3)-O(6)	1.669	0.008
Si(3)-O(7')	1.600	0.007
Si(3)-O(8''')	1.558	0.008
<u>Si(3)-O(9)</u>	<u>1.681</u>	0.007
Average	1.627	

Table 15. Bond Angles for High-Pressure  $\text{CaSiO}_3$ . Atoms with a Primed Number are Equivalent by Symmetry to Atoms of the same Number without Primes.

Atoms	angle	Atoms	angle
0(4)-Ca(1)-0(5')	148°06'	0(3)-Si(2)-0(6)	100°56'
0(1')-Ca(1)-0(4')	79°54'	0(4''')-Si(2)-0(3)	110°56'
0(1')-Ca(1)-0(5'')	71°30'	0(4''')-Si(2)-0(5'')	118°29'
0(5'')-Ca(1)-0(3)	60°37'	0(4''')-Si(2)-0(6)	110°08'
0(3)-Ca(1)-0(7)	78°28'	0(5'')-Si(2)-0(3)	107°37'
0(7)-Ca(1)-0(6')	72°45'	0(5'')-Si(2)-0(6)	107°11'
0(4)-Ca(1)-0(6')	73°21'		
0(2'')-Ca(2)-0(7)	131°40'	0(1)-Si(1)-0(2)	108°03'
0(5')-Ca(2)-0(1'')	70°25'	0(1)-Si(1)-0(3)	112°23'
0(1'')-Ca(2)-0(2'')	61°11'	0(1)-Si(1)-0(9)	108°55'
0(2'')-Ca(2)-0(8)	73°20'	0(2)-Si(1)-0(9)	108°43'
0(5')-Ca(2)-0(8)	91°10'	0(3)-Si(1)-0(2)	115°10'
0(7)-Ca(3)-0(8)	174°11'	0(3)-Si(1)-0(9)	130°19'
0(1)-Ca(3)-0(4)	79°59'		
0(4)-Ca(3)-0(2)	96°41'		
0(4)-Ca(3)-0(8)	97°37'		
0(1)-Ca(3)-0(8)	92°34'		

Table 15. Continued.

Atoms	angle
O(6)-Si(3)-O(7')	109°58'
O(6)-Si(3)-O(8''')	111°14'
O(6)-Si(3)-O(9)	104°40'
O(7')-Si(3)-O(8''')	108°16'
O(8''')-Si(3)-O(9)	112°39'
O(9)-Si(3)-O(7')	110°01'
Si(1)-O(3)-Si(2)	122°56'
Si(1)-O(9)-Si(3)	123°20'
Si(3)-O(6)-Si(2)	124°03'
O(3)-O(6)-O(9)	59°23'
O(3)-O(9)-O(6)	59°03'
O(6)-O(3)-O(9)	61°34'
Si(1)-Si(3)-Si(2)	61°10'
Si(2)-Si(1)-Si(3)	59°47'
Si(3)-Si(2)-Si(1)	59°03'

The Si atoms are tetrahedrally coordinated by oxygens. The tetrahedra share corners to form three-member rings, seen in Fig. 11, which are located between the layers and next to Ca(2). A schematic presentation of this arrangement is given in Fig. 14. This shows that two rings in the central interlayer space are separated by a pair of Ca(2) octahedra. The Si rings are rather compact units with only minor distortions, as seen in Fig. 15. The average Si-O distances are roughly equal: Si(1)-O = 1.630 Å, Si(2)-O = 1.638 Å, and Si(3)-O = 1.627 Å. The deviation from the ideal tetrahedral angle = 109°28' does not exceed 11°11'. This is a relative small discrepancy if compared with a deviation of 20°02' reported by Trojer (1968) for wollastonite. The silicons within a Si<sub>3</sub>O<sub>9</sub> group form an equilateral triangle to good approximation as seen from the bond angles listed in Table 15.

The anisotropic temperature coefficients for this high-pressure phase of CaSiO<sub>3</sub> are found in Table 16. The thermal parameters are listed in Table 17. The  $q_i$ 's are the three principal axes of the thermal-vibration ellipsoid. To each magnitude  $q_i$  there corresponds a temperature factor  $B_i$  along the principal axis  $i$ . An average temperature factor  $B$  is defined by  $B = (B_1 + B_2 + B_3)/3$ , which is comparable to the regular isotropic temperature factor; this is given in the last column of this table. The temperature factors found in this crystal structure are slightly higher than those published for wollastonite by Buerger and Prewitt (1961).

Table 16. Anisotropic Temperature Coefficients for High-Pressure CaSiO<sub>3</sub>.

Atoms	$\beta_{11}$	$\beta_{22}$	$\beta_{33}$	$\beta_{12}$	$\beta_{13}$	$\beta_{23}$
Ca(1) $\sigma$	0.0059 0.0006	0.0062 0.0004	0.0029 0.0004	-.0024 0.0003	-.0008 0.0004	0.0005 0.0003
Ca(2) $\sigma$	0.0047 0.0005	0.0065 0.0004	0.0048 0.0004	-.0016 0.0004	-.0007 0.0004	0.0000 0.0003
Ca(3) $\sigma$	0.0048 0.0005	0.0064 0.0004	0.0023 0.0004	-.0019 0.0003	-.0014 0.0003	-.0002 0.0003
Si(1) $\sigma$	0.0023 0.0007	0.0060 0.0005	0.0023 0.0005	-.0010 0.0004	-.0003 0.0005	-.0008 0.0004
Si(2) $\sigma$	0.0048 0.0007	0.0051 0.0005	0.0024 0.0006	-.0016 0.0005	-.0011 0.0005	-.0006 0.0004
Si(3) $\sigma$	0.0050 0.0007	0.0063 0.0005	0.0019 0.0006	-.0018 0.0005	-.0006 0.0005	-.0004 0.0004
O(1) $\sigma$	0.0038 0.0019	0.0110 0.0015	0.0038 0.0015	-.0035 0.0015	-.0030 0.0013	0.0013 0.0011
O(2) $\sigma$	0.0018 0.0016	0.0044 0.0012	0.0040 0.0015	0.0000 0.0011	-.0001 0.0012	-.0009 0.0010
O(3) $\sigma$	0.0106 0.0021	0.0067 0.0014	0.0039 0.0015	-.0057 0.0013	-.0024 0.0013	0.0004 0.0011
O(4) $\sigma$	0.0062 0.0020	0.0096 0.0015	0.0053 0.0016	-.0045 0.0013	-.0047 0.0014	0.0009 0.0011
O(5) $\sigma$	0.0067 0.0019	0.0073 0.0014	0.0067 0.0017	-.0026 0.0012	0.0033 0.0014	0.0004 0.0011
O(6) $\sigma$	0.0059 0.0020	0.0074 0.0014	0.0094 0.0017	-.0036 0.0013	-.0037 0.0014	0.0005 0.0011
O(7) $\sigma$	0.0055 0.0019	0.0100 0.0015	0.0034 0.0016	-.0039 0.0013	-.0024 0.0013	-.0005 0.0011
O(8) $\sigma$	0.0057 0.0019	0.0048 0.0013	0.0034 0.0016	-.0019 0.0012	-.0021 0.0013	0.0000 0.0010
O(9) $\sigma$	0.0038 0.0019	0.0078 0.0014	0.0022 0.0015	-.0021 0.0012	0.0004 0.0013	0.0002 0.0010

Table 17. Thermal Parameters for High-Pressure  $\text{CaSiO}_3$ .

Atom	$\underline{q}_1$	$\underline{B}_{-1}$	$\underline{q}_2$	$\underline{B}_{-2}$	$\underline{q}_2$	$\underline{B}_{-3}$	Equivalent isotropic $\underline{B}$
Ca(1) $\sigma$	0.110 Å 0.005	0.95 Å <sup>2</sup> 0.08	0.161 Å 0.005	2.06 Å <sup>2</sup> 0.13	0.078 Å 0.006	0.48 Å <sup>2</sup> 0.07	1.16 Å <sup>2</sup> 0.05
Ca(2) $\sigma$	0.091 0.004	0.65 0.06	0.167 0.005	2.19 0.12	0.108 0.003	0.92 0.05	1.25 0.05
Ca(3) $\sigma$	0.097 0.005	0.74 0.08	0.164 0.005	2.13 0.12	0.070 0.006	0.39 0.07	1.08 0.05
Si(1) $\sigma$	0.081 0.006	0.52 0.08	0.160 0.007	2.01 0.17	0.059 0.007	0.28 0.07	0.94 0.07
Si(2) $\sigma$	0.096 0.007	0.73 0.10	0.147 0.007	1.70 0.16	0.072 0.010	0.41 0.11	0.95 0.07
Si(3) $\sigma$	0.100 0.007	0.79 0.11	0.164 0.007	2.12 0.17	0.063 0.009	0.31 0.09	1.07 0.07
O(1) $\sigma$	0.074 0.020	0.43 0.23	0.213 0.017	3.58 0.56	0.090 0.016	0.64 0.23	1.55 0.21
O(2) $\sigma$	0.042 0.035	0.36 0.25	0.139 0.018	1.54 0.39	0.095 0.016	0.71 9.24	0.87 0.17
O(3) $\sigma$	0.142 0.014	1.60 0.34	0.162 0.017	2.06 0.44	0.092 0.017	0.67 0.25	1.11 0.19
O(4) $\sigma$	0.093 0.013	0.68 0.19	0.196 0.015	3.04 0.47	0.114 0.012	1.02 0.21	1.58 0.15
O(5) $\sigma$	0.113 0.016	1.00 0.29	0.174 0.016	2.39 0.43	0.120 0.014	1.13 0.27	1.51 0.19
O(6) $\sigma$	0.105 0.018	0.87 0.29	0.174 0.016	2.38 0.45	0.133 0.013	1.40 0.28	1.55 0.20
O(7) $\sigma$	0.102 0.017	0.83 0.28	0.201 0.014	3.18 0.46	0.084 0.019	0.56 0.25	1.52 0.19
O(8) $\sigma$	0.103 0.016	0.84 0.25	0.144 0.018	1.63 0.40	0.118 0.014	1.10 0.26	1.19 0.18
O(9) $\sigma$	0.094 0.016	0.70 0.24	0.181 0.016	2.59 0.45	0.063 0.020	0.32 0.20	1.20 0.18

Table 18. Observed and Calculated Structure Factors of High-Pressure  $\text{CaSiO}_3$ .

<u>h</u>	<u>k</u>	<u>l</u>	<u> F<sub>o</sub> </u>	<u>F<sub>c</sub></u>	<u>h</u>	<u>k</u>	<u>l</u>	<u> F<sub>o</sub> </u>	<u>F<sub>c</sub></u>
0	0	1	10.20	10.34	5	0	-3	49.50	-46.38
0	0	2	4.42	3.58	5	0	-2	5.54	6.62
0	0	3	10.10	8.14	5	0	-1	30.84	-29.00
0	0	4	3.04	-1.76	5	0	0	11.68	-11.64
0	0	5	22.42	19.38	5	0	1	13.66	12.34
0	0	6	74.26	-70.92	5	0	2	33.16	-31.24
0	0	7	2.24	6.78	5	0	3	54.64	52.64
1	0	-6	5.14	4.28	5	0	5	15.44	13.56
1	0	-5	4.82	-4.78	5	0	4	10.80	10.20
1	0	-4	55.36	-55.46	6	0	-3	10.20	-10.34
1	0	-3	25.80	-25.28	6	0	-2	13.54	16.14
1	0	-2	31.24	-29.50	6	0	-1	6.38	-5.98
1	0	-1	1.40	-1.80	6	0	0	32.46	-37.54
1	0	0	2.60	-0.12	6	0	1	8.96	-9.64
1	0	1	17.70	-17.06	6	0	2	4.78	-7.06
1	0	2	68.20	64.82	6	0	3	7.82	-5.88
1	0	3	63.18	60.06	6	0	4	25.24	-29.20
1	0	4	40.66	39.74	6	0	5	10.74	14.00
1	0	5	16.92	15.98	7	0	-1	1.80	1.58
1	0	6	18.64	-16.10	7	0	0	2.74	-6.52
1	0	7	28.28	26.88	7	0	2	3.12	-3.32
2	0	-7	20.68	20.92	7	0	3	2.86	-0.28
2	0	-6	30.56	30.16	-7	1	-3	1.64	-1.50
2	0	-5	39.16	37.82	-7	1	-1	10.32	-11.72
2	0	-4	24.02	-23.00	-7	1	0	2.08	-1.72
2	0	-3	9.14	-9.26	-6	1	-5	13.32	11.86
2	0	-2	11.88	11.62	-6	1	-4	21.36	-21.60
2	0	-1	59.96	-56.90	-6	1	-3	2.84	3.84
2	0	0	109.86	-99.38	-6	1	-2	48.72	48.94
2	0	1	56.18	-48.78	-6	1	-1	11.18	9.66
2	0	2	21.68	18.94	-6	1	1	10.14	-9.66
2	0	3	26.50	-25.12	-5	1	-6	32.02	-31.36
2	0	4	32.66	-31.10	-5	1	-5	23.10	-22.76
2	0	5	17.38	-16.56	-5	1	-4	9.98	-11.48
2	0	6	45.00	42.80	-5	1	-3	15.96	-15.48
2	0	7	7.40	-5.06	-5	1	-2	39.18	-38.46
3	0	-6	22.22	20.86	-5	1	-1	2.74	-2.26
3	0	-5	18.18	17.28	-5	1	0	18.14	15.06
3	0	-4	12.78	9.94	-5	1	1	20.52	23.22
3	0	-3	62.90	62.44	-5	1	2	36.42	39.76
3	0	-2	0.56	3.10	-5	1	3	6.90	6.76
3	0	-1	27.02	25.44	-5	1	4	8.88	8.28
3	0	0	20.42	-18.30	-4	1	-7	7.86	11.84
3	0	1	5.84	5.60	-4	1	-6	20.34	-18.56
3	0	2	4.42	-1.20	-4	1	-5	19.94	19.30
3	0	3	71.22	-67.90	-4	1	-4	2.00	2.28
3	0	4	50.02	-49.46	-4	1	-3	5.54	-1.98
3	0	5	18.20	-17.02	-4	1	-2	38.44	-36.92
3	0	6	4.82	5.58	-4	1	-1	27.14	-25.48
4	0	-5	23.14	-20.88	-4	1	0	20.90	19.74
4	0	-4	42.40	38.76	-4	1	1	41.86	-40.82
4	0	-3	10.16	8.10	-4	1	2	22.06	-20.92
4	0	-2	43.46	-40.84	-4	1	3	2.02	-0.28
4	0	-1	41.40	37.32	-4	1	4	25.60	23.02
4	0	0	26.66	22.76	-4	1	5	9.28	8.54
4	0	1	36.60	33.10	-3	1	-7	11.62	-10.84
4	0	2	26.58	-24.34	-3	1	-6	52.56	53.26
4	0	3	18.30	15.84	-3	1	-5	54.70	51.80
4	0	4	88.12	84.32	-3	1	-4	9.68	-9.06
4	0	5	38.90	-33.94	-3	1	-3	91.72	88.56
4	0	6	18.18	-17.94	-3	1	-2	32.86	-30.92
4	0	7	23.96	-22.74	-3	1	-1	25.58	23.04
5	0	-4	18.72	-17.40	-3	1	0	13.02	-10.76
					-3	1	1	32.68	-30.74

Table 18. Continued.

<u>h</u>	<u>k</u>	<u>l</u>	<u> F<sub>o</sub> </u>	<u>F<sub>c</sub></u>	<u>h</u>	<u>k</u>	<u>l</u>	<u> F<sub>o</sub> </u>	<u>F<sub>c</sub></u>
-3	1	2	19.52	20.50	2	1	-3	25.10	23.96
-3	1	3	44.36	-44.62	2	1	-2	100.64	101.26
-3	1	4	16.16	16.38	2	1	-1	35.44	-33.56
-3	1	5	6.44	-7.42	2	1	0	7.84	3.22
-3	1	6	32.26	-28.78	2	1	1	23.76	-16.54
-2	1	-7	21.40	-21.66	2	1	2	73.06	70.38
-2	1	-6	26.62	26.80	2	1	3	6.38	5.04
-2	1	-5	7.72	-6.22	2	1	4	65.26	-63.54
-2	1	-4	18.90	-18.32	2	1	5	33.50	32.86
-2	1	-3	27.96	28.84	2	1	6	13.90	14.10
-2	1	-2	68.08	65.62	2	1	7	4.72	5.34
-2	1	-1	40.68	35.66	3	1	-6	26.28	-25.72
-2	1	0	43.88	-39.72	3	1	-5	13.52	-13.80
-2	1	1	5.36	5.46	3	1	-4	3.12	3.08
-2	1	2	47.52	47.52	3	1	-3	23.38	-20.50
-2	1	3	17.94	-17.90	3	1	-2	22.14	-21.16
-2	1	4	10.70	-11.18	3	1	-1	37.36	-36.42
-2	1	5	29.62	-28.20	3	1	0	74.74	69.32
-2	1	6	25.82	26.28	3	1	1	51.78	47.86
-1	1	-7	14.78	-14.90	3	1	2	40.16	37.24
-1	1	-6	52.36	-52.26	3	1	3	14.76	-14.28
-1	1	-5	51.38	-49.90	3	1	4	25.94	-26.38
-1	1	-4	2.62	.02	3	1	5	2.50	-1.78
-1	1	-3	3.56	-2.02	3	1	6	32.28	-33.28
-1	1	-1	27.94	-25.18	3	1	7	3.30	-2.70
-1	1	-2	6.90	-7.02	4	1	-5	31.70	29.92
-1	1	0	4.44	-4.00	4	1	-4	26.16	23.80
-1	1	1	11.56	10.94	4	1	-3	7.74	-7.34
-1	1	2	66.40	-66.46	4	1	-2	21.96	-18.88
-1	1	3	27.36	26.22	4	1	-1	9.92	-8.42
-1	1	4	21.92	-20.64	4	1	0	34.76	32.38
-1	1	5	24.66	23.84	4	1	1	15.58	-15.26
-1	1	6	24.08	21.92	4	1	2	29.04	-28.22
-1	1	7	29.76	-28.46	4	1	3	46.02	44.54
0	1	-7	11.62	11.84	4	1	4	43.00	40.80
0	1	-6	10.12	11.72	4	1	5	10.42	-10.46
0	1	-5	10.54	-8.44	4	1	6	16.98	-16.62
0	1	-4	29.54	29.82	4	1	7	11.96	-11.30
0	1	-3	67.22	-67.84	5	1	-4	0.	-1.06
0	1	-2	85.28	-84.92	5	1	-3	29.62	27.64
0	1	-1	4.56	-2.62	5	1	-2	9.28	-9.78
0	1	1	10.02	-8.14	5	1	-1	11.32	11.36
0	1	2	53.54	-54.02	5	1	0	9.14	-9.08
0	1	3	20.28	21.50	5	1	1	41.64	-40.32
0	1	4	23.60	23.42	5	1	2	8.06	5.80
0	1	5	20.52	-20.32	5	1	3	6.92	-7.50
0	1	6	6.20	-6.98	5	1	4	39.84	39.12
0	1	7	1.36	1.38	5	1	5	5.44	3.86
1	1	-7	17.26	17.16	5	1	6	6.44	-5.26
1	1	-6	25.24	24.62	5	1	7	28.00	29.36
1	1	-5	10.94	9.02	6	1	-3	12.70	11.92
1	1	-4	30.18	29.76	6	1	-2	11.36	9.12
1	1	-3	43.80	-43.34	6	1	-1	26.40	26.20
1	1	-2	56.68	54.50	6	1	0	67.32	-64.76
1	1	-1	7.62	-7.30	6	1	1	21.44	20.40
1	1	1	47.02	41.60	6	1	2	14.90	15.54
1	1	2	79.32	-79.18	6	1	3	50.78	-50.46
1	1	3	43.30	43.34	6	1	4	16.56	-16.74
1	1	4	8.08	-6.34	6	1	5	29.62	-31.94
1	1	5	12.96	12.68	6	1	6	37.80	37.70
1	1	6	15.76	14.50	7	1	-1	0.	-3.38
1	1	7	2.44	.70	7	1	0	3.70	-.06
2	1	-6	15.14	-14.44	7	1	1	7.08	8.86
2	1	-5	14.20	13.26					
2	1	-4	60.96	-61.60					



Table 18. Continued.

<u>h</u>	<u>k</u>	<u>l</u>	<u> F<sub>o</sub></u>	<u>F<sub>c</sub></u>	<u>h</u>	<u>k</u>	<u>l</u>	<u> F<sub>o</sub></u>	<u>F<sub>c</sub></u>
7	1	2	7.68	-9.66	-1	2	7	33.56	32.72
7	1	3	7.56	-12.02	0	2	-7	1.08	2.54
7	1	4	3.80	-4.90	0	2	-6	20.40	-20.58
-6	2	-4	14.28	-14.30	0	2	-5	14.24	13.64
-6	2	-3	13.64	-15.06	0	2	-4	30.48	30.74
-5	2	-6	1.22	4.10	0	2	-3	40.00	41.48
-5	2	-5	10.84	11.46	0	2	-2	52.30	-52.24
-5	2	-4	21.96	21.56	0	2	1	28.00	-29.80
-5	2	-3	18.46	-18.92	0	2	3	63.02	-62.32
-5	2	-2	.14	-1.46	0	2	4	45.94	45.42
-5	2	-1	15.94	-15.06	0	2	5	29.26	-27.74
-5	2	0	18.60	-19.96	0	2	6	8.42	8.20
-5	2	2	2.30	-4.98	0	2	7	4.04	2.52
-4	2	-6	28.12	-27.00	1	2	7	15.76	-16.84
-4	2	-5	0.	0.	1	2	-6	22.22	22.46
-4	2	-4	6.20	5.20	1	2	-5	19.74	20.90
-4	2	-3	5.46	6.40	1	2	-4	5.52	-5.28
-4	2	-2	16.40	-16.56	1	2	-3	9.78	10.48
-4	2	-1	42.74	-43.46	1	2	-2	47.20	46.44
-4	2	0	52.60	53.66	1	2	-1	13.96	14.24
-4	2	1	21.74	-22.60	1	2	1	13.86	-15.26
-4	2	2	25.22	-24.48	1	2	2	44.86	-44.10
-4	2	3	14.14	-13.56	1	2	3	12.58	-13.08
-4	2	4	6.36	-6.52	1	2	4	31.60	-31.60
-3	2	-7	4.04	-3.72	1	2	5	44.98	-43.80
-3	2	-6	3.06	-3.50	1	2	6	46.84	-45.10
-3	2	-5	3.18	-3.74	1	2	7	18.90	-16.84
-3	2	-4	0.	-3.28	2	2	-6	23.18	24.64
-3	2	-3	20.58	-21.02	2	2	-5	48.34	-50.04
-3	2	-2	20.96	20.30	2	2	-4	24.96	-25.54
-3	2	-1	6.68	-5.30	2	2	-3	5.42	6.20
-3	2	0	26.36	24.34	2	2	-2	29.46	30.50
-3	2	1	4.44	-3.24	2	2	-1	52.46	52.94
-3	2	2	22.92	-22.74	2	2	0	46.16	-42.06
-3	2	3	9.12	10.02	2	2	1	102.68	94.80
-3	2	4	8.84	-8.26	2	2	2	9.38	8.30
-3	2	5	12.46	-12.50	2	2	3	12.72	-12.62
-2	2	-7	15.30	16.52	2	2	4	2.24	-1.82
-2	2	-6	9.82	-9.40	2	2	5	0.	-2.22
-2	2	-4	32.78	-35.36	2	2	6	35.32	34.78
-2	2	-3	9.30	8.64	2	2	7	24.24	-23.94
-2	2	-2	50.34	50.62	3	2	-6	6.66	-6.38
-2	2	-1	52.78	-53.94	3	2	-4	23.20	26.30
-2	2	0	14.52	15.68	3	2	-4	26.50	26.30
-2	2	1	10.52	11.38	3	2	-3	85.60	-82.94
-2	2	2	74.88	76.72	3	2	-2	20.92	-19.44
-2	2	3	41.36	43.66	3	2	-1	46.16	-43.66
-2	2	4	24.92	-24.02	3	2	0	56.48	-51.38
-2	2	5	9.92	11.22	3	2	1	53.32	49.28
-2	2	6	0.	-1.40	3	2	2	15.56	-14.46
-1	2	-7	14.80	-16.58	3	2	3	65.50	65.12
-1	2	-6	8.56	-9.40	3	2	4	4.22	4.32
-1	2	-5	8.56	8.54	3	2	5	6.06	4.64
-1	2	-3	25.54	27.80	3	2	6	63.22	62.74
-1	2	-2	18.58	-17.96	3	2	7	1.10	-3.20
-1	2	-1	42.68	38.46	4	2	-5	19.74	20.14
-1	2	0	1.64	5.48	4	2	-4	29.52	30.38
-1	2	1	47.32	-47.80	4	2	-3	14.14	-12.82
-1	2	2	43.40	44.56	4	2	-2	42.14	-43.14
-1	2	3	0.	-2.04	4	2	-1	24.66	-24.36
-1	2	4	15.90	19.12	4	2	0	6.32	5.16
-1	2	5	33.94	36.60	4	2	1	29.46	-27.88
-1	2	6	31.30	29.00	4	2	2	66.04	-65.58
					4	2	3	.94	3.34

Table 18. Continued.

<u>h</u>	<u>k</u>	<u>l</u>	<u> F<sub>o</sub> </u>	<u>F<sub>c</sub></u>	<u>h</u>	<u>k</u>	<u>l</u>	<u> F<sub>o</sub> </u>	<u>F<sub>c</sub></u>
4	2	4	8.26	-9.18	-2	3	1	61.18	-62.12
4	2	5	4.36	3.32	-2	3	2	5.40	3.48
4	2	6	15.86	-15.64	-2	3	3	4.56	3.92
4	2	7	13.38	13.02	-2	3	4	28.86	-29.70
5	2	-4	7.32	8.42	-2	3	5	10.08	10.96
5	2	-3	11.58	11.76	-2	3	6	17.44	18.42
5	2	-2	43.20	46.10	-1	3	-7	21.16	22.70
5	2	-1	25.26	26.56	-1	3	-6	1.48	-0.58
5	2	0	16.14	16.50	-1	3	-5	2.18	4.00
5	2	1	12.02	-12.56	-1	3	-4	51.26	51.28
5	2	2	4.14	5.32	-1	3	-3	1.38	.80
5	2	3	11.52	-12.66	-1	3	-2	78.88	78.08
5	2	4	3.34	.96	-1	3	-1	40.50	-38.68
5	2	5	23.88	-24.10	-1	3	0	2.50	-2.96
5	2	6	37.68	-38.64	-1	3	1	20.90	22.52
6	2	-3	0.	.94	-1	3	2	10.54	-12.42
6	2	-2	35.80	35.76	-1	3	3	17.78	-18.50
6	2	-1	27.28	-26.34	-1	3	4	57.14	-59.72
6	2	0	14.94	17.02	-1	3	5	4.34	-2.22
6	2	1	41.22	44.12	-1	3	6	2.92	5.96
6	2	2	52.94	52.26	0	3	-7	4.08	-2.02
6	2	3	28.16	29.80	0	3	-6	73.82	-75.42
6	2	5	26.98	30.04	0	3	-5	2.74	2.70
6	2	6	5.10	-9.20	0	3	-4	9.68	10.60
7	2	-1	9.90	-13.12	0	3	-3	16.78	-18.28
7	2	0	4.20	-4.80	0	3	-2	17.96	18.58
7	2	1	30.56	-31.06	0	3	0	40.30	129.90
6	2	4	11.62	-12.18	0	3	1	36.90	35.82
7	2	2	22.92	24.60	0	3	2	38.82	-38.20
7	2	3	11.28	-12.76	0	3	3	64.54	66.64
7	2	4	16.00	17.64	0	3	4	19.46	18.86
-5	3	-5	15.50	14.10	0	3	5	22.82	23.04
-5	3	-4	6.70	7.00	0	3	6	32.08	-32.22
-5	3	-3	47.94	50.10	0	3	7	14.16	-12.40
-5	3	-2	13.82	16.02	1	3	-7	8.36	-8.60
-5	3	-1	4.24	6.74	1	3	-6	9.80	-10.70
-5	3	0	0.	.80	1	3	-5	18.20	-20.02
-5	3	2	0.	.68	1	3	-4	32.12	-33.42
-4	3	-6	11.60	-11.88	1	3	-3	7.68	-9.26
-4	3	-5	24.54	-24.28	1	3	-2	21.86	-25.02
-4	3	-4	35.46	36.56	1	3	-1	41.44	-43.74
-4	3	-3	13.46	13.42	1	3	1	34.80	-34.50
-4	3	-2	28.66	-32.86	1	3	2	30.22	32.68
-4	3	-1	48.06	50.78	1	3	3	26.56	26.98
-4	3	0	40.80	43.72	1	3	4	63.26	66.84
-3	3	-7	2.70	2.22	1	3	5	27.50	27.94
-3	3	-6	11.76	10.88	1	3	6	18.22	-20.46
-3	3	-5	27.40	-26.10	1	3	7	27.46	27.98
-3	3	-4	18.48	-19.04	2	3	-6	33.40	35.52
-3	3	-3	60.16	-62.28	2	3	-5	15.60	17.88
-3	3	-2	17.40	-17.68	2	3	-4	23.40	-24.24
-3	3	-1	14.44	-15.58	2	3	-3	0.	.22
-3	3	0	7.04	-10.22	2	3	-2	15.02	15.78
-3	3	1	34.62	36.48	2	3	-1	39.38	42.64
-3	3	2	21.34	-22.30	2	3	0	64.92	-69.46
-3	3	3	43.52	42.88	2	3	1	16.26	-14.76
-3	3	4	12.54	14.62	2	3	2	6.60	-7.46
-3	3	5	.70	.78	2	3	3	44.62	-47.38
-2	3	-7	4.92	3.58	2	3	5	23.82	-25.56
-2	3	-5	32.40	32.34	2	3	6	39.18	40.94
-2	3	-4	20.24	-19.92	2	3	7	15.66	16.14
-2	3	-3	9.38	-8.50	3	3	-6	0.	-1.56
-2	3	-2	5.86	3.46	3	3	-5	26.54	30.08
-2	3	-1	51.98	-50.90					
-2	3	0	93.58	-92.44					

Table 18. Continued.

<u>h</u>	<u>k</u>	<u>l</u>	$ F_o $	$F_c$	<u>h</u>	<u>k</u>	<u>l</u>	$ F_o $	$F_c$
3	3	-4	7.20	7.00	-3	4	-6	17.96	19.82
3	3	-3	59.58	58.46	-3	4	-5	46.66	46.96
3	3	-2	22.64	25.04	-3	4	-4	6.28	-9.46
3	3	-1	25.46	26.50	-3	4	-3	21.10	20.72
3	3	0	22.92	22.26	-3	4	-2	2.52	-7.78
3	3	1	3.76	-5.48	-3	4	-1	2.94	3.88
3	3	2	41.00	42.46	-3	4	0	43.28	42.44
3	3	3	65.90	-67.32	-3	4	1	24.06	-22.20
3	3	4	29.88	-32.42	-3	4	2	14.50	15.44
3	3	5	9.16	-11.30	-3	4	3	5.82	-7.70
3	3	6	7.84	9.32	-3	4	4	2.94	5.26
4	3	-5	17.14	-19.44	-3	4	5	0.	1.50
4	3	-4	21.18	24.04	-2	4	-7	25.18	-23.44
4	3	-3	3.48	-4.84	-2	4	-6	25.70	24.06
4	3	-2	44.96	-48.78	-2	4	-5	17.84	-18.18
4	3	-1	50.66	54.26	-2	4	-4	27.86	-27.94
4	3	0	14.10	13.70	-2	4	-3	24.90	24.98
4	3	1	31.84	32.06	-2	4	-2	44.16	45.06
4	3	2	4.58	-3.58	-2	4	-1	41.80	43.06
4	3	3	4.44	6.30	-2	4	1	34.00	32.80
4	3	4	43.00	46.86	-2	4	2	33.52	34.48
4	3	5	28.64	-31.30	-2	4	3	22.26	-20.54
3	3	7	11.86	-14.02	-2	4	4	8.82	-9.80
4	3	6	27.66	-25.94	-2	4	5	13.96	-16.86
4	3	7	3.92	1.24	-1	4	-7	2.00	.22
5	3	-4	9.18	-9.32	-1	4	-6	16.76	-16.92
5	3	-3	35.86	-39.48	-1	4	-5	24.28	-23.60
5	3	-2	16.00	-16.26	-1	4	-4	16.58	16.76
5	3	-1	13.26	-14.68	-1	4	-3	23.10	-23.22
5	3	0	20.28	-22.66	-1	4	-2	6.78	-7.02
5	3	1	29.82	30.44	-1	4	-1	20.40	-20.34
5	3	2	35.32	-39.68	-1	4	0	13.24	-14.60
5	3	3	9.32	8.54	-1	4	1	48.22	48.34
5	3	4	18.32	20.42	-1	4	2	15.12	-15.66
5	3	5	17.42	-20.16	-1	4	3	5.84	5.10
5	3	6	11.24	13.96	-1	4	4	9.70	-11.62
5	3	7	8.14	-8.94	-1	4	5	19.52	-19.44
6	3	-3	4.70	2.20	0	4	-7	7.78	7.34
6	3	-2	6.06	7.58	0	4	-6	17.92	18.68
6	3	-1	19.50	-21.66	0	4	-5	0.	.88
6	3	0	43.16	-46.50	0	4	-4	42.48	42.62
6	3	1	7.00	-7.74	0	4	-3	9.46	-9.92
6	3	2	4.58	4.60	0	4	-2	81.26	-82.22
6	3	3	6.24	10.36	0	4	-1	.38	7.06
6	3	4	19.10	-21.06	0	4	0	10.32	-12.62
6	3	6	4.96	4.92	0	4	1	19.36	22.42
7	3	-1	7.26	8.42	0	4	2	36.64	-40.86
7	3	0	8.72	-11.48	0	4	3	17.48	17.46
7	3	1	9.60	11.60	0	4	4	26.64	28.42
7	3	2	6.08	7.50	0	4	5	14.56	-15.28
7	3	3	7.26	-8.46	0	4	6	14.46	-14.36
7	3	4	4.76	-3.26	1	4	-6	6.16	5.78
7	3	5	5.16	7.02	1	4	-5	5.08	1.58
-5	4	-4	12.66	-15.48	1	4	-4	45.44	45.62
-5	4	-3	5.36	-7.52	1	4	-3	16.18	-17.78
-5	4	0	4.24	9.22	1	4	-2	26.02	26.40
-5	4	1	0.	-3.66	1	4	-1	11.94	10.36
-4	4	-6	29.88	-28.08	1	4	1	44.24	-44.42
-4	4	-5	18.76	17.16	1	4	2	60.82	-62.88
-4	4	-4	1.74	.98	1	4	3	22.38	23.12
-4	4	-3	3.08	-3.74	1	4	4	48.42	49.92
-4	4	-2	21.10	-26.30	1	4	5	5.34	-4.64
-4	4	3	0.	1.10	1	4	6	14.90	14.60
					1	4	7	13.96	15.02

Table 18. Continued.

<u>h</u>	<u>k</u>	<u>l</u>	<u> F<sub>o</sub></u>	<u>F<sub>c</sub></u>	<u>h</u>	<u>k</u>	<u>l</u>	<u> F<sub>o</sub></u>	<u>F<sub>c</sub></u>
2	4	-6	5.90	-4.18	7	4	1	18.56	19.30
2	4	-5	8.34	-9.36	7	4	2	3.20	1.98
2	4	-4	35.56	-36.24	7	4	3	3.42	1.70
2	4	-3	15.22	-15.90	7	4	4	12.74	-12.92
2	4	-2	86.04	87.94	7	4	5	13.12	-11.70
2	4	-1	37.32	-41.18	-5	5	-3	18.14	-19.02
2	4	0	39.50	-35.58	-5	5	-2	11.60	11.66
2	4	1	4.04	4.96	-5	5	-1	9.90	-8.76
2	4	2	11.58	11.46	-5	5	0	17.58	-18.10
2	4	3	8.22	8.72	-4	5	-5	2.16	2.76
2	4	4	82.38	-85.28	-4	5	-4	17.74	18.84
2	4	5	29.06	29.80	-4	5	-3	9.80	-9.94
2	4	6	13.38	14.46	-4	5	-2	.80	-1.04
2	4	7	2.76	2.98	-4	5	-1	16.06	-18.94
3	4	-6	16.78	-17.42	-4	5	0	19.78	21.22
3	4	-5	10.12	-10.76	-4	5	1	14.92	-16.92
3	4	-4	14.06	-14.38	-4	5	2	54.44	-52.22
3	4	-3	8.58	-7.48	-3	5	-6	9.58	9.46
3	4	-2	5.68	-5.44	-3	5	-5	2.78	-2.86
3	4	-1	0.	-.26	-3	5	-4	5.14	4.54
3	4	0	32.02	32.18	-3	5	-3	8.56	-11.64
3	4	1	16.26	15.66	-3	5	-2	21.34	20.94
3	4	2	35.18	35.02	-3	5	-1	2.54	.06
3	4	3	34.12	-33.66	-3	5	0	1.92	4.78
3	4	4	20.74	-19.80	-3	5	1	1.42	-2.12
3	4	5	10.84	10.52	-3	5	2	9.08	-11.48
3	4	6	13.94	-15.58	-3	5	3	5.24	-3.90
3	4	7	8.28	-10.82	-3	5	4	8.22	-7.80
4	4	-5	0.	.36	-2	5	-6	2.98	-4.28
4	4	-4	27.72	27.86	-2	5	-5	5.78	-6.98
4	4	-3	5.06	-6.22	-2	5	-4	32.86	-31.42
4	4	-2	17.20	-15.72	-2	5	-3	13.96	-12.42
4	4	-1	6.06	4.76	-2	5	-1	12.06	-11.18
4	4	0	34.68	33.86	-2	5	0	5.06	5.02
4	4	1	6.42	7.16	-2	5	-2	36.58	35.58
4	4	2	13.36	-14.00	-2	5	1	39.94	40.34
4	4	3	26.08	26.30	-2	5	2	27.64	27.36
4	4	4	51.26	52.00	-2	5	3	19.98	18.56
4	4	5	11.98	12.64	-2	5	4	8.90	-10.60
4	4	6	9.22	-10.24	-2	5	5	13.54	12.96
4	4	7	6.64	5.28	-1	5	-6	21.06	-21.52
5	4	-4	25.08	-24.48	-1	5	-5	10.82	10.74
5	4	-3	14.62	16.16	-1	5	-4	38.70	-38.88
5	4	-2	31.54	-33.60	-1	5	-3	5.64	3.98
5	4	-1	13.34	15.20	-1	5	-2	26.94	-28.00
5	4	0	27.92	29.64	-1	5	-1	22.08	-20.90
5	4	1	32.82	-33.22	-1	5	0	15.32	14.60
5	4	2	15.24	15.92	-1	5	1	31.68	-32.06
5	4	3	5.82	-7.66	-1	5	2	54.44	54.24
5	4	4	27.12	27.84	-1	5	3	7.54	-7.34
5	4	5	5.44	-8.56	-1	5	4	10.14	11.74
5	4	6	8.88	-10.42	-1	5	5	32.08	33.08
5	4	7	47.58	48.00	-1	5	6	23.76	22.42
6	4	-3	23.90	25.48	0	5	-6	1.90	-3.50
6	4	-2	5.34	4.58	0	5	-5	19.24	19.62
6	4	-1	9.64	10.04	0	5	-4	49.56	51.26
6	4	0	36.34	-38.08	0	5	-3	3.24	1.78
6	4	1	5.34	-5.76	0	5	-2	65.36	-66.24
6	4	2	34.12	36.98	0	5	-1	1.54	5.32
6	4	3	52.80	-55.80	0	5	0	2.66	-.70
6	4	4	19.36	-21.52	0	5	1	18.16	-19.30
6	4	5	19.08	-21.58	0	5	2	26.86	-28.98
6	4	6	0.	1.30	0	5	3	22.54	-21.60
7	4	-1	8.78	7.38					
7	4	0	11.52	-13.44					

Table 18. Continued.

<u>h</u>	<u>k</u>	<u>l</u>	<u> F<sub>o</sub> </u>	<u>F<sub>c</sub></u>	<u>h</u>	<u>k</u>	<u>l</u>	<u> F<sub>o</sub> </u>	<u>F<sub>c</sub></u>
0	5	4	29.10	29.14	5	5	6	36.92	-38.48
0	5	5	29.36	-28.60	6	5	-3	21.18	-22.24
0	5	6	22.64	-20.84	6	5	-2	24.52	26.02
1	5	-6	10.22	10.38	6	5	-1	25.12	-27.14
1	5	-5	14.24	16.10	6	5	0	11.32	12.18
1	5	-4	3.28	3.62	6	5	1	38.42	39.54
1	5	-3	24.50	27.00	6	5	2	48.48	49.00
1	5	-2	46.10	43.16	6	5	3	23.28	23.04
1	5	-1	51.36	53.64	6	5	4	8.48	-9.66
1	5	1	6.06	5.74	6	5	5	26.14	25.36
1	5	2	11.34	-12.10	6	5	6	8.78	7.84
1	5	3	7.56	-6.62	7	5	-1	29.86	-30.16
1	5	4	0.	-2.68	7	5	0	8.20	-8.00
1	5	5	46.98	-45.90	7	5	1	20.04	-19.94
1	5	6	17.04	-18.06	7	5	2	16.90	18.04
2	5	-6	27.94	28.76	7	5	3	8.64	-9.22
2	5	-5	40.04	-41.58	7	5	4	5.60	-4.62
2	5	-4	19.66	-19.88	-4	6	-4	8.48	9.08
2	5	-3	22.10	22.10	-4	6	-3	9.94	10.36
2	5	-2	16.52	16.12	-4	6	-2	22.12	-24.06
2	5	-1	30.64	31.16	-4	6	-1	45.50	43.16
2	5	2	51.32	50.96	-4	6	0	21.26	21.80
2	5	3	2.70	-2.46	-4	6	1	25.76	25.60
2	5	4	19.44	17.32	-3	6	-5	25.12	-22.84
2	5	5	13.88	13.44	-3	6	-4	1.96	-2.48
2	5	6	9.50	9.70	-3	6	-3	19.18	-20.34
2	5	7	16.66	-17.32	-3	6	-2	13.04	-14.40
3	5	-5	20.86	-23.56	-3	6	-1	5.36	-6.06
3	5	-4	8.68	10.20	-3	6	0	15.56	-17.06
3	5	-3	24.16	-24.84	-3	6	1	12.38	15.18
3	5	-2	39.20	-40.10	-3	6	2	18.06	-19.98
3	5	-1	16.66	-17.74	-3	6	3	11.56	11.90
3	5	0	85.96	-78.60	-2	6	-5	11.96	12.40
3	5	1	32.38	27.74	-2	6	-4	0.	-1.30
3	5	2	9.14	-7.90	-2	6	-3	7.00	-6.16
3	5	3	4.32	-2.72	-2	6	-2	26.22	26.76
3	5	4	19.58	18.36	-2	6	-1	18.26	-20.26
3	5	5	4.86	3.04	-2	6	0	40.40	-40.10
3	5	6	53.76	54.80	-2	6	1	21.32	-22.00
3	5	7	7.84	-7.82	-2	6	2	16.78	-15.12
4	5	-5	15.90	18.06	-2	6	3	0.	-1.72
4	5	-4	38.02	39.26	-2	6	4	38.18	-37.14
4	5	-3	11.80	-12.16	-1	6	-6	5.62	5.26
4	5	-2	5.98	-8.16	-1	6	-4	32.64	31.64
4	5	-1	6.56	-10.00	-1	6	-3	3.26	.68
4	5	0	34.92	32.60	-1	6	-2	27.86	27.42
4	5	1	74.18	-67.94	-1	6	-1	21.66	22.36
4	5	2	93.88	-89.46	-1	6	1	24.06	25.98
4	5	3	10.66	-11.26	-1	6	2	6.00	-7.12
4	5	4	19.68	-16.90	-1	6	3	26.32	-25.34
4	5	5	3.64	5.76	-1	6	4	35.70	-35.06
4	5	6	17.10	-17.46	-1	6	5	10.96	-9.00
4	5	7	13.62	16.36	0	6	-6	41.00	-39.24
5	5	-4	1.30	.40	0	6	-5	8.84	-8.58
5	5	-3	7.82	7.18	0	6	-4	19.80	20.28
5	5	-2	23.48	23.82	0	6	-3	42.78	-42.52
5	5	-1	30.84	31.56	0	6	-1	8.08	-7.56
5	5	0	26.28	25.98	0	6	0	41.44	38.68
5	5	1	1.88	-1.16	0	6	1	16.20	17.30
5	5	2	7.68	7.06	0	6	2	11.60	-14.18
5	5	3	5.52	7.06	0	6	3	46.84	47.60
5	5	4	21.70	-20.76	0	6	4	8.96	8.84
5	5	5	18.58	-18.38	0	6	5	4.06	3.94
					0	6	6	14.80	-15.06

Table 18. Continued.

<u>h</u>	<u>k</u>	<u>l</u>	<u> F<sub>0</sub> </u>	<u>F<sub>c</sub></u>	<u>h</u>	<u>k</u>	<u>l</u>	<u> F<sub>0</sub> </u>	<u>F<sub>c</sub></u>
1	6	-6	3.48	-5.56	6	6	5	9.90	9.46
1	6	-5	1.88	-1.26	7	6	-1	3.38	1.70
1	6	-4	39.60	-41.52	7	6	0	5.52	6.30
1	6	-3	2.32	-2.68	7	6	1	8.24	9.08
1	6	-2	52.24	-52.70	7	6	2	8.70	-9.28
1	6	-1	32.78	-31.46	7	6	3	13.08	-15.74
1	6	1	20.48	-23.88	7	6	4	18.20	-20.86
1	6	2	19.24	20.02	-3	7	-4	1.74	-3.04
1	6	3	2.54	.52	-3	7	-3	10.44	10.78
1	6	4	31.08	29.82	-3	7	-2	2.16	.40
1	6	5	18.72	16.70	-3	7	-1	4.14	1.76
1	6	6	26.74	-25.64	-3	7	0	15.56	17.46
2	6	-6	31.38	32.22	-3	7	1	18.76	-20.56
2	6	-5	7.52	9.32	-3	7	2	5.40	-5.06
2	6	-4	14.18	-16.62	-2	7	-5	24.68	-24.02
2	6	-3	16.36	17.00	-2	7	-4	21.28	-20.26
2	6	-2	13.64	15.20	-2	7	-3	20.06	20.40
2	6	-1	8.88	-10.06	-2	7	-2	16.38	16.90
2	6	2	38.48	37.38	-2	7	-1	22.80	24.74
2	6	3	40.30	-37.84	-2	7	0	35.68	-31.08
2	6	4	4.26	-1.00	-2	7	1	.78	3.44
2	6	5	1.54	.04	-2	7	2	22.90	25.18
2	6	6	7.02	7.96	-2	7	3	24.60	-25.76
3	6	-5	23.40	24.30	-1	7	-5	13.56	-12.64
3	6	-4	13.70	15.58	-1	7	-4	4.22	-5.48
3	6	-3	47.48	46.30	-1	7	-3	7.94	-7.20
3	6	-2	10.34	11.84	-1	7	-2	10.88	-10.10
3	6	-1	7.74	7.02	-1	7	-1	21.22	24.94
3	6	0	11.10	9.26	-1	7	0	17.14	-18.58
3	6	2	26.00	23.52	-1	7	1	40.82	35.32
3	6	3	7.54	-3.98	-1	7	2	9.48	8.90
3	6	4	8.74	-8.86	-1	7	3	11.06	-11.70
3	6	5	13.98	14.02	-1	7	4	5.50	-5.30
3	6	6	4.12	3.70	0	7	-5	6.28	1.78
4	6	-5	10.76	-11.28	0	7	-4	20.70	20.74
4	6	-4	3.48	-.30	0	7	-2	27.86	-28.72
4	6	-3	1.98	.88	0	7	0	27.94	27.42
4	6	-2	27.68	-28.12	0	7	1	2.78	.24
4	6	-1	50.94	51.08	0	7	3	1.80	2.92
4	6	0	33.04	29.56	0	7	4	21.08	22.22
4	6	1	17.78	-16.16	0	7	5	8.02	6.58
4	6	2	12.70	9.48	1	7	-5	4.90	-5.16
4	6	3	7.84	-8.00	1	7	-4	25.46	24.74
4	6	4	28.16	26.30	1	7	-3	6.70	-8.06
4	6	5	16.58	-17.14	1	7	-2	9.26	-10.72
4	6	6	9.52	-10.26	1	7	2	35.56	-33.64
5	6	-4	.90	-1.04	1	7	3	13.16	14.22
5	6	-3	18.12	-17.64	1	7	4	19.50	21.56
5	6	-2	17.54	-16.24	1	7	5	8.88	-9.02
5	6	-1	18.12	16.90	2	7	-5	5.22	-5.02
5	6	0	27.26	-24.46	2	7	-4	6.84	-8.72
5	6	1	21.56	19.86	2	7	-3	18.12	-17.62
5	6	2	39.92	-36.72	2	7	-2	42.36	39.26
5	6	3	4.68	3.28	2	7	3	5.26	-5.70
5	6	4	21.50	18.36	2	7	4	57.46	-58.10
5	6	5	24.54	-22.58	2	7	5	6.46	-4.28
5	6	6	4.22	3.94	2	7	6	3.32	3.88
6	6	-3	15.12	15.20	3	7	-4	6.08	-5.42
6	6	-2	18.60	17.02	3	7	-2	8.18	6.74
6	6	-1	26.20	-25.84	3	7	-1	6.88	-5.98
6	6	0	24.70	-24.90	3	7	2	28.20	24.50
6	6	1	2.84	1.24	3	7	3	4.86	4.06
6	6	2	10.90	11.68	3	7	4	28.40	-28.70
6	6	3	3.28	-4.16					
6	6	4	21.70	-20.44					

Table 18. Continued.

<u>h</u>	<u>k</u>	<u>l</u>	<u> F<sub>o</sub> </u>	<u>F<sub>c</sub></u>
3	7	5	19.38	21.20
3	7	6	15.04	-17.90
4	7	-4	8.68	7.72
4	7	-3	3.14	-3.38
4	7	-2	23.68	-23.24
4	7	-1	5.26	-3.06
4	7	0	27.32	23.78
4	7	1	9.26	-9.46
4	7	2	12.74	11.92
4	7	3	13.26	13.60
4	7	4	44.24	46.54
4	7	5	15.80	15.62
4	7	6	0.	-.70
5	7	-2	6.56	-6.64
5	7	-1	16.52	-15.00
5	7	0	23.80	23.74
5	7	1	39.54	-37.24
5	7	2	9.06	-8.36
5	7	3	10.76	11.40
5	7	4	7.74	7.60
5	7	5	14.08	15.32
6	7	-1	3.52	2.98
6	7	0	15.72	-14.74
6	7	1	14.52	-13.28
6	7	2	13.84	14.46
6	7	2	13.84	14.46
6	7	3	40.30	-41.54
6	7	4	10.80	-10.72
6	7	5	4.92	-4.72
7	7	1	32.32	32.42
7	7	2	9.44	8.22
7	7	3	2.58	-2.86

## STRUCTURAL TYPES OF CALCIUM METASILICATE

## Introduction

The following structures of calcium metasilicate have been determined and refined: wollastonite, parawollastonite, and a high-pressure  $\text{CaSiO}_3$ ; in addition, a structure proposal for pseudowollastonite based on the analogous compound  $\text{SrGeO}_3$  has been given. It is the purpose of this chapter to describe some structural relations and to show structural similarities and differences between the various phases of calcium metasilicate in order to establish a means for a classification of them. The main attention will be focused on the two principal building blocks of silicates: namely, the tetrahedrally coordinated silicon atoms and the arrangement of the cation polyhedra. In a systematic classification of silicates, Bragg (1930) considered the assemblage of the silicon-oxygen tetrahedra to be the dominant building block, whereas the other cations are of secondary importance and occupy the remaining space. On the other hand, in a survey of silicate structures by Liebau (1962), the significant role played by the cations is acknowledged. Belov (1960) goes even further and shows that actually the cation polyhedra determine the structure and the silicon-oxygen tetrahedra adjust themselves according to the arrangement of the cation polyhedra. He demonstrated this idea with the examples of a pyroxene chain and the pyrooxnoid chains in wollastonite and rhodonite. In each case the arrangement of the cation polyhedra determines the repeating unit and the shape of the silicon chain. In view of the important influence on the structure emanating from the cation polyhedra, not only the configuration of the silicon-oxygen tetrahedra but also the arrangement of the cation polyhedra will be examined. Since calcium metasilicate occurs in



several modifications which can be transformed into one another, it will be interesting to know which of the two building blocks, namely the silicon tetrahedra or the calcium polyhedra, is altered the most in a phase transformation. Hence the third chapter is initiated with a discussion of the structural relation between wollastonite and parawollastonite. In continuing the comparison, walstromite, a high-pressure  $\text{CaSiO}_3$  and pseudowollastonite are investigated and a structural relation of these compounds to wollastonite as well as parawollastonite is sought.

### Structural Relation Between Wollastonite and Parawollastonite

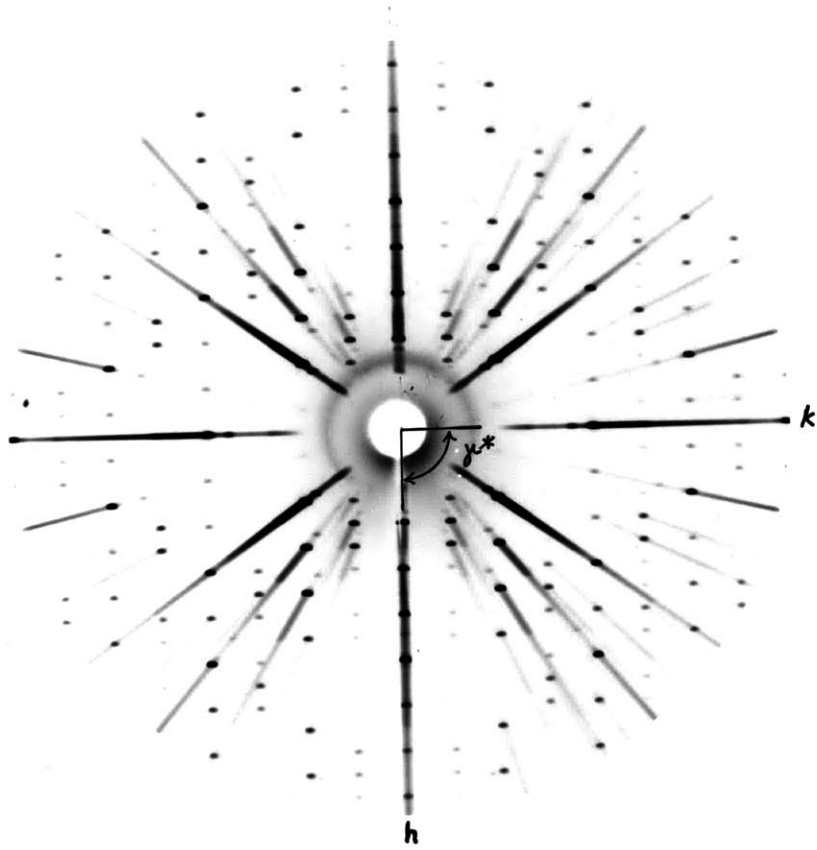
During the x-ray investigation of triclinic wollastonite Warren (1931) detected an unusual pseudomonoclinic symmetry in the diffraction pattern of oscillation photographs. He noted that the triclinic angle  $\gamma$  is such that the direction  $[410]$ , makes an  $90^\circ$  angle with  $\underline{b}$ . In addition Warren observed that the even layer lines of  $\underline{b}$  axis oscillation photographs have perfect monoclinic symmetry. Therefore, he suggested, although wollastonite is triclinic, that a diffraction pattern having monoclinic symmetry could be obtained if adjacent cells of wollastonite are shifted by the amount  $\underline{b}/2$ . In a somewhat different way these findings are illustrated in Fig. 17 by precession photographs along the  $\underline{c}$  axis of wollastonite and parawollastonite. These diffraction patterns are identical if the odd numbered reciprocal lattice levels of index  $\underline{k}$  for both compounds are omitted. Using the triclinic cell of wollastonite as a reference system, it is evident from Fig. 17b that the direction  $[\bar{1}40]$  makes an  $90^\circ$  angle with  $\underline{a}^*$  and in addition  $[\bar{1}40]$  is parallel to the  $\underline{b}^*$  direction of monoclinic parawollastonite. Based on these observations a structural relation between the two phases can be deduced.

Ito (1950) suggested that both the triclinic and monoclinic varieties of calcium metasilicate can be constructed from a pseudomonoclinic cell by alternating shifts of  $\pm \frac{1}{2} \underline{b}$  of a hypothetical monoclinic cell. Prewitt and Beurger (1963) followed the idea outlined by Ito and proposed the space group  $P2_1/\underline{a}$  for parawollastonite with additional local centers of symmetry which are not required by this space group.

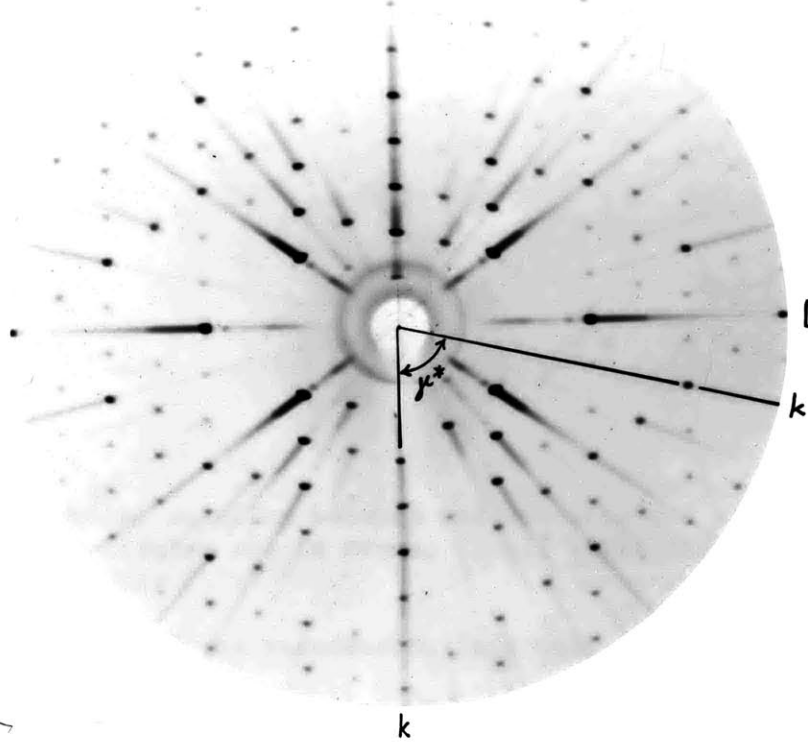
Figure 17. Precession photographs of the reciprocal plane  $hk0$  using  $MoK\alpha$  radiation.

(a) Parawollastonite.

(b) Wollastonite.



(a)



(b)

- Figure 18. Structural relation between wollastonite and parawollastonite. Double circles are Ca atoms. Small solid circles are centers of symmetry.
- (a) Selection of the pseudomonoclinic unit, shaded.
  - (b) Stacking scheme of the pseudomonoclinic units in parawollastonite.

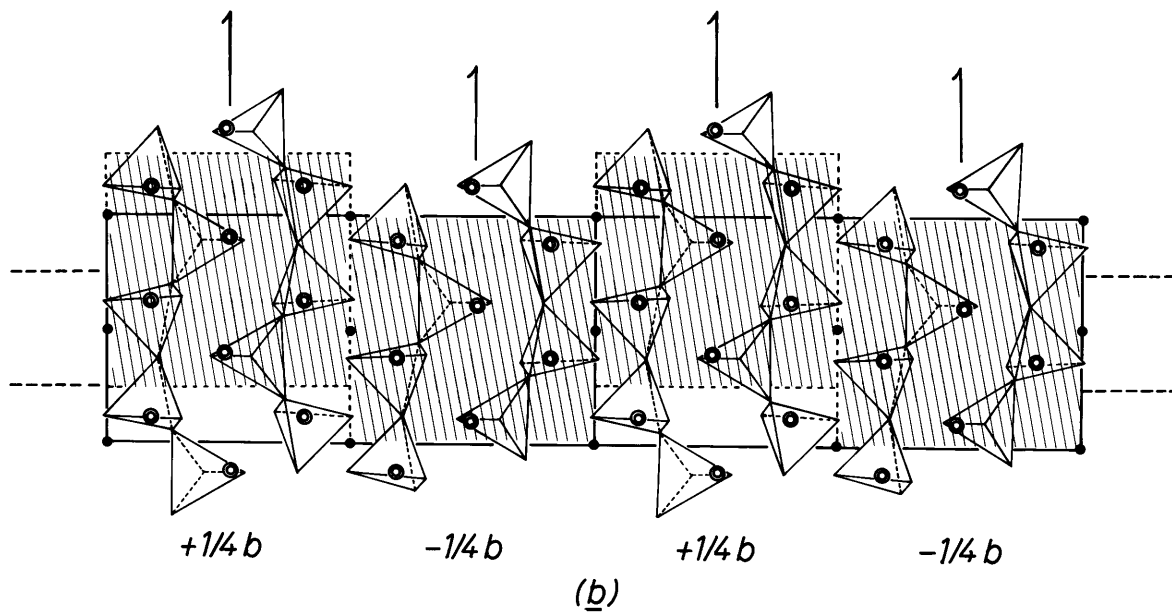
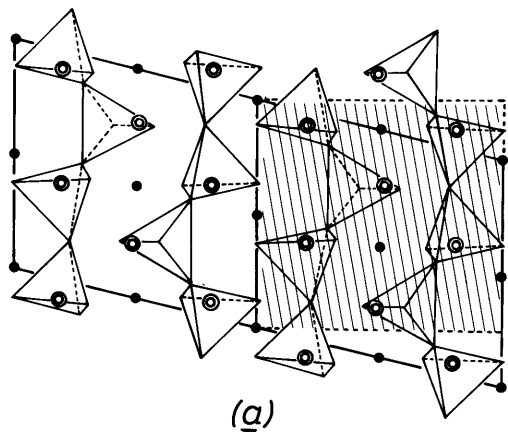


Table 19. Comparison of the  $y$  Coordinates of the Atoms in Parawollastonite with the position  $(2n + 1)/8$ .

$(2n + 1)/8$	$1/8$ 0.1250	$3/8$ 0.3750	$5/8$ 0.6250	$7/8$ 0.8750
Atom	$y$			
Ca(1)		$0.3758 \pm 0.0004$		
Ca(2)			$0.6265 \pm 0.0006$	
Ca(3)	$0.1209 \pm 0.0006$			
Si(1)	$0.0906 \pm 0.0003$			
Si(2)			$0.6597 \pm 0.0003$	
Si(3)		$0.3760 \pm 0.0004$		
O(1)		$0.3747 \pm 0.0013$		
O(2)		$0.3759 \pm 0.0013$		
O(3)	$0.1397 \pm 0.0014$			
O(4)			$0.6157 \pm 0.0015$	
O(5)	$0.1226 \pm 0.0020$			
O(6)			$0.6176 \pm 0.0019$	
O(9)				$0.8755 \pm 0.0010$
O(7)	$0.1962 \pm 0.0007$			
O(8)			$0.5533 \pm 0.0008$	

These postulates are approximately verified in the results of the present investigation. Figure 18a illustrates how a cell, regarded as having pseudomonoclinic symmetry, can be selected from the structure of wollastonite. When those units are stacked together as shown in Fig. 18b, a rough model of the structure of parawollastonite is obtained. For example, in wollastonite as well as in the pseudomonoclinic unit, the Ca atoms are related by inversion centers. In parawollastonite, however, these atoms are related by the operations of a  $2_1$  axis, but they are located in almost the same positions as would be generated by the inversion centers of the pseudomonoclinic unit. Both symmetry operations give rise to identical positions if all atoms have  $y$  coordinates of  $(2n + 1)/8$ , except O(7) and O(8). Table 19 shows that the deviations of the  $y$  coordinate from  $(2n + 1)/8$  for the atoms in parawollastonite are small, but above the limit of error. These specialized locations are responsible for the additional pseudosymmetry elements which were discussed in the first chapter. Figures 18a and 18b show furthermore that the positions of the Ca atoms are almost identical in both structures. This means that the displacement, introduced by the alternating shifts  $\pm 1/4 b$  of pseudomonoclinic units, is an integral part of the distance between two Ca atoms along a direction parallel  $b$ . Hence these shifts occur without subjecting the whole structure to appreciable strains.



Common Structural Features in Walstromite, High-Pressure  $\text{CaSiO}_3$  and Pseudowollastonite.

The existence of  $\text{Si}_3\text{O}_9$  rings was known in chemically different compounds long before the possibility of rings in calcium metasilicates was suggested. Zachariassen (1930) determined the crystal structure of benitoite,  $\text{BaTiSi}_3\text{O}_9$ , and found  $\text{Si}_3\text{O}_9$  rings as a new type of arrangement for  $\text{SiO}_4$  tetrahedra. The crystal structure of wadeite,  $\text{K}_2\text{ZrSi}_3\text{O}_9$ , was successfully investigated by Henshaw (1955). This mineral has irregular layers formed by Zr-O and K-O polyhedra and  $\text{Si}_3\text{O}_9$  rings between the layers. Based on comparison of cell constants, Liebau (1960) suggested that  $\text{SrSiO}_3$  and  $\text{BaSiO}_3$  have the same structure as pseudowollastonite. The latter compound is assumed to be analogous to  $\text{SrGeO}_3$ , whose structure was worked out by Hilmer (1958). She described the structure as having  $\text{Ge}_3\text{O}_9$  rings sandwiched by Sr layers. Glasser and Glasser (1961) published the structure walstromite,  $\text{Ca}_2\text{BaSi}_3\text{O}_9$ , which is chemically very similar and structurally related to this compound.

Some of the compounds listed above will be examined in more detail to illustrate structural features common with high-pressure  $\text{CaSiO}_3$ . Glasser and Glasser (1961) predicted the presence of  $\text{Si}_3\text{O}_9$  rings in walstromite on the basis of cell constants similar to those of benitoite, wadeite, and pseudowollastonite. Unfortunately the cell used by Glasser and Glasser is not the reduced cell so that its dimensions cannot be compared directly with those of the new form of  $\text{CaSiO}_3$ . The transformation from their cell to the reduced cell is:

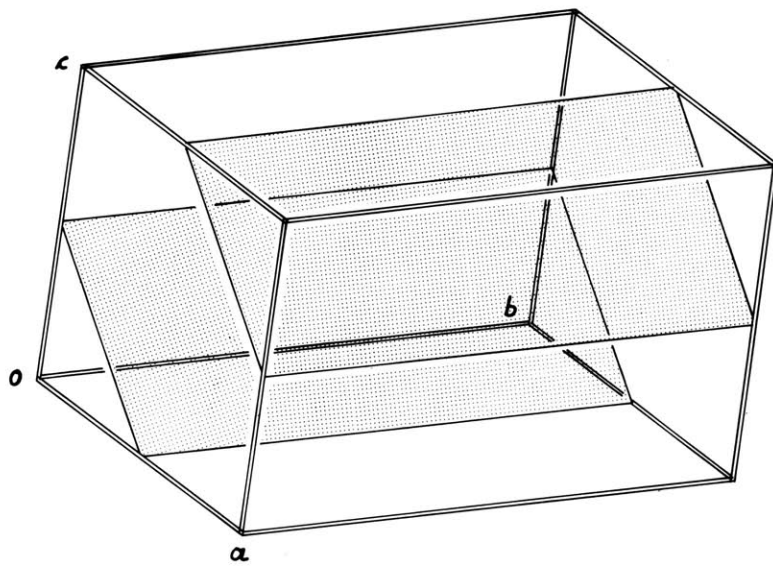
$$\begin{pmatrix} 0 & 0 & 1 \\ 0 & 1 & 0 \\ \bar{1} & 0 & 0 \end{pmatrix}$$

The reduced cell dimensions for the two compounds are listed in Table 20. Both compounds have almost identical reduced cells.

Table 20. Cell Constants of Walstromite and High-Pressure  $\text{CaSiO}_3$ .

Cell Constants	Walstromite $\text{Ca}_2\text{Basi}_3\text{O}_9$		High-Pressure $\text{CaSiO}_3$
	as published	referred to reduced cell	
<u>a</u>	6.733 Å	6.723 Å	6.695 Å
<u>b</u>	9.616 Å	9.616 Å	9.257 Å
<u>c</u>	6.723 Å	6.733 Å	6.666 Å
<u><math>\alpha</math></u>	69°37'	83°06'	86°38'
<u><math>\beta</math></u>	102°20'	77°40'	76°08'
<u><math>\gamma</math></u>	96°54'	69°37'	70°23'

Figure 19. The orientation of the Ca planes in the reduced cell of walstromite. The Ca planes are shaded.



In walstromite the silicon atoms also form  $\text{Si}_3\text{O}_9$  rings and the Ca atoms are arranged in layers. The Ba atoms connect these Ca layers like the Ca(2) atoms in the high-pressure phase of  $\text{CaSiO}_3$ . In both structures the separation of the Ca layers from each other amounts to roughly  $5 \text{ \AA}$ . The orientation of the Ca layers, however, is different as illustrated in Figures 16 and 19. The cell of walstromite contains only two layers which are orientated parallel to (101) and intersect  $\underline{a}$  and  $\underline{c}$  at  $\frac{1}{2}$ . High-pressure  $\text{CaSiO}_3$  on the other hand has three layers within its cell which are orientated parallel (111).

As a consequence of the different orientation of the Ca layers in the two structures, an interesting relation in the stacking sequence can be derived. For this purpose both structures will be examined in a direction perpendicular to their layers. A different and larger cell is to be selected so that the Ca layers are parallel to the basal plane of the new cell. Figures 20 and 21 demonstrate the relation of larger cells labeled  $\underline{A}$ ,  $\underline{B}$  and  $\underline{C}$  with their reduced cell. Figure 20 presents the case of walstromite where the repeat unit along  $\underline{C}$  contains two layers. Using the large cell as the system of reference, Fig. 22a shows that the Ca layers and their adjacent  $\text{Si}_3\text{O}_9$  rings are displaced in respect to each other by the amount  $\underline{A}/2$ . This shift is indicated in Fig. 22a by an arrow on an  $\text{Si}_3\text{O}_9$  ring. On the other hand, in high-pressure  $\text{CaSiO}_3$ , three layers form the repeat unit along  $\underline{C}$ . In respect to the large cell the layers and their adjacent rings are displaced relative to each other by the amount  $\underline{B}/3$  as indicated by an arrow in Fig. 22b. As a consequence it is feasible to consider the structure of high-pressure  $\text{CaSiO}_3$  as having layers like the ones observed in walstromite but with each of them shifted by an amount different from the one for walstromite. This structural relation is

Figure 20. Walstromite: Selection of a cell whose basal plane is a Ca-O layer. The Ca planes are shaded. The new cell vectors  $\underline{A}$ ,  $\underline{B}$ ,  $\underline{C}$ , expressed in terms of the ones for the reduced cell, are  $\underline{A} = \underline{a} - \underline{c}$ ,  $\underline{B} = \underline{b}$ ,  $\underline{C} = \underline{a} + \underline{c}$ .

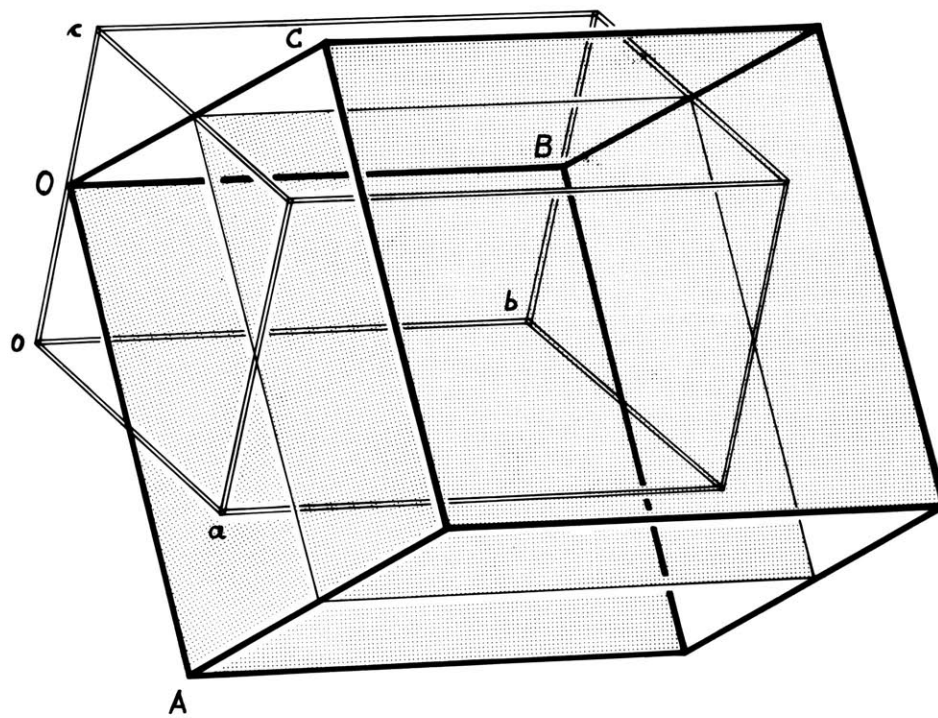
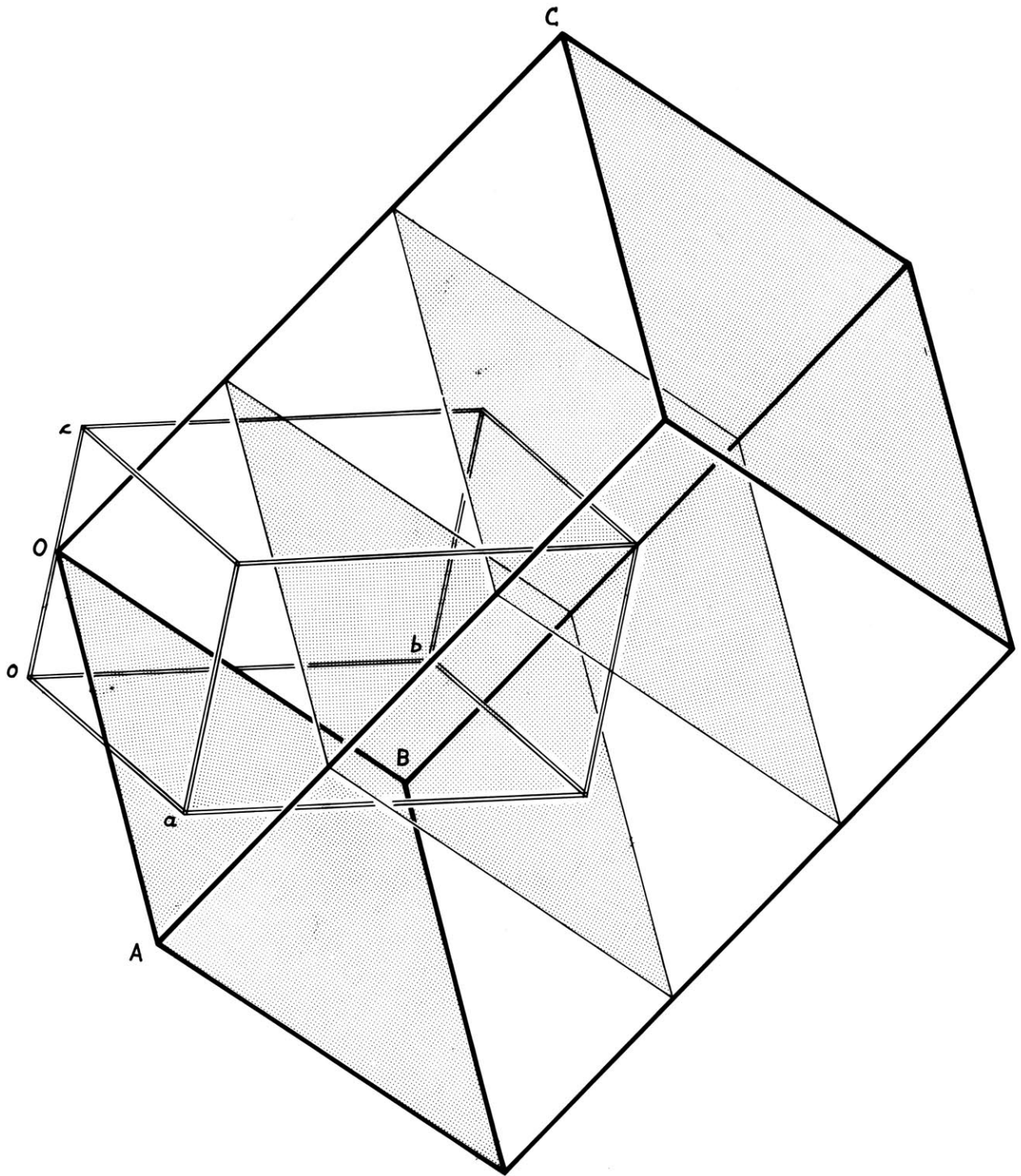


Figure 21. High-pressure  $\text{CaSiO}_3$  : Selection of a cell whose basal plane is a Ca-O layer. The Ca planes are shaded. The new cell vectors  $\underline{A}$ ,  $\underline{B}$ ,  $\underline{C}$ , expressed in terms of the ones for the reduced cell, are  $\underline{A} = \underline{a} - \underline{c}$ ,  $\underline{B} = \underline{b} - \underline{c}$ ,  $\underline{C} = \underline{a} + \underline{b} + \underline{c}$ .





analogous to a transformation mechanism which requires only chemical bonds reaching to the next layer to be disconnected, the layer itself remains intact. Such a relation corresponds to Buerger's (1961) definition of polytypism in layer structures. Based on this classification, and disregarding the substitution of one Ca atom by a Ba atom, it is possible to consider walstromite and this high-pressure phase of  $\text{CaSiO}_3$  to be polytypes.

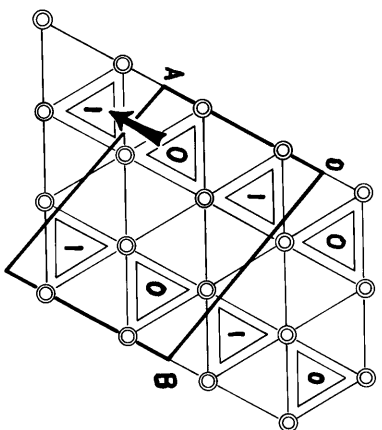
Since the nature of the structural relation of walstromite and this high-pressure phase of  $\text{CaSiO}_3$  has been established, an additional comparison of both structures with  $\text{SrGeO}_3$ , as well as with pseudowollastonite, is of great interest. Hilmer (1963) considered the atomic arrangement in  $\text{SrGeO}_3$  to be an analog of pseudowollastonite. As mentioned in the discussion of the structure of high-pressure  $\text{CaSiO}_3$ , it is possible to reconstruct complete Ca layers like the Sr layers found in  $\text{SrGeO}_3$  by stuffing the Ca(2) atoms into the voids of the imperfect Ca layers. This reconstruction would require chemical bonds to the nearest neighbors to be broken and would require a change of coordination around Ca(1). Simultaneously minor displacive adjustments would be necessary. Assuming complete Ca layers, Fig. 22 compares the three structures: walstromite, high-pressure  $\text{CaSiO}_3$ , and pseudowollastonite. In order to stress common structural features, a representation chosen by Dornberger-Schiff (1962) for  $\text{SrGeO}_3$  is applied to all three compounds. It is evident from Fig. 22 that the Ca atoms form a hexagonal network in all three structures. The shapes of the  $\text{Si}_3\text{O}_9$  rings, however, are different. Neglecting small distortions, the rings of walstromite and high-pressure  $\text{CaSiO}_3$  have symmetry  $3\bar{m}$  while those of  $\text{SrGeO}_3$  and possibly pseudowollastonite have symmetry  $\bar{6}m2$ .

An interesting relation between these structures can be found in the stacking sequence of the rings. Hilmer (1963) describes the atomic arrangement of  $\text{SrGeO}_3$ , and hence pseudowollastonite, as follows: The structure is composed of layers having hexagonal symmetry. Six of these layers and their adjacent rings are superposed on one another in such a way that the symmetry for the whole structure is monoclinic. Dornberger-Schiff (1962) showed that the stacking sequence can be represented graphically by a projection of the structure onto the hexagonal layer as it is shown in Fig. 22c. The relative heights of the rings in a direction perpendicular to the hexagonal layer are labeled with the numbers 0, 1, 2, 3, 4, 5. The lower picture in Fig. 22c shows that the stacking arrangement can be expressed in terms of successive shifts applied on each layer.

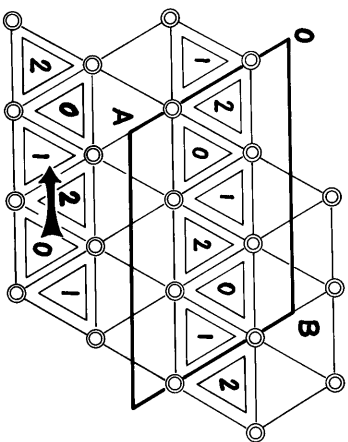
Examined in the same manner, this high-pressure phase of  $\text{CaSiO}_3$  shows a repeating unit containing three Ca layers. The  $\text{Si}_3\text{O}_9$  rings, projected onto the hexagonal network, occupy only half of the interstices within a hexagon. The resulting stacking arrangement is similar to that of pseudowollastonite if only half of its repeat unit in a direction perpendicular to the hexagonal network is considered. Walstromite, on the other hand, has only two layers, and the rings associated with them occupy only a third of the interstices within a hexagon.

These structural properties can be summed up in the following way: walstromite, high-pressure  $\text{CaSiO}_3$ , and pseudowollastonite each have hexagonal Ca layers. The three structures can be distinguished by the stacking sequence of the layers and their adjacent rings and by the number of layers in each case. As a consequence it is justifiable to consider pseudowollastonite and

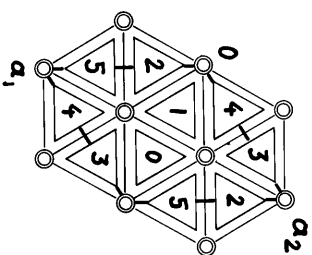
- Figure 22. Stacking sequence of the  $\text{Si}_3\text{O}_9$  rings in walstromite, high-pressure  $\text{CaSiO}_3$ , and pseudowollastonite. For each compound the upper figure represents schematically a projection of the structure onto the Ca layer, while the lower figure is a view parallel to this layer. The double circles are Ca atoms. The numbers give the relative heights of the  $\text{Si}_3\text{O}_9$  rings.
- (a) Walstromite. The heavy lines outline the cell, A, B, C derived in Fig. 20.
  - (b) High-pressure  $\text{CaSiO}_3$ . The heavy lines outline the cell A, B, C derived in Fig. 21.
  - (c) Pseudowollastonite, assumed analogous to  $\text{SrGeO}_3$ .
  - (d) Wadeite. The Zr atoms are represented by full circles. The shaded tetrahedron in the lower figure masks the third tetrahedron below it.



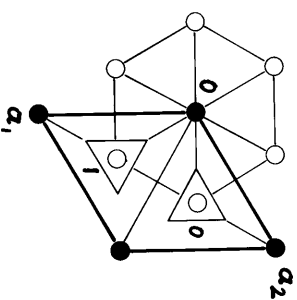
(a)



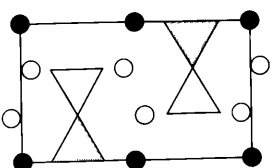
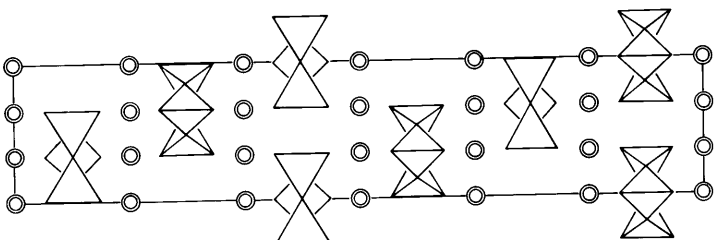
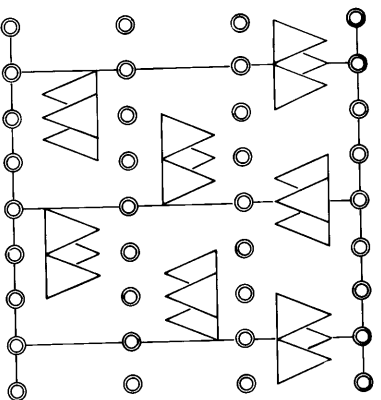
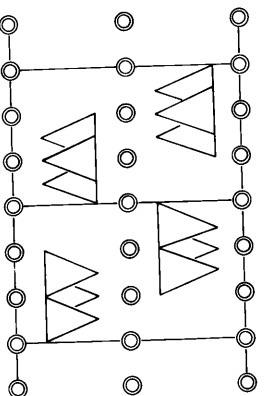
(b)



(c)



(d)



high-pressure  $\text{CaSiO}_3$  as polytypes. Since polytypism is a subdivision of polymorphism, one can say that walstromite, the high-pressure phase of  $\text{CaSiO}_3$ , and pseudowollastonite belong to one polymorphic set.

Comparison of Wollastonite and Parawollastonite with High-Pressure  $\text{CaSiO}_3$ .

At the first glance, the structures of the two modifications of wollastonite and high-pressure  $\text{CaSiO}_3$  appear to be quite different from each other. The wollastonites have triclinic and monoclinic symmetry, slabs built by Ca-O octahedra, and  $\text{Si}_3\text{O}_9$  chains. High-pressure  $\text{CaSiO}_3$ , on the other hand, has  $\text{Si}_3\text{O}_9$  rings, incomplete Ca-O layers, and triclinic symmetry. A close examination of these structural features shows however, that only minor reconstructive processes would be necessary to transform one structure into the other. It will be demonstrated in this section that the basic building principle, namely sheets of Ca polyhedra alternating with sheets of Si tetrahedra, is retained in both structure types. Dornberger-Schiff (1962) describes a similar structural relation between foshagite,  $\text{Ca}_4\text{Si}_3\text{O}_9(\text{OH})_2$ , whose structure was worked out by Gard and Taylor (1960), and  $\text{SrGeO}_3$ . Dornberger-Schiff concluded that the transformation of pseudowollastonite to wollastonite is accomplished by merely pulling apart the octahedral layers in pseudowollastonite.

Figures 23 and 24 present a schematic projection of both structures, wollastonite and high-pressure  $\text{CaSiO}_3$ . Wollastonite and parawollastonite give the same picture in projection if they are viewed parallel to the Ca-O slabs as seen in Fig. 23. High-pressure  $\text{CaSiO}_3$  is seen in a direction parallel to the Ca planes. First the arrangement of the Ca-O polyhedra will be examined. Figure 23 shows that the individual slabs of Ca polyhedra are separated by small channels within a sheet. As it was pointed out in the discussion of the structure of parawollastonite, it is possible to consider the arrangement of the Ca octahedra to constitute slabs cut out of an octahedral layer where the Ca atoms form a hexagonal network. Hence if these slabs were pushed

Figure 23. A schematic picture of the structure of wollastonite, as well as parawollastonite, viewed along the direction of the chains.



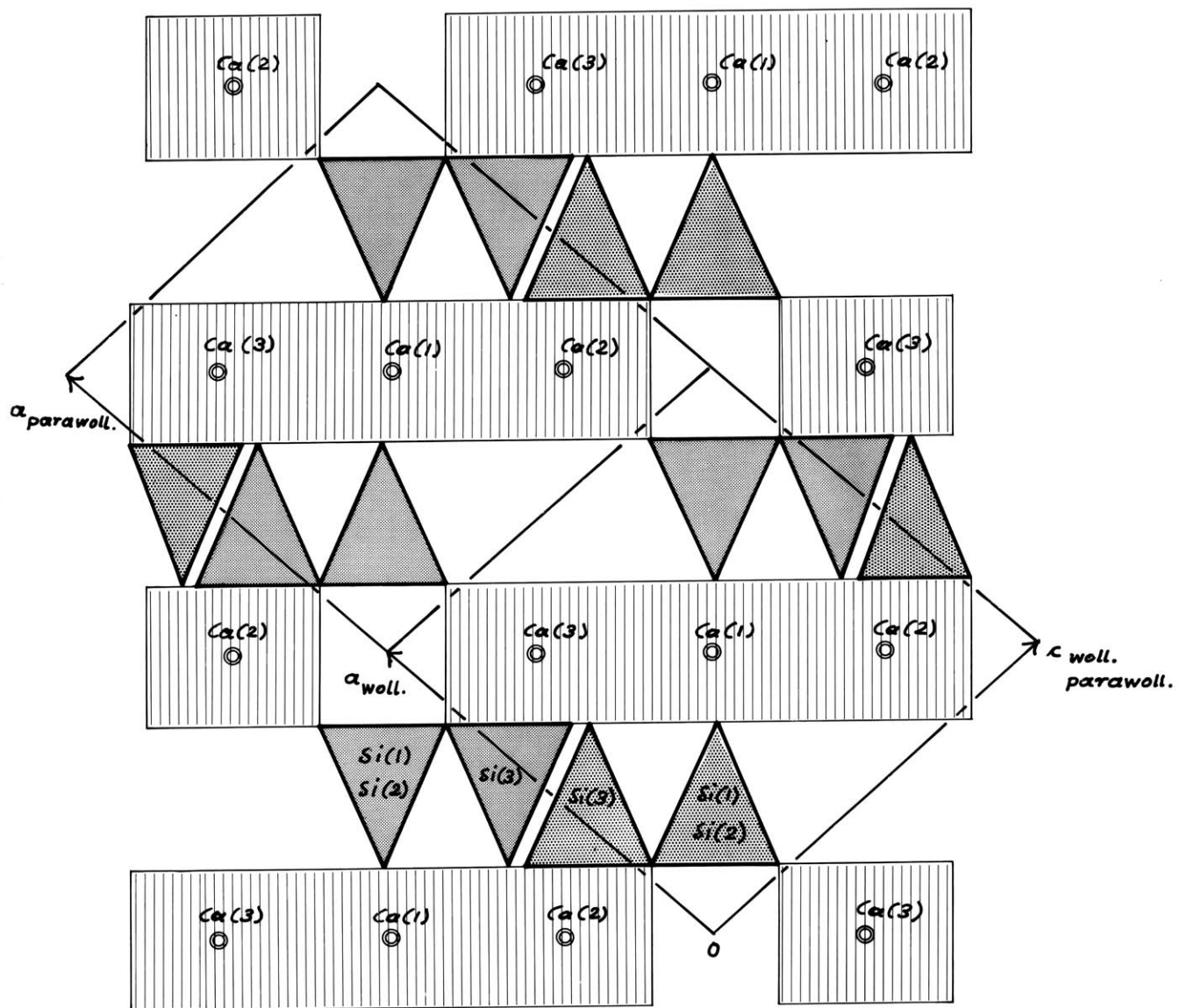


Figure 24. A schematic picture of the structure of high-pressure  $\text{CaSiO}_3$  viewed along a direction parallel to the Ca layers.

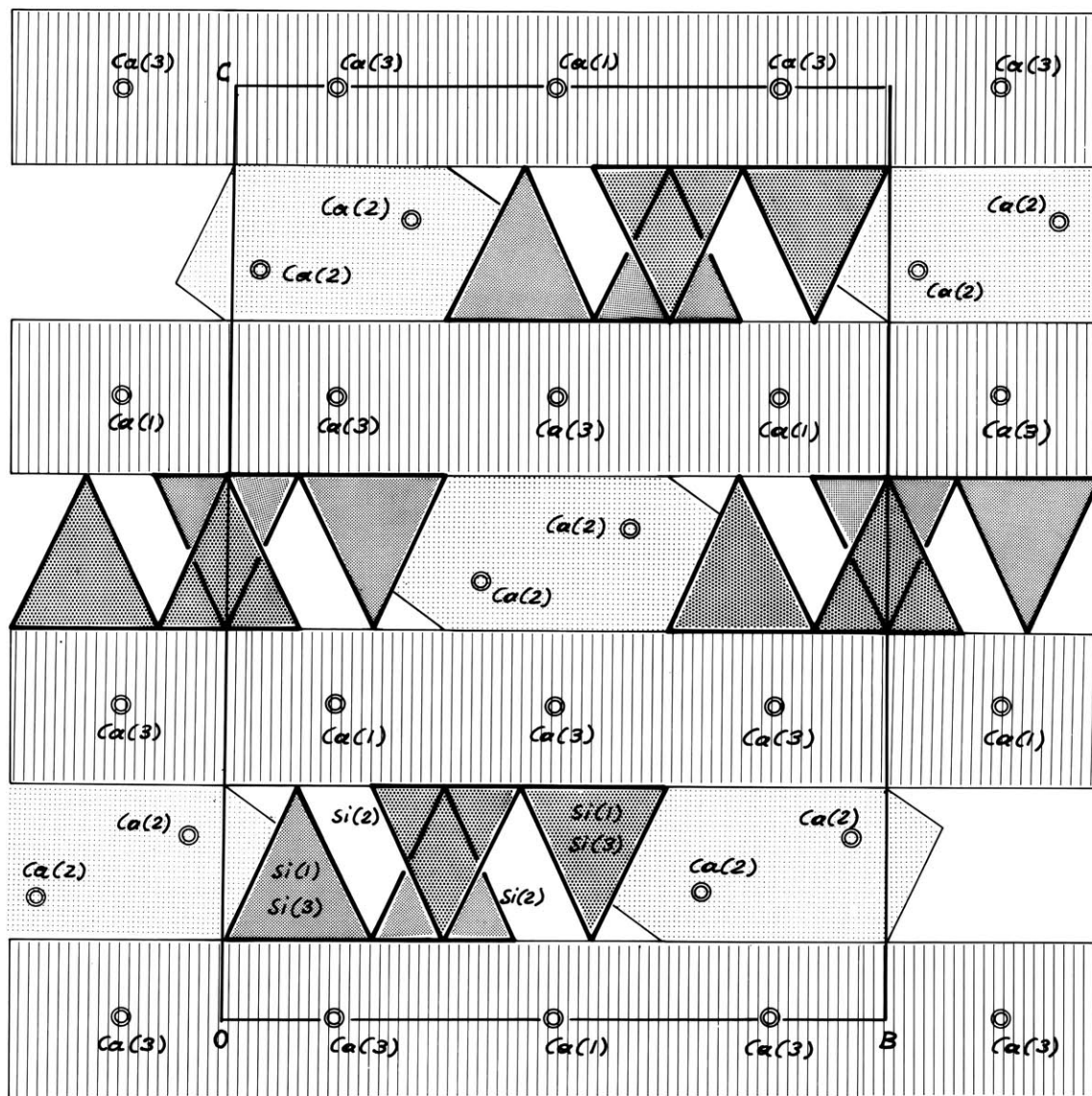
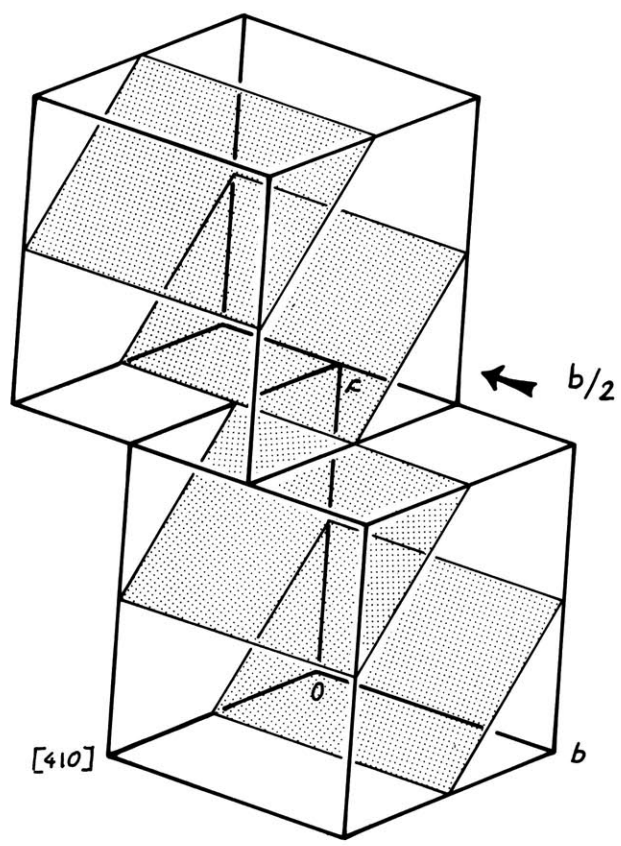


Figure 25. Two pseudomonoclinic units of wollastonite displaced relative to each other by the amount  $b/2$  parallel the plane (001). The shaded planes represent the layerlike arrangement of the Ca atoms, the  $\text{Si}_3\text{O}_9$  chains are located between those planes.

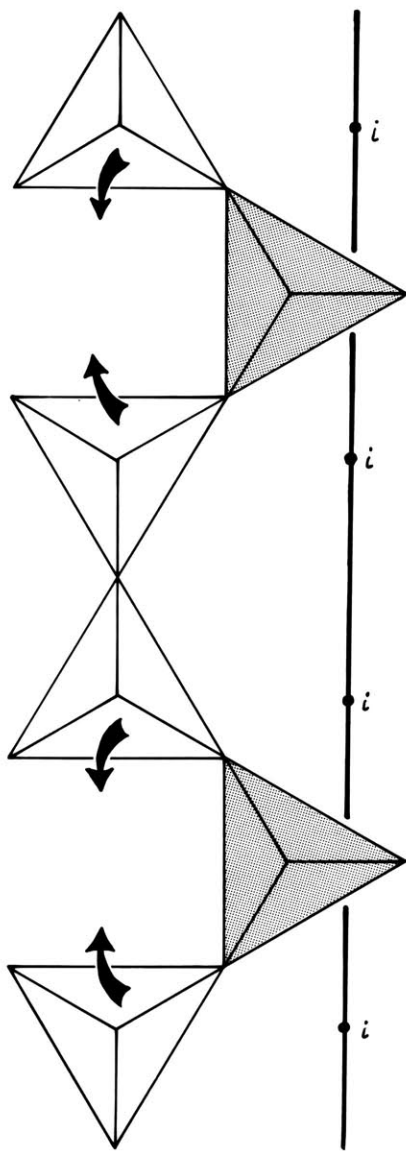


together, for example by high-pressure, then a somewhat hexagonal looking network of Ca atoms could be obtained, as Fig. 27 illustrates in projection. Assuming that such layers can be produced at a certain stage of transition from wollastonite to a phase stable at higher temperatures and pressure, it is natural to ask what changes might occur in the  $\text{Si}_3\text{O}_9$  chains. Again looking at Figures 23 and 24, a remarkable resemblance in the location of the chains in wollastonite with the rings in high-pressure  $\text{CaSiO}_3$  between the respective Ca-O sheets is evident. The two modifications of wollastonite occur together in the same paragenetic environment and are often intergrown. Evidently a very small amount of energy seems to be necessary to transform one phase into the other. The transformation mechanism consists of successive shifts of Ca-O slabs with their associated  $\text{SiO}_4$  tetrahedra parallel to the elongation of the slabs. Hence it is likely that a similar mechanism is acting in the transformation of wollastonite to a phase like high-pressure  $\text{CaSiO}_3$ . Relying again on the pseudomonoclinic units which were discussed at the beginning of this chapter, the type of displacement for such a transformation is illustrated in Fig. 25. These units are shifted in respect to each other by the amount  $b/2$  parallel to the basal plane of such a unit. A view perpendicular to the idealized, hexagonal network of the Ca atoms and also showing the  $\text{Si}_3\text{O}_9$  chains is given in Fig. 27a. The shaded tetrahedra indicate the chains belonging to the layer which has been shifted by the amount suggested above. Based on this intermediate arrangement of the  $\text{Si}_3\text{O}_9$  chains, a possible mechanism to reconnect the Si tetrahedra in form of rings of the type found in high-pressure  $\text{CaSiO}_3$  is proposed in Fig. 26. The figure on the right shows a chain as it occurs in wollastonite and parawollastonite. The inversion centers

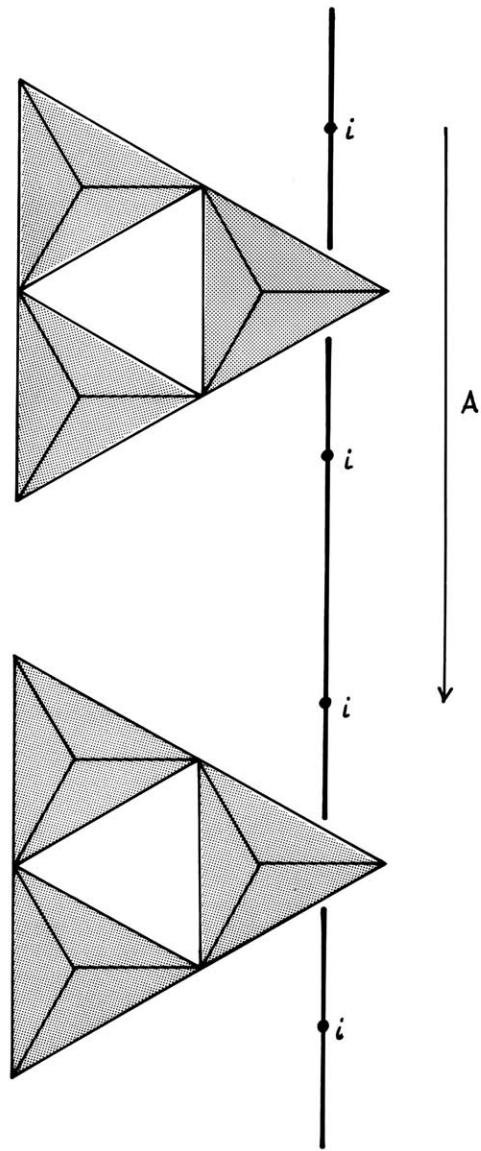
Figure 26. A possible mechanism for constructing  $\text{Si}_3\text{O}_9$  rings out of  $\text{Si}_3\text{O}_9$  chains.

(a)  $\text{Si}_3\text{O}_9$  chain in wollastonite and parawollastonite.

(b)  $\text{Si}_3\text{O}_9$  rings in high-pressure  $\text{CaSiO}_3$ .



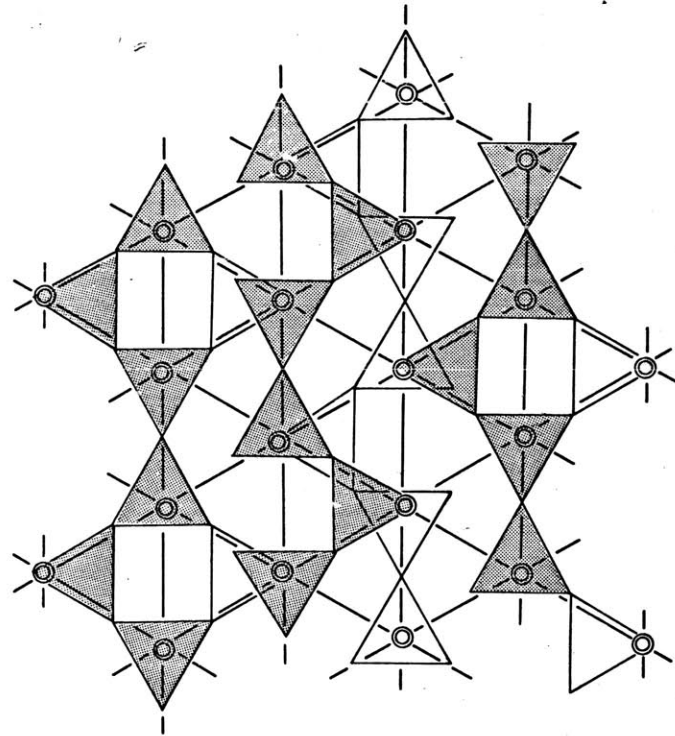
(a)



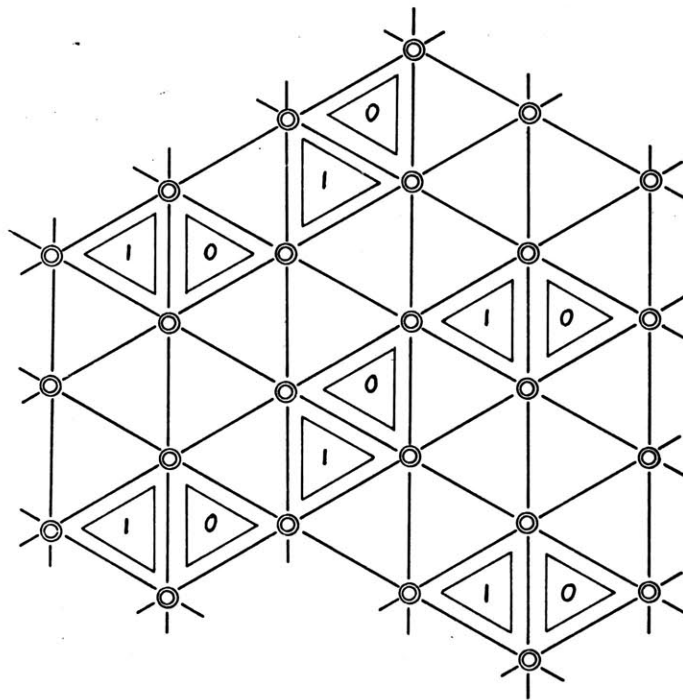
(b)



- Figure 27. An idealized structure of wollastonite projected perpendicular to the Ca network.
- (a) The  $\text{SiO}_4$  tetrahedra form chains, the shaded tetrahedra are above the unshaded ones and are shifted by the amount  $b/2$ .
  - (b) The  $\text{SiO}_4$  tetrahedra are rearranged into rings, the relative heights of the  $\text{Si}_3\text{O}_9$  rings are indicated by numbers. Only the Si atoms forming an equilateral triangle are shown.



(a)



(b)

are located on a direction parallel to  $\underline{b}$ . This direction corresponds to the location of the  $2_1$  axis in parawollastonite. In order to introduce as little change as possible these centers of symmetry ought to be retained and therefore the unshaded tetrahedra are rotated in a position as indicated by the arrows so that they form three-member rings. It is worth while to notice that this procedure produces the rings exactly as they are located along the  $\underline{A}$  axis in high-pressure  $\text{CaSiO}_3$ , thus giving some credibility to this transformation. From Fig. 23 it can be seen that the repeating unit for wollastonite in the direction normal to the Ca-O sheet contains two layers of slabs and their adjacent  $\text{SiO}_4$  tetrahedra. Therefore, if transformed into a ring structure, two layers of different relative heights in direction normal to the layer are expected. Figure 27b shows schematically the rings as obtained by the transformation mechanism just outlined, and projected onto an idealized, hexagonal network of Ca atoms. The heights normal to the layer of the rings are indicated by numbers. This figure has a striking similarity to the presentation of an idealized structure of high-pressure  $\text{CaSiO}_3$  illustrated in Fig. 22b.

This fictitious ring structure derived from wollastonite can be used as a basic structure in order to describe other modifications of  $\text{CaSiO}_3$  which have a larger number of layers. In looking at the projection of the fictitious ring structure of Fig. 27b it is seen that the rings occupy a third of the interstices within a hexagon. By adding a third Ca-O layer with their adjacent  $\text{Si}_3\text{O}_9$  rings and by placing it on top of the second layer so that the positions of its Ca atoms register with the hexagonal network of the Ca atoms underneath, a structure like the idealized structure of high-pressure  $\text{CaSiO}_3$  is obtained.

In this manner up to six layers, each of them in a different position, can be stacked on top of one another. If, in addition, the Ca octahedra forming layers are undistorted, then the orientation of the  $\text{SiO}_4$  tetrahedra would change so that the  $\text{Si}_3\text{O}_9$  rings reach the ideal configuration having symmetry  $\bar{6}m2$ . The result is a structure model identical to the one proposed by Hilmer (1958) and Dornberger-Schiff (1962) for pseudowollastonite.

### Classification of the Calcium Metasilicates.

In order to classify minerals according to the character of their structures it is useful to differentiate between structural features which are shared by all members within the group to be considered and those features which are specific to each individual mineral. Therefore the structural properties of the hitherto known phases of calcium metasilicate are briefly recapitulated.

#### Wollastonite:

- a The cation polyhedra are separated into two kinds of sheets, one is formed by Ca-O octahedra, the other by  $\text{SiO}_4$  tetrahedra.
- b The distribution of octahedrally coordinated Ca atoms is such that they form bands with a width of three octahedra. The octahedra share edges with each other.
- c The repeating unit normal to the sheets consists of two layers of each kind.
- d The  $\text{SiO}_4$  tetrahedra are linked into chains which run parallel to the octahedral slabs. The repeating unit of the chains contains three tetrahedra.
- e There are three different coordinations for the oxygens: O coordinated by one Si and two Ca, O coordinated by one Si and three Ca, and O coordinated by two Si and one Ca.

#### Parawollastonite:

- a The same as in wollastonite.
- b The same as in wollastonite.

- c The repeating unit normal to the sheets contains four layers of each kind as seen in Fig. 23.
- d The same as in wollastonite.
- e The same as in wollastonite.

#### High-Pressure $\text{CaSiO}_3$ :

- a Essentially the same as in the two previous phases.
- b The distribution of the Ca polyhedra results in a continuous layer. However, this layer is incomplete and the missing Ca octahedra is located in the interlayer space thus sharing the space with the  $\text{Si}_3\text{O}_9$  rings. Hence the arrangement of the Ca polyhedra in high-pressure  $\text{CaSiO}_3$  may also be interpreted as being a three-dimensional framework where the interlayer Ca octahedra connect two neighboring layers. The Ca polyhedra share edges as well as corners with each other.
- c The repeating unit normal to the sheets contains three layers of Ca polyhedra as well as three layers of  $\text{Si}_3\text{O}_9$  rings.
- d The  $\text{SiO}_4$  tetrahedra are connected to three-member rings with symmetry  $3\bar{m}$ .
- e The same as in wollastonite.

#### Pseudowollastonite (assumed to be isotypic with $\text{SrGeO}_3$ )

- a The same as in all the other phases.
- b The Ca octahedra are arranged in a continuous layer in which the Ca atoms form a hexagonal network. The octahedra share edges with each other.

- c The repeating unit normal to the layers contains six layers of Ca octahedra and six layers of  $\text{Si}_3\text{O}_9$  rings.
- d The  $\text{SiO}_4$  tetrahedra form three-member rings with symmetry  $\bar{6}m2$ .
- e There are only two different coordinations for the oxygens: O coordinated by two Si, and O coordinated by two Si and three Ca. This results from the fact that the  $\text{SiO}_4$  tetrahedra share only corners with the octahedra.

In the classification of pyroxenes and pyroxenoids Prewitt and Peacor (1964) attribute the following structural characters to the pyroxenoids:

- I The cations are arranged in alternating layers between sheets of oxygens.
- II The distribution of the cations in the octahedral layer is such that they form continuous bands. In contrast to the bands found in the pyroxenes, the pyroxenoid band is either three octahedra wide, as in wollastonite, or is a combination of segments of the pyroxene band and wollastonite band. The various combinations of these segments determine the repeating unit of the bands and the shape of the chains as well.
- III The repeating unit of the silicate chain may contain 3, 5, 7, or 9 tetrahedra.
- IV The oxygens have three different coordinations: O coordinated by one Si and two Ca, O coordinated by one Si and three Ca, and O coordinated by two Si and one Ca.

In comparing these criteria stated above with the structural properties of wollastonite and parawollastonite, it is evident that these two phases of calcium metasilicate belong to the pyroxenoids, as has been concluded by several previous investigators. However, it is impossible to find a substantial agreement with the properties of high-pressure  $\text{CaSiO}_3$  and parawollastonite. The disagreement lies mainly in points b, d and for parawollastonite also in e. High-pressure  $\text{CaSiO}_3$  and pseudowollastonite belong to the group of cyclo-silicates or also named ring-silicates with three-member rings. Several minerals have already been classified into this structural group, for example, benitoite,  $\text{BaTiSi}_3\text{O}_9$ , wadeite,  $\text{K}_2\text{ZrSi}_3\text{O}_9$ , and walstromite,  $\text{Ca}_2\text{BaSi}_3\text{O}_9$ . Benitoite was successfully investigated by Zachariasen (1930) and was the first mineral known to have  $\text{Si}_3\text{O}_9$  rings. A schematic view of the structures of walstromite, pseudowollastonite, and wadeite is illustrated in Figures 22a, 22c, and 22d. The principal structural features as seen in these pictures can be characterized by the following criteria:

- I Sheets of oxygen polyhedra around large cations, e.g. Ba, Ca, K, alternate with sheets composed of  $\text{SiO}_4$  tetrahedra.
- II The large cation polyhedra **form** continuous layers in which the cations are arranged approximately in a hexagonal network.
- III The repeating unit normal to the layers can vary.
- IV The  $\text{SiO}_4$  tetrahedra are connected to three-member rings.
- V In the ideal case, as exemplified by pseudowollastonite, there are two cation coordinations of the oxygens: O coordinated by two Si, and O coordinated by two Si and three Ca.



If these five criteria are compared with the structural properties listed for high-pressure  $\text{CaSiO}_3$  it is obvious, although some are only approximately fulfilled, that this compound belongs to the cyclosilicates. In one point, that is the coordination of the oxygens, it resembles the coordination found in pyroxenoids. This stems from the fact that the tetrahedra in high-pressure  $\text{CaSiO}_3$  share not only corners with the octahedra but also edges. The structure proposed for pseudowollastonite represents the ideal case of cyclosilicate with three-member rings. The layers are a continuous complete arrangement of octahedrally coordinated Ca atoms, and the Si tetrahedra of the  $\text{Si}_3\text{O}_3$  rings share corners with the octahedra so that only two types of oxygen coordination result.

In conclusion it can be said that these four phases of calcium metasilicate crystallize in two distinct structural types, namely pyroxenoids and cyclosilicates. In agreement with Liebau (1962), a significant influence on the type of tetrahedral assemblage is exerted by the arrangement of the Ca polyhedra. The basic feature, sheets of Ca polyhedra alternating with sheets of Si tetrahedra, is common to both types thus greatly facilitating phase transformations which can even be reversible as has been observed in some cases. Polymorphic transitions between pyroxenoids are well known, for instance wollastonite and parawollastonite are considered by Ito (1950) to be members of a polymorphic set using a pseudomonoclinic unit as the basic structure. Layer structures usually have the tendency to show polymorphism; hence it was no surprise to find a polymorphic set whose members, as of now, are walstromite (neglecting the substitution of one Ca by a Ba), high-pressure  $\text{CaSiO}_3$ , and pseudowollastonite.

The  $p$ - $T$  stability Field of the Calcium Metasilicates in relation to their Structures.

Recent studies of phase equilibria of the calcium metasilicates have shown that the various modifications of  $\text{CaSiO}_3$  have stability regions which are quite distinct from one another. Obviously this feature should be reflected in certain characteristics found in the individual structures. Wollastonite and parawollastonite are known to be low temperature forms of  $\text{CaSiO}_3$ . Jeffery (1953) considers the stability region of wollastonite and parawollastonite to be almost the same since intergrowth between the two modifications is frequently observed. Buckner and Roy (1960) determined that wollastonite is stable up to  $1120^\circ \text{C}$  under atmospheric pressure. Above this temperature a different phase, namely pseudowollastonite, is existing. In an analysis of the system  $\text{CaSiO}_3 - \text{H}_2\text{O}$  Buckner, Roy, and Roy (1960) found a rather wide range of pressure, up to 35 kilobars, within which wollastonite is a stable phase. A similar observation was made by Ringwood and Major (1967), they determined a maximum pressure of 30 kilobars for wollastonite. Unfortunately very little is known about pressure conditions of the stability field for pseudowollastonite. Buckner and Roy indicated that the temperature of inversion under pressure between wollastonite and pseudowollastonite is probably higher than  $1120^\circ \text{C}$ . However, these authors did not give any detailed information about existing pressure conditions for the stability field of pseudowollastonite. Since the transformation of wollastonite to pseudowollastonite does not require the presence of pressure, both phases should have similar densities. This is indeed the case, the densities are: wollastonite,  $\rho = 2.88 \text{ g/cc}$ ; pseudowollastonite,  $\rho = 2.92 \text{ g/cc}$ . High-pressure

$\text{CaSiO}_3$ , on the other hand, has a significantly higher density of  $\rho = 3.05$  g/cc. Evidently this is the result of the  $p$ - $T$  conditions under which this high-pressure phase was synthesized, namely 65 kilobars and  $1300^\circ\text{C}$ . Hence a structure which is more closely packed than those of wollastonite, parawollastonite, and pseudowollastonite has to be expected for high-pressure  $\text{CaSiO}_3$ . Prewitt and Peacor (1964) pointed out that the structure of calcium metasilicate have two-dimensional layers of approximately closest packed oxygens in common. Hence there is no way to pack the oxygens closer together than they are already. The only possibility to account for the different densities lies in the arrangement of these layers. The relatively low density of wollastonite and parawollastonite can be explained by the fact that there are slabs of Ca atoms coordinated by closest packed oxygens and these slabs are separated by empty channels. Pseudowollastonite, on the other hand, has continuous layers and hence a slightly higher density than wollastonite. Jeffery and Heller (1953) determined the cell dimensions for pseudowollastonite. These authors give a value of  $19.65 \text{ \AA}$  for the  $c$  axis. According to Dornberger-Schiff (1962) pseudowollastonite has a repeating unit of six layers. This requires a  $c$  axis of twice the length given by Jeffery and Heller. Hence the repeating unit normal to the layers becomes  $39.3 \text{ \AA}$  which allows for a separation of  $6.5 \text{ \AA}$  between the layers. Yet the density of high-pressure  $\text{CaSiO}_3$  is even higher. This in turn can be explained by the smaller separation of the octahedral layers in high-pressure  $\text{CaSiO}_3$ . If the value  $6.5 \text{ \AA}$  is compared with the separation of  $5 \text{ \AA}$  found in high-pressure  $\text{CaSiO}_3$  it is evident that the high-pressure phase has a structure where the octahedral layers are spaced much closer than in pseudowollastonite. This feature is obviously the result of the high pressure of 65 kilobars. In addition the small separation would

account for the eight-fold coordination of Ca(1) since some oxygens belonging to other coordination polyhedra come close enough to be considered as additional nearest neighbors.

In conclusion it can be said that the structures reflect to good approximation the different  $p$ - $T$  conditions of each phase. It seems that the main influence upon the type of structure is exerted by the temperature rather than the pressure. Apparently the energy threshold between a chain structure and a ring structure is quite high, so that pressure alone is not enough to change one structural type into the other. This is exemplified by the inversion of wollastonite to pseudowollastonite induced by high temperature. Therefore it can be said that the calcium metasilicates prefer the pyroxenoid structure at low temperatures and the cyclosilicate structure at high temperatures.

### Acknowledgement

I wish to thank Professor Martin J. Buerger for suggesting the investigation of calcium metasilicates and for his kind and thorough advice during the research work. I also thank Dr. Charles T. Prewitt for supplying me with suitable specimens and x-ray powder photographs. I am very grateful to Mrs. Lyneve Waldrop who helped me not only to overcome difficulties in the English language but also to improve the content of this thesis. Furthermore I am indebted to my colleagues Professor Wayne A. Dollase, Dr. Peter Süssse, and Dr. Herbert Thurn for valuable discussions and detection of errors. The computations were carried out on an IBM 7094 computer at the Massachusetts Institute of Technology Computation Center. After the IBM 7094 computer was replaced by the more modern IBM 360 at the Massachusetts Institute of Technology Computation Center, the computations were concluded at the Harvard University Computation Center in order to avoid the initial defects of the IBM 360 computer. This work was supported by a grant from the National Science Foundation GA-1308.

## References

- E.T. Allen, W.P. White, and F.E. Wright (1906), On wollastonite and pseudo-wollastonite, polymorphic forms of calcium metasilicate. *Am. Jour. Sc.* 21, 89-108.
- A.W. Barnik (1936) Strukturuntersuchung des natürlichen Wollastonite. *Mitt. K.-Wilh.-Inst. Silikatforsch.* No. 172; abstracted in *Strukturbericht* 4, 207-209.
- N.V. Belov (1960), Chapter B of the crystal chemistry of silicates. *Fortschr. Miner.* 38, 4-6.
- L. Bourgeois (1882), Essai de production artificielle de wollastonite et de meionite. *Bull. Soc. Min. France*, 5, 13-16.
- W.L. Bragg (1930), The structure of silicates. *Z. Kristallogr.* 74, 237-305.
- D.A. Buckner and R. Roy (1960), Note on a subsolidus study of the system  $\text{CaSiO}_3$ - $\text{SrSiO}_3$ . *Jour. Am. Ceram. Soc.* 43, 52-53.
- D.A. Buckner, D.M. Roy, and R. Roy (1960), Studies in the system  $\text{CaO-Al}_2\text{O}_3$  -  $\text{SiO}_2$  -  $\text{H}_2\text{O}$  . II: The system  $\text{CaSiO}_3$  -  $\text{H}_2\text{O}$  . *Am. Jour. Sc.* 258, 132-147.
- M.J. Buerger (1956), The determination of the crystal structure of pectolite,  $\text{Ca}_2\text{NaHSi}_3\text{O}_9$  . *Z. Kristallogr.* 108, 248-262.
- M.J. Buerger (1961), Polymorphism and phase transformations. *Fortschr. Miner.* 39, 1, 9-24.
- M.J. Buerger and C.T. Prewitt (1961), The crystal structures of wollastonite and pectolite. *Proc. Nat. Acad. Sc.* 12, 1884-1888.

- C. Dähler (1886), Synthetische Studien. N. Jb. Min. 1, 119-135.
- K. Dornberger-Schiff, F. Liebau und E. Thilo (1955), Zur Struktur des Wollastonite, des Madrellschen Salzes und des Natrium-polyarsenate. Acta Cryst. 8, 752-754.
- K. Dornberger-Schiff (1962), The symmetry and structure of strontium germanate,  $\text{Sr}(\text{GeO}_3)$ , as a structure model for  $\beta$ - wollastonite,  $\text{Ca}(\text{SiO}_3)$ . Soviet Physics-Crystallography vol. 6, no. 6, 694-700.
- J.A. Gard and H.F.W. Taylor (1960), The crystal structure of foshagite. Acta Cryst. 13, 785-793.
- F.P. Glasser and L.S. Dent Glasser (1961), Crystallographic study of  $\text{Ca}_2\text{BaSi}_3\text{O}_9$ . Z. Kristallogr. 116, 263-265.
- D.E. Henshaw (1955), The structure of wadeite. Min. Mag. 30, 585-595.
- W. Hilmer (1958), Zur Strukturbestimmung von Strontiumgermanat,  $\text{SrGeO}_3$ . Naturwiss, 19, 238.
- W. Hilmer (1963), An x-ray investigation of strontium germanate,  $\text{SrGeO}_3$ . Soviet Physics-Crystallography, vol. 7, no. 5, 573-576.
- H. Hauptman, and J. Karle (1953), Solution of the phase problem, I the centrosymmetric crystal. A.C.A. Monograph no. 3, Brooklyn: Polycrystal Book Service.
- T. Ito (1950), X-ray studies on polymorphism. Maruzen, Tokyo, 93-110.

W.J. Jeffery (1953), Unusual x-ray diffraction effects from a crystal of wollastonite. Acta Cryst. 6, 821-825.

W.J. Jeffery and L. Heller (1953), Preliminary x-ray investigation of pseudo-wollastonite. Acta Cryst. 6, 807-808.

I.L. Karle and J. Karle (1966), An application of the symbolic procedure to space group  $P2_1$  and the structure of the alkaloid panamine,  $C_{20} H_{33} N_3$ . Acta Cryst. 21, 860-868.

J. Karle and H. Hauptman (1958), Phase determination for colemanite,  $CaB_3O_4 \cdot (OH)_3 H_2O$ . Acta Cryst. 11, 757-761.

C.A. Larsen (1965), The crystal structure of  $Li_2SO_4 \cdot H_2O$ . A three-dimensional refinement. Acta Cryst. 18, 717-727.

F. Liebau (1960), Zur Kristallchemie der Silikate, Germanate und Fluoberyllates des Formeltyps  $ABX_3$ . N. Jb. Miner. Abh. 94, 1209-1222.

F. Liebau (1962), Die Systematik der Silikate. Naturwiss. 21, 481-491.

F. Machatschki (1928), Zur Frage der Struktur und Konstitution der Feldspate. Zbl. Mineral Abt. A, 97-104.

Kh. S. Mamedov and N.V. Belov (1956), Crystal structure of wollastonite, (Kristallicheskaia structura wollastonite). Doklady Akad. Nauk. SSSR, 107 (3), 463-466.



T. Monticelli e N. Covelli (1825), Podromo della mineralogia vesuviane.  
Vol. I. Napoli da Torchi del Tramater.

H.H. Onken (1964), Manual for some computer programs for x-ray analysis.  
Cambridge, Massachusetts Institute of Technology.

M.A. Peacock (1935), On wollastonite and parawollastonite. Am. Jour. Sc.  
30, 495-529.

D.R. Peacor and M.J. Beurger (1962), Determination and refinement of the  
crystal structure of bustamite,  $\text{CaMnSi}_2\text{O}_6$ . Z. Kristallogr. 117, 331-343.

D.R. Peacor and C.T. Prewitt (1963), Comparison of the crystal structures of  
bustamite and wollastomite. Am. Min. 48, 588-596.

C.T. Prewitt and M.J. Buerger (1963), Comparison of the crystal structures  
of wollastonite and pectolite. Min. Soc. Am. Special Paper 1, 293-302.

C.T. Prewitt and D.R. Peacor (1964), Crystal chemistry of the pyroxenes and  
pyroxenoids. Am. Min. 49, 1527-1542.

A.E. Ringwood and A. Major (1967), Some high-pressure transformations of  
geophysical significance. Earth and Planetary Science Letters 2, 106-110.

H. Strunz (1966), Mineralogische Tabellen. Akademische Verlagsgesellschaft  
Geest & Portig K.-G. , Leipzig.

E. Thilo und I. Plaetschke (1949), Über die Herstellung und Eigenschaften  
von Meta-Arsenophosphaten und die Konstitution des Maddrellschen Salzes  
( $\text{NaPO}_3$ )<sub>x</sub>. Z.anorg. Chemie 260, 297-314.

J. Tolliday (1958), Crystal structure of  $\beta$ -wollastonite. Nature 182, 1012-1013.

F.J. Trojer (1966), The refinement of the structure of sulvanite,  $\text{Cu}_3\text{VS}_4$ . M.S. Thesis, Massachusetts Institute of Technology, Cambridge.

F.J. Trojer (1968), The crystal structure of parawollastonite. Z. Kristallogr. In press.

A. de Vries (1965), On weights for a least-squares refinement. Acta Cryst. 18, 1077-1078.

B.E. Warren and J. Bischof (1931), The crystal structure of the monoclinic pyroxenes. Z. Kristallogr. 80, 391-401.

B.T.M. Willis (1958), An optical method of studying the diffraction from imperfect crystals, III layer structures with stacking faults. Proc. Roy. Soc. A, 248, 183-198.

W.H. Zachariasen (1930), The crystal structure of benitoite,  $\text{BaTiSi}_3\text{O}_9$ . Z. Kristallogr. 74, 139-146.

## Biography

The author was born in Graz, Austria on August 20, 1939 and attended elementary and high schools in Radenthein and Graz, Austria. He studied on the Karl-Franzens-University in Graz from 1958-1964 receiving the degree of Doctor of Philosophy.

From September 1964 until 1969 he has been enrolled at the Massachusetts Institute of Technology. He received the degree of Master of Science in June, 1966. He continued his studies on a Ph.D. program at the same institute.

The author is a member of the American Crystallographic Association. The publications of the author are listed on the following page.

## Publications by the Author

Strukturuntersuchung an einer Hornblende aus dem eklogitischen Gestein von Stramez, südliche Koralpe. Tschermaks min. petr. Mitt. 10, 233-240, (1965).

Coauthor.

Refinement of the Structure of Sulvanite. Am. Min. 51, 890-894, (1966).

Crystal Structure of Parawollastonite. Naturwiss. 20, 536, (1967).

Kurzmitteilung (abstract).

The Crystal Structure of Parawollastonite. Z. Kristallogr. (1968).

Crystal structure of a High-Pressure Polymorph of  $\text{CaSiO}_3$ . Naturwiss. 9, 442, (1968). Kurzmitteilung (abstract).

The Crystal Structure of a High-Pressure Polymorph of  $\text{CaSiO}_3$ . Z. Kristallogr. (1969). In press.